The Dissertation Committee for Luiz Otávio Schmall dos Santos Certifies that this is the approved version of the following dissertation:

DEVELOPMENT OF A MULTI-FORMULATION COMPOSITIONAL SIMULATOR

Committee:

Kamy Sepehrnoori, Supervisor

Mojdeh Delshad

Gary A. Pope

Matthew Balhoff

Lee Chin

Daniel N. de Miranda Filho

DEVELOPMENT OF A MULTI-FORMULATION COMPOSITIONAL SIMULATOR

by

Luiz Otávio Schmall dos Santos, Eng., M.S.

Dissertation

Presented to the Faculty of the Graduate School of

The University of Texas at Austin

in Partial Fulfillment

of the Requirements

for the Degree of

Doctor of Philosophy

The University of Texas at Austin

May 2013

Dedication

This dissertation is dedicated to my beloved wife Rúbia, my partner in life and a constant source of inspiration; to my daughter Cloe, a blessing in our lives; and to my parents Waldir and Glória, my earliest supporters and guides.

Acknowledgements

Foremost, I would like to express my profound gratitude to my supervisor Prof. Kamy Sepehrnoori. No words can express how thankful I am for his guidance, support, patience, and friendship during all these years.

Additionally, I would like to thank Drs. Daniel Miranda, Gary Pope, Lee Chin, Matthew Balhoff, and Mojdeh Delshad for their comments and contributions for the improvement of this dissertation.

I would also like to thank Petrobras (Petróleo Brasileiro S.A.), especially my immediate managers Dr. Anelise Lara, Ms. Roberta Mendes, and Ms. Priscila Moczydlower for providing me with all the necessary support. My sincere thanks also goes to Dr. Daniel Miranda who motivated and helped me to pursue this endeavor.

A special thanks goes to Dr. Francisco Marcondes and Dr. Abdoljalil Varavei who made substantial contributions to this work, and Dr. Chowdhury Mamun who reviewed the text of this dissertation.

Finally, I thank my friends at the Department of Petroleum and Geosystems Engineering for the memorable experiences shared during this period, including the endless hours studying together.

DEVELOPMENT OF A MULTI-FORMULATION COMPOSITIONAL SIMULATOR

Luiz Otávio Schmall dos Santos, Ph.D.

The University of Texas at Austin, 2013

Supervisor: Kamy Sepehrnoori

Compositional simulation is a complex task that involves solving several equations simultaneously for all grid blocks representing a petroleum reservoir. Usually, these equations are separated into two groups: primary and secondary equations. Similarly, the unknowns of the system are also separated into primary and secondary variables. Considering the large number of unknowns, there are many ways to separate such variables in order to deal with the primary variables.

This work aims at comparing a number of formulations for compositional reservoir simulation. It also aims at enhancing the formulations with new features not provided in the original publications. To accomplish these objectives, various formulations prevailing in the literature are implemented in The University of Texas at Austin in-house fully implicit simulator named GPAS (General Purpose Adaptive Simulator) and their performances were compared. Subsequently, some of the formulations were enhanced and tested for various applications.

The comparison of the formulations studied indicated differences in efficiency for each approach. These differences come from the fact that when one is solving for a different set of primary variables, the manipulation of the equations is analogous to the

use of a preconditioner applied to a linear system of equations. Furthermore, unlike a preconditioner, changing the primary variables affects the non-linear solver. Therefore, differences in terms of the number of Newton-Raphson iterations, used for solution of nonlinear equations resulting from discretization of nonlinear partial differential equations representing fluid flow in the reservoir, are expected. In addition to these differences in the non-linear solver, many formulations explore the fact that a reduced number of equations need to be solved implicitly, thus considerably reducing the CPU time dedicated to the linear solver.

Finally, new features not provided in the original published formulations such as three-phase flash calculation, physical dispersion, and unstructured grid were implemented and verified. Additionally, it was demonstrated that, in certain situations, these enhancements are essential to properly model the physical phenomena occurring in oil and gas reservoirs.

Table of Contents

List of Tables

List of Figures

Chapter 1. Introduction

In this chapter, it is presented a brief summary of compositional reservoir simulation and explained various formulations used to solve problems that may affect simulator performance. In upcoming sections, it will be described the objectives of this research and summarized the organization of this dissertation.

1.1 Problem Description

Development of a compositional simulator is a complex task that involves solving several nonlinear equations simultaneously for each grid block (mass balance and fugacity equations for each component, saturation and mole fraction constraints). Through thermodynamic arguments, it can be proved that only n_c+1 equations need to be solved simultaneously in a fully implicit system, where n_c is the number of components in the system (Cao, 2002; Wong and Aziz, 1988). These n_c+1 equations solved implicitly are referred to as primary equations and the remaining, solved explicitly, are secondary equations.

Similarly, the unknowns of the system are separated into primary and secondary variables, where the primary variables are calculated implicitly using the primary equations and the secondary variables are subsequently calculated using the primary variables. Due to a large number of unknowns, there are many ways to solve such a system by choosing different sets of primary variables.

Several compositional formulations have been developed and exist in the literature (Acs et al., 1985; Branco and Rodriguez, 1996; Cao, 2002; Chang et al., 1990a; Chien et al., 1985; Coats, 1980; Collins et al., 1992; Fussell and Fussell, 1979; Kazemi et al., 1978; Kendall et al., 1983; Lins, 2010; Nghiem et al., 1981; Quandalle and Savary, 1989; Wang et al., 1997; Watts, 1986; Wei et al., 2004; Young and Stephenson, 1983).

These formulations differ in the selection of the primary variables, the degree of implicitness, and the choice of primary equations. Aziz and Wong (1988) provided a comprehensive study regarding the most widely used formulations.

From the large set of currently available models, an important issue emerges: which of the formulations is the most efficient and robust for the same degree of implicitness? Thele et al. (1983) compared three different formulations for 1D and 2D problems. Cao (2002) and Voskov et al. (2009) addressed this problem by comparing different sets of primary variables in a fully implicit model.

Another issue is the dependence of those formulations with respect to the physical problem. For example, can different formulations have different performances in terms of computational efficiency when solving different classes of problems, such as miscible gas injection, immiscible gas injection, and gas condensate?

Compositional simulation problems have been addressed by researchers at The University of Texas at Austin for more than 20 years, resulting in the development of various in-house compositional simulators, such as UTCOMP (University of Texas Compositional Simulator) and GPAS (General Purpose Adaptive Simulator) by Chang (1990b) and Wang et al. (1997), respectively. Research and further development of these simulators have resulted in a complex and robust set of tools. Based on the GPAS framework, we intend to implement two fully implicit formulations, one IMPSAT formulation, and one sequential IMPEC formulation; and then compare their performance for different physical problems. Subsequently, we will improve the capabilities of these formulations in terms of phase behavior and also by implementation of a physical dispersion term in one of the formulations.

1.2 RESEARCH OBJECTIVES

This work aims at comparing a number of formulations to determine the efficiency of each approach. It also aims at enhancing and testing the applicability of new features not provided in the referred publications.

Various compositional formulations available in the literature such as Coats (1980), Collins et al. (1992), Branco and Rodriguez (1996) and sequential IMPEC will be implemented in GPAS. These implementations will allow the comparison of three different fully implicit formulations published by Wang et al. (1997), Coats (1980), and Collins et al. (1992); and two semi-implicit formulations: Branco and Rodriguez (1996) and sequential IMPEC.

Additionally, we will enhance and test the applicability of new features not available in the referred publications. These implementations aim at improving the performance and accuracy of the formulations. Furthermore, we will compare these formulations when applied to different physical problems such as water flooding, miscible gas injection, retrograde gas and lean gas production.

For miscible gas injection, for example, phenomena such as dispersion and four-phase flow (three hydrocarbon phases and one aqueous phase) can play an important role in the process. Therefore, the dispersion tensor and a three-phase flash calculation will be implemented in some of the above mentioned formulations.

The final objective of this research is to compare all the formulations implemented for solving different physical problems. Changing the primary variables changes the non-linearity of the resulting equations involved. Furthermore, the main difference among the compositional formulations available is the choice for the selection of various sets of primary variables. Hence, there is a possibility that one set of primary variables would outperform other sets of primary variables for solving a specific physical

problem, with regards to computational effort. Identifying such a set of primary variables can improve the outcome of a reservoir simulation study in terms of overall results as well as computational costs.

1.3 REVIEW OF CHAPTERS

In Chapter 2, a literature review on the four topics covered in this dissertation is performed: different formulations for compositional reservoir simulation, three-phase flash in compositional reservoir simulation, physical dispersion, and unstructured gridding.

In Chapter 3, we show the mathematical model, the background for the numerical model, and the phase behavior concepts involved in compositional reservoir simulation. This chapter is divided into five sections: basic assumptions, mathematical model, equation of state, treatment of phase appearance and disappearance, and discretization of the mathematical model.

In Chapter 4, we describe the techniques used to implement the different formulations in GPAS. The implemented formulations are Coats (1980), Collins et al. (1992), Branco and Rodriguez (1996), and sequential IMPEC. Also in this chapter, we describe the original GPAS formulation proposed by Wang et al. (1997).

In Chapter 5, we describe the enhancements implemented in some of the formulations. These enhancements include three-phase flash calculation (four phase flow), physical dispersion modeling, and unstructured grid.

In Chapter 6, we present a performance comparison of the formulations for various case studies. The studies presented are the following: a water flooding problem, an immiscible gas injection problem, a miscible gas injection problem, a dry gas problem, and an immiscible gas injection in a large heterogeneous reservoir.

In Chapter 7, we present few applications for the enhancements implemented in some of the formulations.

In Chapter 8 we present the conclusions of this work, followed by recommendations for future work.

In Appendices A, B, and C, we present various validation cases using GPAS, an application of various techniques to calculate saturation pressure and an application of Coats formulation (1980) in conjunction with corner point mesh, respectively.

Chapter 2. Literature Survey

In this chapter, we present the literature review related to various topics considered in this dissertation. The chapter will be divided into four sections: (1) solution methods for compositional simulation, (2) three-phase flash, (3) dispersion tensor, and (4) unstructured gridding.

2.1 Solution Methods for Compositional Simulation

Although compositional simulation has been studied for the past three decades, it is still a challenging task. The complexity arises from solving a large number of nonlinear equations and accurately calculating the unknowns that represent the physical variables for the given model. Many authors have developed different formulations for this problem. A brief summary of some formulations is presented below.

Fussel and Fussel (1979) were the first authors to introduce an equation-of-state to calculate phase equilibrium in a reservoir simulator (Wong and Aziz, 1988). Their IMPEC (implicit in pressure and explicit concentrations) formulation uses a method called MVNR (minimum variable Newton-Raphson), which consists of reducing the number of equations and variables by a Gauss elimination procedure. Different from other formulations, the Fussel and Fussel (1979) formulation uses the constraint equations (fugacity equations and volume constraint) as primary equations instead of the usual material balance equations. Another distinction about this formulation is the variable-dependent ordering scheme, which means that the choice of primary variables depends on the predominance of liquid or gas in the grid block. In case of a predominantly liquid grid block, the primary variables are N^g (number of moles of gas per pore volume), $y_i \quad i = 2,\ldots,n_c$ (gas mole fractions for components 2 through n_c), and P (pressure). For a predominantly gas grid block, the primary variables are N^o (number of

moles of liquid per pore volume), $x_i \;\; i = 2,\ldots,n_c$ (liquid mole fractions for components 2 through n_c), and P (pressure).

Another set of primary variables was presented by Coats (1980) in a fully implicit formulation called natural variables (Cao, 2002; Wong and Aziz, 1988). This formulation uses a procedure similar to that of Fussel and Fussel (1979) to reduce the number of unknowns in the full Jacobian matrix. Therefore, the full Jacobian matrix is calculated with respect to the variables P, y_i, x_i, S_o, and S_g, followed by a Gauss elimination scheme to eliminate the secondary variables (y_1, y_2, and $x_i \;\; i = 1,\ldots,n_c$). After this elimination, the system reduces to $(n_c+1)x(n_c+1)$ equations per grid block.

Young and Stephenson (1983) developed an IMPEC formulation where the primary variables are given by P, $z_i \;\; i = 1,\ldots,(n_c-1)$ where z_i is the global mole fraction of the component i, N_w is the number of moles of water per pore volume, and N_T is the total number of moles of hydrocarbon per pore volume. Similar to Coats (1980), Young and Stephenson (1983) formulation uses the fugacity equations to eliminate the secondary variables (y_i and v, the vapor mole fraction) from the primary equations.

Chien et al. (1985) developed a formulation based on K-values instead of mole fractions (where $K_i = \frac{y_i}{x_i}$). Slightly different from Coats (1980) and from Young and Stephenson (1983), this formulation eliminates the secondary variables (K-values and $N_{i\max}$: number of moles of the component for which the derivative of the saturation constraint is the largest per pore volume) from the material balance equations before the Jacobian calculation. Therefore, the primary equations (after eliminating the secondary variables) are directly derived with respect to the primary variables, which are defined by N_i, $i=1,\ldots,n_c$, $i \neq i_{\max}$; N_w; and P.

Another class of formulation was introduced by Acs et al. (1985). They developed a pressure equation for an IMPEC formulation fully decoupled from the fugacity equations, starting from a volume conservation equation. This formulation served as a basis for Kendall et al. (1983), Watts (1986) and Chang (1990a; 1990b) formulations. Kazemi et al. (1978) and Nghiem et al. (1981) presented an IMPEC formulations as well. But differently from Acs et al. (1985), these authors developed the pressure equation by a linear combination of the material balance equations. Moreover, Collins et al. (1992) developed a fully implicit formulation, in which the phase equilibrium is decoupled from the material balance equations. The decoupling process is performed in a way similar to that developed by Acs et al. (1985).

Quandalle and Savary (1989) introduced an IMPSAT formulation (implicit pressure and saturations and explicit concentrations). This model has the advantage of being more stable than a usual IMPEC formulation, because of the implicit treatment of the saturations. Also, this formulation is computationally less expensive than a fully implicit formulation due to the reduced number of equations. Branco and Rodriguez (1996) developed another IMPSAT formulation, which they called a semi-implicit formulation. The main difference between this formulation and that of Quandalle and Savary (1989) is the choice for updating the concentrations at each iteration.

Cao (2002) developed a formulation similar to that of Branco and Rodriguez (1996). However, the choice of the primary equations is different. Instead of the regular Gauss elimination performed for all the material balance equations, Cao (2002) neglected the influence of composition on density and considered the sum of all hydrocarbon material balance equations as a function of pressure and saturations only.

Some additional formulations are available. Bowen and Crumpton (2003) presented another implicit compositional formulation to improve efficiency and CPU

performance. Wei et al. (2004) applied the streamline method to simulate WAG in a three-phase simulator. Li (2004) developed a four-phase simulator using streamlines. He also discussed the advantages of using streamlines instead of the finite difference method in terms of efficiency and reduced numerical dispersion. Voscov and Tchelepi (2008) used the compositional space parameterization (CSP) approach to improve the phase behavior and to garner a premium in performance. Jessen and Rastegar Moghadam (2009) presented an automatic lumping technique to reduce the number of components, thus to improve the computational time.

A final fully implicit formulation considered here was developed by Wang et al. (1997) at The University of Texas at Austin. This formulation uses $\ln K_i \;\; i=1,\ldots,n_c$, $N_i \;\; i=1,\ldots,n_c$, N_w , and P as primary variables. Wang et al. (1997) used GPAS as the framework for their development and the same framework will serve as the basis for this work.

Wong and Aziz (1988) provided a comprehensive study regarding the most widely used formulations.

GPAS was developed under a framework called IPARS which was developed specifically for parallel reservoir simulation research (Gropp et al., 1996; Parashar et al., 1997; Wheeler et al., 1999). This framework was extensively tested for different reservoir simulation models on cluster of PCs and parallel supercomputers with excellent speed-up using large number of processors (Wang et al., 1999; Wang et al., 1997).

Several models have been developed under the GPAS framework such as compositional modeling (Wang et al., 1997), thermal EOS compositional modeling (Varavei, 2009), chemical flooding (Han et al., 2005), unstructured gridding (Marcondes and Sepehrnoori, 2010), and geomechanics coupling (Pan, 2009; Pan et al., 2007).

We implemented all the different formulations compared in this work under the GPAS framework. This procedure guarantees a fair comparison in terms of efficiency and performance.

2.2. THREE-PHASE FLASH ON COMPOSITIONAL RESERVOIR SIMULATION

Three-phase flash can be important in cases of CO_2 injection because of the formation of a second liquid phase rich in super critical CO_2 at low temperatures as reported by various authors (Creek and Sheffield, 1993; Henry and Metcalfe, 1983; Orr et al., 1981; Shelton and Yarborough, 1977; Turek et al., 1988). Despite, the obvious importance of properly modeling such an important phenomenon, most commercial simulators neglect it (Okuno et al., 2010).

The appropriate incorporation of a new phase in a compositional reservoir simulator involves significant changes in the structure with direct impact on the performance of the simulator. A three-phase flash subroutine needs to be implemented. A new term for this phase has to be incorporated in the accumulation and in the convection terms in the material balance equations for each component. A new set of n_c fugacity equations has to be considered in the system and a new mole fraction constraint equation has to be added to the system in a fully implicit model.

Nghiem and Li (1986) compared results of different simulations using a two-phase flash scheme and a three-phase flash scheme. From their results, they concluded that the differences are small because just a small part of the reservoir had all the three hydrocarbon phases coexisting at the same time. This conclusion comes from the fact that the three phase region of the phase envelope is small. Several authors demonstrated the opposite. Simulations using a two-phase flash scheme and a three-phase flash scheme

give significantly different results (Guler et al., 2001; Khan et al., 1992; Wang and Strycker, 2000).

Some authors (Khan et al., 1992; Okuno et al., 2010; Wang and Strycker, 2000) also reported convergence problems in simulation when performing two-phase flash calculations in a case where three hydrocarbon phases were expected to appear. According to Okuno (2010), these problems are the result of discontinuities in the overall composition created when the third phase is neglected.

Fong (1992) developed a methodology to overcome this problem by tuning the EOS in a way that the third hydrocarbon phase does not appear, but, as demonstrated by Okuno (2010), such methodology requires much EOS tuning and simplifications which do not have theoretical basis.

Lins et al. (2011) also proposed a procedure to reduce instability in reservoir simulations in cases when three hydrocarbon phases coexist. This procedure consists of changing by a small amount the calculated pressure in grid blocks with convergence problems in the flash subroutine. This is done only in the flash calculations in order to escape from the three-phase region. Although it improves the stability of the system, it does not have a reasonable theoretical basis, since the whole problem is coupled.

2.3 DISPERSION TENSOR

Gas injection is one of the most important methods for enhanced oil recovery, but requires careful modeling in order to correctly predict production performance. One of the key physical parameters associated with miscible gas displacement is physical dispersion. Although the importance of physical dispersion is known in miscible gas processes, most commercial simulators do not consider this term in the recovery processes. This is mainly due to trappings of the full dispersion tensor that gives rise to

approximate equations whose Jacobian matrix stencil is much large than the one we obtain when the dispersion term is not included in a fully implicit compositional simulator.

Several authors demonstrated the importance of appropriate modeling of physical dispersion (Haajizadeh et al., 1999; Shrivastava et al., 2002; Solano et al., 2001; Stalkup, 1990) in miscible gas processes. In order to incorporate the effects of physical dispersion, some authors have tried to find a grid block size whose numerical dispersion results mimics the physical dispersion (Haajizadeh et al., 1999). The main idea of this approach is to explore the inherent numerical dispersion in the finite difference method to find a grid block size capable of accurately representing the mass transport with the physical dispersion. As pointed out by Fanchi (1983), this methodology is difficult to apply to real field cases and can lead to errors in one or more cross-flow directions. Important to mention that efforts to reduce numerical dispersion using high order methods are object of research as in Liu et al. (1994)

Chang (1990b) presented a method to incorporate physical dispersion in an IMPEC compositional reservoir simulator. Later, Chang et al. (1994) investigated the formation of viscous fingering in different dispersivity scenarios for CO_2 injection. Shrivastava et al. (2005a; 2005b) presented a similar approach to that of Chang et al. (1994) to incorporate physical dispersion in a fully implicit compositional reservoir simulator.

In this study, we introduce a similar dispersion methodology to that proposed by Chang (1990b) in a fully implicit compositional reservoir simulator based on the Coats (1980) formulation for Cartesian grids. The original formulation of Coats (1980) is implemented using an Element-based Finite-Volume Method (EbFVM) as described in Marcondes and Sepehrnoori (2007; 2010) and Marcondes et al. (2013). This approach has

been implemented for several gas flooding reservoir simulation studies and has been shown to be less prone to numerical dispersion. Using this approach, we aim at having the correct physical dispersion effects properly modeled in reservoir simulation (Santos et al., 2013).

2.4 UNSTRUCTURED GRID

Unlike structured mesh formulations, the unstructured grid brings lots of flexibility to the representation of complex geometries such as faults, fractures, and anisotropies occurring in most cases of interest. This advantage arises from the possibility of using either triangles or quadrilaterals, adjusting the element angles to properly comply with the reservoir geometry. Because of this important advantage, many authors have been developing new ideas applied to formulations capable of handling unstructured grids in the petroleum industry.

Another way of modeling complex geometries is the use of corner point meshes. These meshes keep some advantages of the Cartesian and unstructured meshes together. Marcondes et al. (2008) presented a methodology using a full permeability tensor instead of equivalent volumes methodology commonly used in commercial simulators. Appendix C presents one application of this methodology.

Forsyth (1990) used a methodology called Control Volume-based Finite Element Method (CVFEM) to simulate cases of cyclic steam injection with 2D triangular elements. His objective was to apply this methodology to the local-mesh-refinement problem to prove the advantage of flexible unstructured meshes. A similar methodology was also developed by Fung et al. (1992) using triangular elements to simulate thermal processes in two dimensional cases. Gottardi and Dall´Olio (1992) applied this methodology to two-phase (water-oil) cases. Verna and Aziz (1997) presented the

CVFEM formulation among other gridding techniques such as Voronoi and boundary adapting grids (BAG) in two and three-dimensions. Edwards (2000; 2002) used a mixed grid scheme (triangular and quadrilateral elements) to simulate two phase cases. Prevost et al. (2002) extended the streamline formulation for unstructured grid using the CVFEM method.

Cordazzo et al. (2004a; 2004b) demonstrated the problem associated with negative transmissibilities in the CVFEM formulation. But, based on the ideas of the CVFEM formulation, Cordazzo et al. (2005) developed a method called Element-based Finite-Volume Method (EbFVM). In this method, the authors approximate the multi-phase flow equations and overcome the problems related to negative transmissibilities associated with elements with angles greater than 90^{o}.

Marcondes and Seperhnoori (2007; 2010) applied the EbFVM for two-dimensional compositional simulation cases. In their development, they used triangular, quadrilateral and mixed meshes to simulate cases of gas injection in homogeneous and heterogeneous reservoirs. Although the meshes used for most of the investigations presented several elements with angles equal or greater than right angles, the results obtained with triangles and quadrilateral indicated good agreement. Following a similar approach used by the other EbFVM papers, Paluszny et al. (2007) presented a full 3D discretization using hexahedron, tetrahedron, prism, and pyramid elements. They applied their approach to the simulation of the water flooding problem in naturally fractured reservoirs. Marcondes et al. (2013) presented a full 3D discretization using hexahedron, tetrahedron, prism, and pyramid elements for cases of gas injection in a compositional reservoir simulator.

Chapter 3. Compositional Modeling and Background

In this chapter, we present a brief background for compositional reservoir simulation, which sets the foundation for the developments in this dissertation. The chapter will be divided into five sections as follows: (1) basic assumptions, (2) mathematical model, (3) equation of state, (4) treatment of phase appearance and disappearance, and (5) discretization of material balance equations.

3.1 BASIC ASSUMPTIONS

The assumptions associated with the development of the mathematical model in this dissertation are as follows:

- isothermal system;
- multiphase Darcy's law;
- local equilibrium;
- no reaction between rock and fluids (inert rock);
- diagonal permeability tensor for Cartesian grids, but full tensor for unstructured grids;
- dispersion given by a full tensor, with isotropic geometric dispersivity;
- no chemical reactions between the injected fluid and the reservoir fluids;
- slightly compressible porous media;
- there is no mass transfer among the water phase and the hydrocarbon phases;
- no flow boundaries;
- no capillary pressure;
- constant water viscosity;
- no fractures;
- Peaceman's well model.

3.2 MATHEMATICAL MODEL

The mathematical problem for compositional modeling consists of $\left(n_p-1\right)n_c+n_p+1$ equations (where n_c is the number of components, and n_p is the number of phases present in the system) and $\left(n_p-1\right)n_c+n_p+1$ unknowns as follows:

For each component i there is one material balance equation defined by

$$V_b\frac{\partial}{\partial t}\left(\phi N_i\right)-V_b\vec{\nabla}\cdot\sum_{j=2}^{n_p}\left(\frac{\bar{\bar{k}}k_{rj}}{\mu_j}\xi_j x_{ij}\left(\nabla P_j-\gamma_j\nabla D\right)-\phi\xi_j S_j\bar{\bar{K}}_{ij}\nabla x_{ij}\right)-q_i=0\,, \tag{3.2.1}$$

where V_b is the bulk volume of the referred control volume, ϕ is the porosity of the control volume, $\bar{\bar{k}}$ is the absolute permeability tensor of the control volume, k_{rj} is the relative permeability of the phase j, μ_j is the viscosity of the phase j, ξ_j is the density of the phase j, P_j is the pressure of the phase j, γ_j is the specific weight of the phase j, D is the depth, S_j is the saturation of the phase j, $\bar{\bar{K}}_{ij}$ is the full dispersion tensor for the component i for phase j, x_{ij} is the mole fraction of the component i in phase j, q_i is the molar flow rate of the component i due to well injection/production, and N_i is the number of moles of component i per pore volume and is defined by

$$N_i=\sum_{j=2}^{n_p}\xi_j S_j x_{ij}\,. \tag{3.2.2}$$

For the water phase, there is an additional material balance equation as given bellow:

$$V_b\frac{\partial}{\partial t}\left(\phi N_w\right)-V_b\vec{\nabla}\cdot\frac{\bar{\bar{k}}k_{rw}}{\mu_w}\xi_w\left(\nabla P_w-\gamma_w\nabla D\right)-q_w=0\,, \tag{3.2.3}$$

where parameters with w subscript refer to the water phase.

For each component there are n_p-2 fugacity constraints as follows:

$$f_i^2 - f_i^j = 0 \quad for\ j = 3...n_p, \tag{3.2.4}$$

where f_i^j is the fugacity of component *i* in phase *j*. We notice from Equation (3.2.4) that the fugacity of phase *2* was selected as the base for the fugacity of all other phases when three or more hydrocarbon phases are present.

There are $n_p - 1$ mole fraction constraints:

$$\sum_{i=1}^{n_c} x_{ij} = 1 \quad for\ j = 2...n_p\,. \tag{3.2.5}$$

Finally, there is one volume constraint defined by

$$\sum_{j=1}^{n_p} \frac{N_j}{\xi_j} - 1 = 0 \text{ or } \sum_{j=1}^{n_p} S_j - 1 = 0\,. \tag{3.2.6}$$

For the material balance equation defined in Equation (3.2.1), we can see from the second term inside the summation that the transport of mass by diffusion/dispersion has been considered. For this term, we define $\bar{\bar{K}}_{ij}$ as the full dispersion tensor given by

$$\bar{\bar{K}}_{ij} = \begin{pmatrix} K_{xx} & K_{xy} & K_{xz} \\ K_{yx} & K_{yy} & K_{yz} \\ K_{zx} & K_{zy} & K_{zz} \end{pmatrix}_{ij}, \tag{3.2.7}$$

where each term in Equation (3.2.7) was defined by Bear (1988) as

$$K_{mn} = \sum_{k=1}^{3}\sum_{l=1}^{3} \alpha_{klmn} \frac{v_k v_l}{|v|}\,. \tag{3.2.8}$$

In Equation (3.2.8), we can see a new parameter, α, which Bear (1988) defined as the medium (geometrical) dispersivity. This parameter depends on the rock properties and

also by the scale of the experiment (Lake, 1989). The other parameter v is the interstitial velocity.

For an isotropic medium, the following equations (Lake, 1989) are simplified version of Equation (3.2.8):

$$K_{xx} = \frac{D_{ij}}{\tau} + \frac{\alpha_{lj}}{\phi S_j}\frac{u_{xj}^2}{|u_j|} + \frac{\alpha_{tj}}{\phi S_j}\frac{u_{yj}^2}{|u_j|} + \frac{\alpha_{tj}}{\phi S_j}\frac{u_{zj}^2}{|u_j|}, \tag{3.2.10a}$$

$$K_{yy} = \frac{D_{ij}}{\tau} + \frac{\alpha_{lj}}{\phi S_j}\frac{u_{yj}^2}{|u_j|} + \frac{\alpha_{tj}}{\phi S_j}\frac{u_{xj}^2}{|u_j|} + \frac{\alpha_{tj}}{\phi S_j}\frac{u_{zj}^2}{|u_j|}, \tag{3.2.10b}$$

$$K_{zz} = \frac{D_{ij}}{\tau} + \frac{\alpha_{lj}}{\phi S_j}\frac{u_{zj}^2}{|u_j|} + \frac{\alpha_{tj}}{\phi S_j}\frac{u_{xj}^2}{|u_j|} + \frac{\alpha_{tj}}{\phi S_j}\frac{u_{yj}^2}{|u_j|}, \tag{3.2.10c}$$

$$K_{xy} = K_{yx} = \frac{\alpha_{lj} - \alpha_{tj}}{\phi S_j}\frac{u_{xj}u_{yj}}{|u_j|}, \tag{3.2.10d}$$

$$K_{xz} = K_{zx} = \frac{\alpha_{lj} - \alpha_{tj}}{\phi S_j}\frac{u_{xj}u_{zj}}{|u_j|}, \tag{3.2.10e}$$

$$K_{yz} = K_{zy} = \frac{\alpha_{lj} - \alpha_{tj}}{\phi S_j}\frac{u_{yj}u_{zj}}{|u_j|}. \tag{3.2.10f}$$

3.3 EQUATION OF STATE

For the equilibrium statements in the last section (Equation 3.2.4), the parameters involved must to be calculated by an Equation of State (EOS). Equations of State relate the state variables of the reservoir fluids such as pressure, temperature, volume, and internal energy.

Since debut of the van der Waals' equation in 1876, many different EOS have been proposed. In the petroleum literature, the Peng-Robinson, and the Soave-Redlich-

Kwong are the most used EOS for compositional simulation because of their simplicity and accurate results for VLE (vapor-liquid equilibrium) calculations. In this research the Peng-Robinson EOS was used for all formulations.

3.3.1 Peng-Robinson Equation of State

Peng and Robinson (1976) proposed a cubic equation of state with two parameters by changing the repulsive term of the original van der Waals equation as follows:

$$P = \frac{RT}{V-b} - \frac{a(\alpha)}{V(V+b)+b(V-b)}, \tag{3.3.1.1}$$

where P is the pressure, R is the universal gas constant, T is the temperature V is the volume, $a(\alpha)$ is given by

$$a(\alpha) = 0.45724\frac{R^2T_c^2}{P_c}\alpha(T), \tag{3.3.1.2}$$

b is given by

$$b = 0.07780\frac{RT_c}{P_c}, \tag{3.3.1.3}$$

$\alpha(T)$ is a function of temperature and is defined by

$$\sqrt{\alpha(T)} = 1+\kappa\left(1-\sqrt{\frac{T}{T_c}}\right), \tag{3.3.1.4}$$

where κ is defined by

$$\kappa = 0.37464+1.54226\omega-0.26992\omega^2, \tag{3.3.1.5}$$

and the subscript c denotes critical point.

3.3.2 Mixing Rules

For mixtures of hydrocarbons, the calculation of parameters a and b in the Peng-Robinson EOS need to be performed using a mixing rule as defined below:

$$a = \sum_{i=1}^{n_c} \sum_{j=1}^{n_c} x_i x_j a_{ij} , \tag{3.3.2.1}$$

$$a_{ij} = \left(1 - K_{ij}\right)\left(a_i a_j\right)^{0.5} , \tag{3.3.2.2}$$

and

$$b = \sum_{i=1}^{n_c} x_i b_i , \tag{3.3.2.3}$$

where K_{ij} are the binary interaction coefficients.

3.4 TREATMENT OF PHASE APPEARANCE AND DISAPPEARANCE

The Section 3.2 of this dissertation presented the mathematical model in the most general way, i.e., considering n_p phases for each control volume. These n_p phases can change for each control volume and for each time-step during the simulation due to global composition and pressure changes. In order to correctly capture the number of phases present in each control volume, a procedure called stability test needs to be performed at each iteration for each control volume. This procedure is one of the most difficult tasks in a compositional simulator and still is a subject for much research.

In this section, we detail the most common procedures to perform a stability test in compositional simulators: comparing the actual control volume pressure with the fluid saturation pressure (Coats, 1980), and the tangent plane procedure proposed by Michelsen (1982).

Appendix B presents a comparison of various methodologies used for the saturation pressure calculation presented in this dissertation.

For the comparisons of different formulations for compositional reservoir simulation presented in Chapter 5, we used Michelsen's stability test method (Michelsen, 1982).

3.4.1 Saturation Pressure Calculation

For single phase control volumes, Coats (1980) suggests comparing the saturation pressure and the actual control volume pressure to determine whether or not the actual phase splits into two phases. If the actual pressure is less than the saturation pressure, the control volume is set as two-phase and a flash calculation is performed to estimate the new phase composition.

Coats (1980) suggested using Fussel and Yanosik (1978) for the saturation pressure calculation, but this approach is entirely dependent on the initial guess as it uses the Newton-Raphson procedure. We investigated Baker and Luks (1980) and Michelsen (1985) approaches in order to improve the robustness of the saturation pressure calculation.

3.4.1.1 Fussel and Yanosik (1978)

This method consists of a Newton-Raphson iteration for the fugacity equations plus one of the constraint equations. Therefore, in their original work, Fussel and Yanosik (1978) suggested to use Equations (3.4.1.1.1) and (3.4.1.1.2) to calculate the saturation pressure of the liquid phase,

$$f_i^g - f_i^o = 0, \tag{3.4.1.1.1}$$

$$P_s - \sum_{i=1}^{n_c} \frac{f_i^o}{\psi_i^g} = 0, \tag{3.4.1.1.2}$$

where the superscripts *o* and *g* represent the oil and gas phases, respectively; P_s is the saturation pressure; and ψ_i^g is the fugacity coefficient of the component *i* in gas phase.

If the gas saturation pressure is desired, Equation (3.4.1.1.2) should be replaced by

$$P_s - \sum_{i=1}^{n_c} \frac{f_i^g}{\psi_i^o} = 0 . \qquad (3.4.1.1.3)$$

Coats (1980) claims to obtain better convergence by switching Equation (3.4.1.1.2) with Equation (3.4.1.1.4) when the liquid saturation pressure is calculated. When the gas saturation pressure is calculated, Equation (3.4.1.1.3) must be replaced by (3.4.1.1.5).

$$\sum_{i=1}^{n_c} y_i = 1.0 , \qquad (3.4.1.1.4)$$

$$\sum_{i=1}^{n_c} x_i = 1.0 . \qquad (3.4.1.1.5)$$

3.4.1.2 Baker and Luks (1980)

Because of the strong non-linearity of the fugacity equations (Equation 3.4.1.1), Fussel and Yanosik (1978) method is entirely dependent on the initial guess. In order to improve the initial guess, Baker and Luks (1980) proposed a successive substitution procedure to be performed before the Newton-Raphson iterations. Therefore, when the estimation gets close enough to the solution, Fussel and Yanosik (1978) can be used to accelerate the convergence.

The successive substitution procedure starts at a low pressure, i.e. *1 psi*, and the compositions are defined by the known phase and an appropriate approximation of the

unknown phase. Therefore, the fugacity coefficients can be calculated by Equations (3.4.1.2.1a) and (3.4.1.2.1b):

$$f_i^o = P\psi_i^o x_i, \qquad (3.4.1.2.1a)$$

$$f_i^g = P\psi_i^g y_i. \qquad (3.4.1.2.1b)$$

Using Equation (3.4.1.1.1), we can calculate the composition of the unknown phase by

$$Y_i = x_i \frac{\psi_i^o}{\psi_i^g}, \qquad (3.4.1.2.2a)$$

for a bubble point calculation, or

$$X_i = y_i \frac{\psi_i^g}{\psi_i^o}, \qquad (3.4.1.2.2b)$$

for a dew point calculation.

If the summation of the calculated composition is greater than one, then this means that the pressure used is too low. If the same summation is less than one, then the pressure used is too high. In order to correct the pressure used, we add *200 psi*, or subtract *200 psi*, depending on the direction established by the summation of the unknown composition.

After the new pressure is calculated, the unknown composition should be normalized for use in the next iteration. Thus, we recalculate the unknown composition using Equations (3.4.1.2.1a) or (3.4.1.2.1b).

If the direction established by the summation of the calculated composition changes, the new pressure should be calculated using half of the interval used before. As

soon as we get close enough to the objective, i.e. the difference among the new pressure calculated and the previous one is small enough, such as $\pm 20\,psi$, the Newton-Raphson procedure (Fussell and Yanosik, 1978) can start.

Baker and Luks (1980) suggest using $\psi_i^g = 1$ as a first guess in case of bubble point calculation and Equation (3.4.1.2.3) in case of dew point calculation.

$$\psi_i^o = \psi_i^0 \exp\left[Z_L^0 \left(\frac{P}{P_{si}} - 1 \right) \right], \tag{3.4.1.2.3}$$

where ψ_i^0 is the pure component fugacity coefficient evaluated at the pure component vapor pressure P_{si}. The estimation of P_{si} can be obtained by Clausius-Clapeyron Equation (3.4.1.2.4).

$$P_{si} = P_{ci} \exp\left[\left(\frac{\Delta H_{\upsilon i}}{T_{ci}} \right) \left(1 - \frac{T_{ci}}{T} \right) \right], \tag{3.4.1.2.4}$$

where $\Delta H_{\upsilon i}$ is the heat of vaporization of component *i*.

3.4.1.3 Michelsen (1985)

Michelsen (1985) proposed a different successive substitution method using the tangent plane distance equation to calculate the pressure for the new iteration. This method seems to be more robust than the one proposed be Baker and Luks (1980).

The first step for this method is to calculate the composition of the unknown phase using Equation (3.4.1.2.2a) or (3.4.1.2.2b). Thus, the tangent plane distance is calculated using Equation (3.4.1.3.1a) or (3.4.1.3.1b):

$$Q^k = 1 - \sum_i Y_i\,, \tag{3.4.1.3.1a}$$

in case of a bubble point calculation, or

$$Q^k = 1 - \sum_i X_i \,, \tag{3.4.1.3.1b}$$

in case of a dew point calculation. The superscript *k* indicates the iteration level.

The new pressure can now be calculated by Equation (3.4.1.3.2)

$$P_s^{k+1} = P_s^k - \frac{Q^k}{\frac{\partial Q^k}{\partial P_s}} \,, \tag{3.4.1.3.2}$$

and the new composition can be normalized by Equation (3.4.1.3.3) in order to calculate the fugacity coefficients for the new iteration

$$y_i^{k+1} = \frac{Y_i^k}{\sum_s Y_s^k} \,. \tag{3.4.1.3.2}$$

With the new composition and the new pressure, the new fugacity coefficients can be calculated and a new iteration can be started from Equation (3.4.1.2.2a) or (3.4.1.2.2b). The procedure needs to be repeated until we get close enough to the boundary, such as $P_s^{k+1} - P_s^k \le 0.1 psi$. Therefore, Fussell and Yanosik (1978) method can be used to refine the solution.

3.4.2 Stability Test by Tangent Plane Distance

The general concept for stability test is search for a new phase, which combined with the existent one, can reduce the Gibbs free energy. This problem can be expressed mathematically by Equation (3.4.2.1) (Chang, 1990b):

$$\Delta G = \sum_i y_i \left[\mu_i(\bar{y}) - \mu_i(\bar{z}) \right], \tag{3.4.2.1}$$

where y_i is the mole fraction of component *i* in the new phase, $\mu_i(\bar{y})$ is the chemical potential of component *i* in the new phase, and $\mu_i(\bar{z})$ is the chemical potential of component *i* in the existent phase.

In case of positive ΔG (calculated by Equation (3.4.2.1)) for all possible compositions $\bar{y}$, the phase is intrinsically stable. Otherwise, if a set of $\bar{y}$ can minimize the Gibbs free energy ($\Delta G < 0$), the system is unstable and needs to be split in two phases.

Equation (3.4.2.1) is non-linear and difficult to be minimized in a multicomponent system because of the existence of local minima. Furthermore, it is not practical to check the entire space of possibilities in Equation (3.4.2.1). Thus, a procedure that reduces the search range should be applied.

Michelsen (1982) proposed to check the Tangent Plane Distance at stationary points. This procedure is much faster than a regular flash calculation and much simpler than a direct minimization for the Gibbs free energy.

The method consists of solving Equation (3.4.2.2) for Y_i,

$$\ln\psi_i(\bar{y}) + \ln Y_i - \ln\psi_i(\bar{z}) - \ln(z_i) = 0, \tag{3.4.2.2}$$

where y_i is the normalization of Y_i, given by Equation (3.4.2.3), and ψ_i is the fugacity coefficient.

$$y_i = \frac{Y_i}{\sum_s Y_s}. \tag{3.4.2.3}$$

After obtaining the solution to Equation (3.4.2.2), we calculate $r = \sum_i Y_i - 1$. In case of a positive value of *r*, the phase is unstable and a flash calculation should be performed. Otherwise, the phase is considered stable.

Equation (3.4.2.2) is a system of non-linear equations, thus requiring an initial guess to be solved. Michelsen (1982) proposed the use of Equations (3.4.2.4) first:

$$Y_i = z_i K_i, \tag{3.4.2.4}$$

and then, the use of Equation (3.4.2.5):

$$Y_i = \frac{z_i}{K_i}, \tag{3.4.2.5}$$

where K_i's are the K values which can be calculated by Equation (3.4.2.6) (Wilson, 1969).

$$K_i = \frac{P_{ci}}{P} \exp\left[5.37\left(1+\omega_i\right)\left(1-\frac{T_{ci}}{T}\right)\right]. \tag{3.4.2.6}$$

The solution can be obtained by Newton-Raphson method or by successive substitution. If the second alternative is chosen, Equation (3.4.2.2) is replaced by Equation (3.4.2.6):

$$Y_i^{k+1} = \exp\left[\ln\psi_i\left(\bar{y}\right)+\ln\psi_i\left(\bar{z}\right)-\ln\left(z_i\right)\right]^k. \tag{3.4.2.6}$$

When the Tangent Plane Distance indicates a two-phase system, the instability of the system is guaranteed and a flash calculation has to be performed. On the other hand, the Michelsen (1982) procedure cannot guarantee stability, if indicated by the solution.

3.5 DISCRETIZATION OF THE MATERIAL BALANCE EQUATIONS

The set of equations representing the mathematical model presented in Section 3.2 of this chapter is a system of non-linear partial differential equations. In order to solve

this system, we need to discretize the material balance equations (Equations (3.2.1) and (3.2.3)).

In this dissertation, the Finite Volume Method (FVD) will be used to discretize the equations in the Cartesian formulation and the Element-based Finite Volume Method (EbFVM) will be used to discretize in the unstructured formulation. In this section, we present the details for the Cartesian formulation and in Section 5.3 we present the details of the unstructured formulation.

The first step for building the numerical model is the integration of Equations (3.2.1) and (3.2.3) as presented below:

$$\int_V V_b \frac{\partial}{\partial t}(\phi N_i)\,dV - \int_V V_b \vec{\nabla}\cdot\sum_{j=2}^{n_p}\left(\frac{\bar{\bar{k}}k_{rj}}{\mu_j}\xi_j x_{ij}\left(\nabla P_j - \gamma_j \nabla D\right) - \phi\xi_j S_j \bar{\bar{K}}_{ij}\nabla x_{ij}\right)dV - \int_V q_i dV = 0\,, \quad (3.5.1)$$

$$\int_V V_b \frac{\partial}{\partial t}(\phi N_w)\,dV - \int_V V_b \vec{\nabla}\cdot\frac{\bar{\bar{k}}k_{rw}}{\mu_w}\xi_w\left(\nabla P_w - \gamma_w \nabla D\right)dV - \int_V q_w dV = 0\,, \quad (3.5.2)$$

Applying the Gauss theorem to Equations (3.5.1) and (3.5.2), we get

$$\int_V \frac{\partial}{\partial t}(\phi N_i)\,dV - \int_A \sum_{j=2}^{n_p}\left(\frac{k_{rj}}{\mu_j}\xi_j x_{ij}\bar{\bar{k}}\cdot\left(\nabla P_j - \gamma_j \nabla D\right) - \phi\xi_j S_j \bar{\bar{K}}_{ij}\cdot\nabla x_{ij}\right)\cdot d\bar{A} - \int_V \frac{q_i}{V_b}dV = 0\,, \quad (3.5.3)$$

$$\int_V \frac{\partial}{\partial t}(\phi N_w)dV - \int_A \frac{k_{rw}}{\mu_w}\xi_w\bar{\bar{k}}\cdot\left(\nabla P_w - \gamma_w \nabla D\right)\cdot d\bar{A} - \int_V \frac{q_w}{V_b}dV = 0\,. \quad (3.5.4)$$

For the Cartesian formulation, we adopt a parallelepiped element. Also, we assume that all properties are constant inside the element. This is a strong assumption (requires small grid block sizes for accurate results), but makes it possible for the integration of Equations (3.5.3) and (3.5.4).

Figure 3.5.1 presents the parallelepiped element used for the Cartesian formulation and its respective geometric properties.

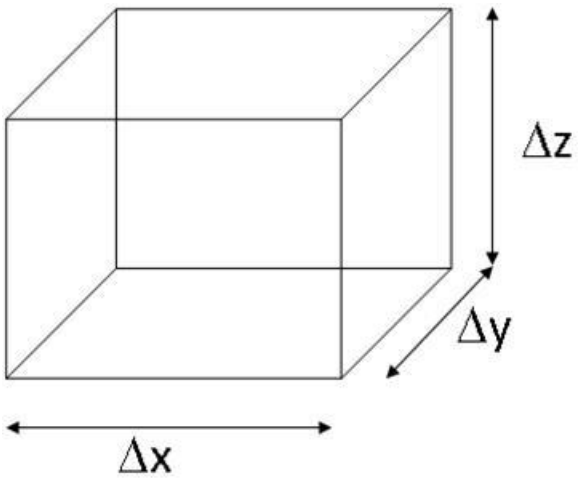

Figure 3.5.1. Parallelepiped element used in the Cartesian formulation.

Using the element showed in **Figure 3.5.1**, we can integrate the accumulation term in Equations (3.5.3) and (3.5.4) as follows:

$$\int_V \frac{\partial}{\partial t}\left(\phi N_i\right) dV = \left[\frac{\partial}{\partial t}\left(\phi N_i\right)\right]_{xyz} \left(\Delta x \Delta y \Delta z\right)_{xyz}, \tag{3.5.5}$$

$$\int_V \frac{\partial}{\partial t}\left(\phi N_w\right) dV = \left[\frac{\partial}{\partial t}\left(\phi N_w\right)\right]_{xyz} \left(\Delta x \Delta y \Delta z\right)_{xyz}. \tag{3.5.6}$$

In a similar way, we can integrate the source/sink term as follows:

$$\int_V \frac{q_i}{V_b} dV = q_i, \tag{3.5.7}$$

$$\int_V \frac{q_w}{V_b} dV = q_w, \tag{3.5.8}$$

where the well model is given by Peaceman's model for nonsquare wellblocks with anisotropic permeability.

Expanding the convective term, we get

$$\begin{aligned}
&\int_A \sum_{j=2}^{n_p} \left(\frac{k_{rj}}{\mu_j} \xi_j x_{ij} \bar{\bar{k}} \cdot \left(\nabla P_j - \gamma_j \nabla D \right) - \phi \xi_j S_j \bar{\bar{K}}_{ij} \cdot \nabla x_{ij} \right) \cdot d\bar{A} = \\
&\sum_{j=2}^{n_p} \int_A \left[\frac{k_{rj}}{\mu_j} \xi_j x_{ij} \bar{\bar{k}} \cdot \left(\nabla P_j - \gamma_j \nabla D \right) \right] \cdot d\bar{A} - \sum_{j=2}^{n_p} \int_A \left(\phi \xi_j S_j \bar{\bar{K}}_{ij} \cdot \nabla x_{ij} \right) \cdot d\bar{A}
\end{aligned} \tag{3.5.9}$$

The first term on the right hand side of Equation (3.5.9) can be integrated using our assumption of a diagonal permeability tensor. Equation (3.5.10) shows an example for a phase *j* (a similar expression can be obtained for the convective term in the water material balance equation).

$$\begin{aligned}
&\int_A \left[\frac{k_{rj}}{\mu_j} \xi_j x_{ij} \bar{\bar{k}} \cdot \left(\nabla P_j - \gamma_j \nabla D \right) \right] \cdot d\bar{A} = \\
&\left(\frac{k_{rj}}{\mu_j} \xi_j x_{ij} k_{xx} \right)_{x+\frac{1}{2}} \left(\frac{\partial P_j}{\partial x} - \gamma_j \frac{\partial D}{\partial x} \right)_{x+\frac{1}{2}} (\Delta y \Delta z)_{x+\frac{1}{2}} - \left(\frac{k_{rj}}{\mu_j} \xi_j x_{ij} k_{xx} \right)_{x-\frac{1}{2}} \left(\frac{\partial P_j}{\partial x} - \gamma_j \frac{\partial D}{\partial x} \right)_{x-\frac{1}{2}} (\Delta y \Delta z)_{x-\frac{1}{2}} + \\
&\left(\frac{k_{rj}}{\mu_j} \xi_j x_{ij} k_{yy} \right)_{y+\frac{1}{2}} \left(\frac{\partial P_j}{\partial y} - \gamma_j \frac{\partial D}{\partial y} \right)_{y+\frac{1}{2}} (\Delta x \Delta z)_{y+\frac{1}{2}} - \left(\frac{k_{rj}}{\mu_j} \xi_j x_{ij} k_{yy} \right)_{y-\frac{1}{2}} \left(\frac{\partial P_j}{\partial y} - \gamma_j \frac{\partial D}{\partial y} \right)_{y-\frac{1}{2}} (\Delta x \Delta z)_{y-\frac{1}{2}} + \\
&\left(\frac{k_{rj}}{\mu_j} \xi_j x_{ij} k_{zz} \right)_{z+\frac{1}{2}} \left(\frac{\partial P_j}{\partial z} - \gamma_j \frac{\partial D}{\partial z} \right)_{z+\frac{1}{2}} (\Delta x \Delta y)_{z+\frac{1}{2}} - \left(\frac{k_{rj}}{\mu_j} \xi_j x_{ij} k_{zz} \right)_{z-\frac{1}{2}} \left(\frac{\partial P_j}{\partial z} - \gamma_j \frac{\partial D}{\partial z} \right)_{z-\frac{1}{2}} (\Delta x \Delta y)_{z-\frac{1}{2}}.
\end{aligned} \tag{3.5.10}$$

Although the integration of the second term on the right hand side of Equation (3.5.9) is made in a similar fashion as in Equation (3.5.10), the dispersion tensor cannot be approximated by a diagonal tensor. The expansion for phase *j* is given by Equation

(3.5.11) and the expressions for each direction are presented in Equations (3.5.12a), (3.5.12b), and (3.5.12c).

$$\int_A \left(\phi\xi_j S_j \bar{\bar{K}}_{ij} \cdot \nabla x_{ij}\right) \cdot d\bar{A} =$$
$$\int_{A_x} \left(\phi\xi_j S_j \bar{\bar{K}}_{ij} \cdot \nabla x_{ij}\right) \cdot d\bar{A}_x + \int_{A_y} \left(\phi\xi_j S_j \bar{\bar{K}}_{ij} \cdot \nabla x_{ij}\right) \cdot d\bar{A}_y + \int_{A_z} \left(\phi\xi_j S_j \bar{\bar{K}}_{ij} \cdot \nabla x_{ij}\right) \cdot d\bar{A}_z, \tag{3.5.11}$$

$$\int_{A_x} \left(\phi\xi_j S_j \bar{\bar{K}}_{ij} \cdot \nabla x_{ij}\right) \cdot d\bar{A}_x =$$
$$\left(\phi\xi_j S_j K_{ij\,xx}\right)_{x+\frac{1}{2}} \left(\frac{\partial x_{ij}}{\partial x}\right)_{x+\frac{1}{2}} (\Delta y \Delta z)_{x+\frac{1}{2}} - \left(\phi\xi_j S_j K_{ij\,xx}\right)_{x-\frac{1}{2}} \left(\frac{\partial x_{ij}}{\partial x}\right) (\Delta y \Delta z)_{x-\frac{1}{2}} +$$
$$\left(\phi\xi_j S_j K_{ij\,xy}\right)_{x+\frac{1}{2}} \left(\frac{\partial x_{ij}}{\partial y}\right)_{x+\frac{1}{2}} (\Delta y \Delta z)_{x+\frac{1}{2}} - \left(\phi\xi_j S_j K_{ij\,xy}\right)_{x-\frac{1}{2}} \left(\frac{\partial x_{ij}}{\partial y}\right) (\Delta y \Delta z)_{x-\frac{1}{2}} + \tag{3.5.12a}$$
$$\left(\phi\xi_j S_j K_{ij\,xz}\right)_{x+\frac{1}{2}} \left(\frac{\partial x_{ij}}{\partial z}\right)_{x+\frac{1}{2}} (\Delta y \Delta z)_{x+\frac{1}{2}} - \left(\phi\xi_j S_j K_{ij\,xz}\right)_{x-\frac{1}{2}} \left(\frac{\partial x_{ij}}{\partial z}\right) (\Delta y \Delta z)_{x-\frac{1}{2}},$$

$$\int_{A_y} \left(\phi\xi_j S_j \bar{\bar{K}}_{ij} \cdot \nabla x_{ij}\right) \cdot d\bar{A}_y =$$
$$\left(\phi\xi_j S_j K_{ij\,yy}\right)_{y+\frac{1}{2}} \left(\frac{\partial x_{ij}}{\partial y}\right)_{y+\frac{1}{2}} (\Delta x \Delta z)_{y+\frac{1}{2}} - \left(\phi\xi_j S_j K_{ij\,yy}\right)_{y-\frac{1}{2}} \left(\frac{\partial x_{ij}}{\partial y}\right) (\Delta x \Delta z)_{y-\frac{1}{2}} +$$
$$\left(\phi\xi_j S_j K_{ij\,yx}\right)_{y+\frac{1}{2}} \left(\frac{\partial x_{ij}}{\partial x}\right)_{y+\frac{1}{2}} (\Delta x \Delta z)_{y+\frac{1}{2}} - \left(\phi\xi_j S_j K_{ij\,yx}\right)_{y-\frac{1}{2}} \left(\frac{\partial x_{ij}}{\partial x}\right) (\Delta x \Delta z)_{y-\frac{1}{2}} + \tag{3.5.12b}$$
$$\left(\phi\xi_j S_j K_{ij\,yz}\right)_{y+\frac{1}{2}} \left(\frac{\partial x_{ij}}{\partial z}\right)_{y+\frac{1}{2}} (\Delta x \Delta z)_{y+\frac{1}{2}} - \left(\phi\xi_j S_j K_{ij\,yz}\right)_{y-\frac{1}{2}} \left(\frac{\partial x_{ij}}{\partial z}\right) (\Delta x \Delta z)_{y-\frac{1}{2}},$$

$$\int_{A_z}\left(\phi\xi_j S_j \bar{\bar{K}}_{ij}\cdot\nabla x_{ij}\right)\cdot d\bar{A}_z =$$

$$\left(\phi\xi_j S_j K_{ij_{zz}}\right)_{z+\frac{1}{2}}\left(\frac{\partial x_{ij}}{\partial z}\right)_{z+\frac{1}{2}}\left(\Delta x\Delta y\right)_{z+\frac{1}{2}} - \left(\phi\xi_j S_j K_{ij\,zz}\right)_{z-\frac{1}{2}}\left(\frac{\partial x_{ij}}{\partial z}\right)\left(\Delta x\Delta y\right)_{z-\frac{1}{2}} +$$

$$\left(\phi\xi_j S_j K_{ij_{zx}}\right)_{z+\frac{1}{2}}\left(\frac{\partial x_{ij}}{\partial x}\right)_{z+\frac{1}{2}}\left(\Delta x\Delta y\right)_{z+\frac{1}{2}} - \left(\phi\xi_j S_j K_{ij\,zx}\right)_{z-\frac{1}{2}}\left(\frac{\partial x_{ij}}{\partial x}\right)\left(\Delta x\Delta y\right)_{z-\frac{1}{2}} + \tag{3.5.12c}$$

$$\left(\phi\xi_j S_j K_{ij_{zy}}\right)_{z+\frac{1}{2}}\left(\frac{\partial x_{ij}}{\partial y}\right)_{z+\frac{1}{2}}\left(\Delta x\Delta y\right)_{z+\frac{1}{2}} - \left(\phi\xi_j S_j K_{ij_{zy}}\right)_{z-\frac{1}{2}}\left(\frac{\partial x_{ij}}{\partial y}\right)\left(\Delta x\Delta y\right)_{z-\frac{1}{2}},$$

where $\bar{\bar{K}}_{ij}$ is the dispersion tensor of component *i* and phase *j*.

The last step in the development of the numerical model is the approximation of derivatives in Equations (3.5.5), (3.5.6), (3.5.10), (3.5.12a), (3.5.12b), and (3.5.12c). For the time derivative in Equations (3.5.5), and (3.5.6) we use the backward Finite Differences Method (FDM), and for the spatial derivatives in Equations (3.5.10), (3.5.12a), (3.5.12b), and (3.5.12c) we use central approximation of the FDM. Therefore, the term inside the brackets in Equations (3.5.5) and (3.5.6) can be replaced by

$$\left[\frac{\partial}{\partial t}\left(\phi N_i\right)\right]_{xyz} \simeq \frac{1}{\Delta t}\left[\left(\phi N_i\right)^{k+1} - \left(\phi N_i\right)^{k}\right]_{xyz}, \tag{3.5.13}$$

$$\left[\frac{\partial}{\partial t}\left(\phi N_w\right)\right]_{xyz} \simeq \frac{1}{\Delta t}\left[\left(\phi N_w\right)^{k+1} - \left(\phi N_w\right)^{k}\right]_{xyz}, \tag{3.5.14}$$

where the superscript *k* indicates the time step.

Furthermore, the spatial derivatives in the first term of the right hand side of Equations (3.5.10), (3.5.12a), (3.5.12b), and (3.5.12c) can be replaced by

$$\left(\frac{\partial P_j}{\partial x}\right)_{x+\frac{1}{2}} = \left(\frac{1}{\Delta x}\right)_{x+\frac{1}{2}}\left(P_{j\,x+1}^{k+1} + P_{jx}^{k+1}\right), \tag{3.5.15}$$

$$\left(\frac{\partial D}{\partial x}\right)_{x+\frac{1}{2}} = \left(\frac{1}{\Delta x}\right)_{x+\frac{1}{2}} \left(D_{x+1} + D_x\right), \tag{3.5.16}$$

$$\left(\frac{\partial x_{ij}}{\partial x}\right)_{x+\frac{1}{2}} = \left(\frac{1}{\Delta x}\right)_{x+\frac{1}{2}} \left(x_{ij\,x+1}^{\;k+1} + x_{ij\,x}^{\;k+1}\right). \tag{3.5.17}$$

The derivatives for the other interfaces are approximated in a similar way.

Substituting Equations (3.5.15), and (3.5.16) in the first term on the right hand side of Equation (3.5.10) gives

$$\begin{aligned}&\left(\frac{k_{rj}}{\mu_j}\xi_j x_{ij} k_{xx}\right)_{x+\frac{1}{2}} \left(\frac{\partial P_j}{\partial x} - \gamma_j \frac{\partial D}{\partial x}\right)_{x+\frac{1}{2}} \left(\Delta y \Delta z\right)_{x+\frac{1}{2}} = \\ &\left(\frac{k_{rj}}{\mu_j}\xi_j x_{ij}\right)_{x+\frac{1}{2}}^{k+1} \left(\frac{\Delta y \Delta z}{\Delta x} k_{xx}\right)_{x+\frac{1}{2}} \left[\left(P_{j\,x+1}^{\;k+1} - P_{j\,x}^{\;k+1}\right) - \gamma_{j\,x+\frac{1}{2}}^{\;k+1} \left(D_{x+1} - D_x\right)\right],\end{aligned} \tag{3.5.18}$$

where $\left(\frac{k_{rj}}{\mu_j}\xi_j x_{ij}\right)_{x+\frac{1}{2}}^{k+1}$ is calculated upwind, the relative permeability model is given by Corey's model (Equation 3.5.20), and the transmissibility is calculated by Equation (3.5.19):

$$\left(\frac{\Delta y \Delta z}{\Delta x} k_{xx}\right)_{x+\frac{1}{2}} = 2\left(\frac{1}{\left(\frac{\Delta y \Delta z}{\Delta x} k_{xx}\right)_{x+1}} + \frac{1}{\left(\frac{\Delta y \Delta z}{\Delta x} k_{xx}\right)_{x}}\right)^{-1}, \tag{3.5.19}$$

$$k_{rj} = k_{rj}^0 S_j^{n_j} \;;\; \bar{S}_j = \frac{S_j - S_j^0}{1 - \sum_{i=1}^{np} S_i^0}, \tag{3.5.20}$$

where S_j^0 denotes the residual saturation of the j-th phase, n_j denotes the Corey's exponent for phase j, and k_{rj} denotes the relative permeability of phase j.

Because of the non-diagonal terms in the dispervisity tensor, additional difficulties need to be addressed in the discretization of the dispersion term. In this dissertation, the dispersion term was included in the numerical model fully implicitly. The discussion and details involved in this method will be addressed in Section 5.2.

Chapter 4. Implementation of Different Formulations for Compositional Simulation

In this chapter, we introduce the basis of the formulations compared in this dissertation. We chose these formulations for comparison because of their success for their application in industry.

4.1 WANG et al. FORMULATION (WANG et al., 1997)

In Wang et al. formulation (1997), the authors selected the primary variables: N_i, N_w, P, and $\ln(K_i)$. This set of primary variables linearizes the accumulation terms associated with the material balance equations (Equations 3.2.1, and 3.2.3). On the other hand, the volume constraint (Equation 3.2.6) becomes non-linear and cannot be eliminated as a secondary equation, as in Coats (1980).

As presented in Chapter 3, the mathematical model (Equations 3.2.1 through 3.2.6) is given by

$$V_b \frac{\partial}{\partial t}\left(\phi N_i\right) - V_b \vec{\nabla} \cdot \sum_{j=2}^{n_p} \left(\frac{\bar{\bar{k}}k_{rj}}{\mu_j} \xi_j x_{ij} \left(\nabla P_j - \gamma_j \nabla D \right) - \phi \xi_j S_j \bar{\bar{K}}_{ij} \nabla x_{ij} \right) - q_i = 0, \tag{3.2.1}$$

$$V_b \frac{\partial}{\partial t}\left(\phi N_w\right) - V_b \vec{\nabla} \cdot \frac{\bar{\bar{k}}k_{rw}}{\mu_w} \xi_w \left(\nabla P_w - \gamma_w \nabla D \right) - q_w = 0, \tag{3.2.3}$$

$$f_i^{\,2} - f_i^{\,j} = 0 \quad for\ j = 3...n_p, \tag{3.2.4}$$

$$\sum_{i=1}^{n_c} x_{ij} = 1 \quad for\ j = 2...n_p. \tag{3.2.5}$$

$$\sum_{j=1}^{n_p} \frac{N_j}{\xi_j} - 1 = 0 \text{ or } \sum_{j=1}^{n_p} S_j - 1 = 0. \tag{3.2.6}$$

The solution method consists of the following steps:

- discretization of the mathematical model;
- linearization of resulting equations by Newton-Raphson scheme and generation of the Jacobian matrix with respect to the primary variables;
- solution of the linearized equations for the primary variables;
- updating the secondary variables.

The method described is repeated until convergence is achieved, i.e. the residuals calculated are sufficiently small, or differences in the calculated primary variables are sufficiently small.

Michelsen (1982) method is used to check the stability of the hydrocarbon phases in the case of a single hydrocarbon phase grid block. In the case of a two hydrocarbon phase grid block, the stability test can be simplified: fluid remains as two-phase if Equations (4.1.1) and (4.1.2) are true; otherwise, single phase fluid resides.

$$K_i z_i > 1, \tag{4.1.1}$$

$$\frac{K_i}{z_i} > 1. \tag{4.1.2}$$

4.2 COATS FORMULATION (COATS, 1980)

In Coats (1980) formulation, also called natural variables formulation, the selected primary variables are pressure (p), oil and gas saturations (S_o and S_g) and $n_c - 2$ mole fractions of the gas phase ($y_i \quad for\ i = 3...n_c$).

Coats (1980) chose Equations (3.2.1) and (3.2.3) as primary equations because they are functions of the variables in the actual grid block and those of their neighbors. All other equations (Equations 3.2.4, 3.2.5, and 3.2.6) are used to eliminate the secondary variables from the primary equations. In this work, the same procedure as that proposed

by Cao (2002) will be used to decouple the primary equations from the secondary variables, which consists of a Gauss elimination technique, as described below.

Assuming that Equations (3.2.1) through (3.2.6) are functions of the saturations (S_o, S_g, and S_w), mole fractions ($x_i \quad i=1...n_c$ and $y_i \quad i=1...n_c$), and pressure (P) as well as eliminating one of the saturations using Equation (3.2.6), we can write the diagonal submatrices of the whole Jacobian matrix (primary and secondary variables included), and the corresponding right hand side for each grid block as follows:

$$\begin{bmatrix} \frac{\partial R_{m1}}{\partial S_o} & \frac{\partial R_{m1}}{\partial S_g} & \frac{\partial R_{m1}}{\partial y_3} & \cdots & \frac{\partial R_{m1}}{\partial y_{nc}} & \frac{\partial R_{m1}}{\partial p} \\ \frac{\partial R_{m2}}{\partial S_o} & \frac{\partial R_{m2}}{\partial S_g} & \frac{\partial R_{m2}}{\partial y_3} & \cdots & \frac{\partial R_{m2}}{\partial y_{nc}} & \frac{\partial R_{m2}}{\partial p} \\ \frac{\partial R_{m3}}{\partial S_o} & \frac{\partial R_{m3}}{\partial S_g} & \frac{\partial R_{m3}}{\partial y_3} & \cdots & \frac{\partial R_{m3}}{\partial y_{nc}} & \frac{\partial R_{m3}}{\partial p} \\ \vdots & \vdots & \vdots & \cdots & \vdots & \vdots \\ \frac{\partial R_{mn_c}}{\partial S_o} & \frac{\partial R_{mn_c}}{\partial S_g} & \frac{\partial R_{mn_c}}{\partial y_3} & \cdots & \frac{\partial R_{mn_c}}{\partial y_{nc}} & \frac{\partial R_{mn_c}}{\partial p} \\ \frac{\partial R_w}{\partial S_o} & \frac{\partial R_w}{\partial S_g} & \frac{\partial R_w}{\partial y_3} & \cdots & \frac{\partial R_w}{\partial y_{nc}} & \frac{\partial R_w}{\partial p} \end{bmatrix} \begin{bmatrix} \frac{\partial R_{m1}}{\partial y_1} & \frac{\partial R_{m1}}{\partial y_2} & \frac{\partial R_{m1}}{\partial x_1} & \cdots & \frac{\partial R_{m1}}{\partial x_{n_c}} \\ \frac{\partial R_{m2}}{\partial y_1} & \frac{\partial R_{m2}}{\partial y_2} & \frac{\partial R_{m2}}{\partial x_1} & \cdots & \frac{\partial R_{m2}}{\partial x_{n_c}} \\ \frac{\partial R_{m3}}{\partial y_1} & \frac{\partial R_{m3}}{\partial y_2} & \frac{\partial R_{m3}}{\partial x_1} & \cdots & \frac{\partial R_{m3}}{\partial x_{n_c}} \\ \vdots & \vdots & \vdots & \cdots & \vdots \\ \frac{\partial R_{mn_c}}{\partial y_1} & \frac{\partial R_{mn_c}}{\partial y_2} & \frac{\partial R_{mn_c}}{\partial x_1} & \cdots & \frac{\partial R_{mn_c}}{\partial x_{n_c}} \\ \frac{\partial R_w}{\partial y_1} & \frac{\partial R_w}{\partial y_2} & \frac{\partial R_w}{\partial x_1} & \cdots & \frac{\partial R_w}{\partial x_{n_c}} \end{bmatrix} \cdots\cdots\cdots \begin{bmatrix} R_{m1} \\ R_{m2} \\ R_{m3} \\ \vdots \\ R_{mn_c} \\ R_w \end{bmatrix}$$

$$\begin{bmatrix} \frac{\partial R_{f1}}{\partial S_o} & \frac{\partial R_{f1}}{\partial S_g} & \frac{\partial R_{f1}}{\partial y_3} & \cdots & \frac{\partial R_{f1}}{\partial y_{nc}} & \frac{\partial R_{f1}}{\partial p} \\ \frac{\partial R_{f2}}{\partial S_o} & \frac{\partial R_{f2}}{\partial S_g} & \frac{\partial R_{f2}}{\partial y_3} & \cdots & \frac{\partial R_{f2}}{\partial y_{nc}} & \frac{\partial R_{f2}}{\partial p} \\ \vdots & \vdots & \vdots & \cdots & \vdots & \vdots \\ \frac{\partial R_{fn_c}}{\partial S_o} & \frac{\partial R_{fn_c}}{\partial S_g} & \frac{\partial R_{fn_c}}{\partial y_3} & \cdots & \frac{\partial R_{fn_c}}{\partial y_{nc}} & \frac{\partial R_{fn_c}}{\partial p} \\ \frac{\partial R_x}{\partial S_o} & \frac{\partial R_x}{\partial S_g} & \frac{\partial R_x}{\partial y_3} & \cdots & \frac{\partial R_x}{\partial y_{nc}} & \frac{\partial R_x}{\partial p} \\ \frac{\partial R_y}{\partial S_o} & \frac{\partial R_y}{\partial S_g} & \frac{\partial R_y}{\partial y_3} & \cdots & \frac{\partial R_y}{\partial y_{nc}} & \frac{\partial R_y}{\partial p} \end{bmatrix} \begin{bmatrix} \frac{\partial R_{f1}}{\partial y_1} & \frac{\partial R_{f1}}{\partial y_2} & \frac{\partial R_{f1}}{\partial x_1} & \cdots & \frac{\partial R_{f1}}{\partial x_{n_c}} \\ \frac{\partial R_{f2}}{\partial y_1} & \frac{\partial R_{f2}}{\partial y_2} & \frac{\partial R_{f2}}{\partial x_1} & \cdots & \frac{\partial R_{f2}}{\partial x_{n_c}} \\ \vdots & \vdots & \vdots & \cdots & \vdots \\ \frac{\partial R_{fn_c}}{\partial y_1} & \frac{\partial R_{fn_c}}{\partial y_2} & \frac{\partial R_{fn_c}}{\partial x_1} & \cdots & \frac{\partial R_{fn_c}}{\partial x_{n_c}} \\ \frac{\partial R_x}{\partial y_1} & \frac{\partial R_x}{\partial y_2} & \frac{\partial R_x}{\partial x_1} & \cdots & \frac{\partial R_x}{\partial x_{n_c}} \\ \frac{\partial R_y}{\partial y_1} & \frac{\partial R_y}{\partial y_2} & \frac{\partial R_y}{\partial x_1} & \cdots & \frac{\partial R_y}{\partial x_{n_c}} \end{bmatrix} \begin{bmatrix} R_{f1} \\ R_{f2} \\ \vdots \\ R_{fn_c} \\ R_x \\ R_y \end{bmatrix} \quad (4.5.1)$$

Equation (4.5.1) shows that the main Jacobian matrix can be divided into 4 sub-matrices: the derivative of the primary equations with respect to the primary variables, the derivative of the primary equation with respect to the secondary variables, the

derivative of the secondary equations with respect to the primary variables, and the derivative of the secondary equations with respect to the secondary variables. These sub-matrices will be called A, B, C and D, respectively. The residuals of the primary equations and the residuals of the secondary equations will be called M and N, respectively. Writing Equation (4.5.1) with this notation, we obtain

$$\begin{bmatrix} A & B \\ C & D \end{bmatrix} \cdots\cdots\cdots \begin{bmatrix} M \\ N \end{bmatrix}. \tag{4.5.2}$$

Then, using Gauss elimination we can eliminate the secondary variables using the procedure illustrated by Equations (4.5.3) through (4.5.6).

$$\begin{bmatrix} A & B \\ D^{-1}C & D^{-1}D \end{bmatrix} \cdots\cdots\cdots \begin{bmatrix} M \\ D^{-1}N \end{bmatrix}, \tag{4.5.3}$$

$$\begin{bmatrix} A & B \\ BD^{-1}C & B \end{bmatrix} \cdots\cdots\cdots \begin{bmatrix} M \\ BD^{-1}N \end{bmatrix}, \tag{4.5.4}$$

$$\begin{bmatrix} A-BD^{-1}C & 0 \\ BD^{-1}C & B \end{bmatrix} \cdots\cdots\cdots \begin{bmatrix} M-BD^{-1}N \\ BD^{-1}N \end{bmatrix}, \tag{4.5.5}$$

$$\begin{bmatrix} A-BD^{-1}C & 0 \\ D^{-1}C & I \end{bmatrix} \cdots\cdots\cdots \begin{bmatrix} M-BD^{-1}N \\ D^{-1}N \end{bmatrix}. \tag{4.5.6}$$

Equation (4.5.6) completely decouples the primary equations from the secondary variables and after solving the primary equations, the secondary variables can be calculated by Equation (4.5.7):

$$\Delta X_s = ND^{-1} - CD^{-1}\Delta X_p. \tag{4.5.7}$$

A similar approach can be used to eliminate the secondary variables from the primary equations for the off-diagonal terms.

As discussed in Section 3.4.1, for single phase control volumes, Coats (1980) suggests comparing the saturation pressure and the actual control volume pressure to determine whether or not the actual phase splits into two phases.

Disappearence of a phase occurs when one of the hydrocarbon saturations of a two-phase grid block becomes negative. Thus, the negative saturation is set equal to zero and the grid block is set to single-phase.

4.3 COLLINS et al. FORMULATION (COLLINS et al., 1992)

The primary variables for this formulation are pressure (P), number of moles of each component per pore volume (N_i), and number of moles of water per pore volume (N_w); the primary equations are Equations (3.2.1), (3.2.3) and (3.2.6). From the primary equations, it can be seen that all the fugacity equations are decoupled from the main Jacobian matrix, which allows much flexibility in the formulation. Therefore, it is easier to use alternative implementations of the phase behavior model.

It is not obvious, but one of the most difficult aspects of this formulation is calculating the derivatives of N^o and N^g with respect to N_i and P. To address this issue, we used the same procedure presented by Wong and Aziz (1988) and Chang (1990b). In this procedure, $n_c + 1$ systems of n_c equations are solved as follows:

$$N_i = N_i^o + N_i^g , \tag{4.6.1}$$

$$f_i^o - f_i^g = 0 . \tag{4.6.2}$$

Deriving Equations (4.6.1) and (4.6.2) with respect to P and N_i gives

$$\frac{\partial N_i^o}{\partial p}+\frac{\partial N_i^g}{\partial p}=0 \quad \Rightarrow \quad \frac{\partial N_i^o}{\partial p}=-\frac{\partial N_i^g}{\partial p}, \tag{4.6.3}$$

$$\frac{\partial N_i^o}{\partial N_m}+\frac{\partial N_i^g}{\partial N_m}=0 \quad \Rightarrow \quad \frac{\partial N_i^o}{\partial N_m}=1-\frac{\partial N_i^g}{\partial N_m}, \tag{4.6.4}$$

and

$$\frac{\partial f_i^o}{\partial p}+\sum_{s=1}^{n_c}\frac{\partial f_i^o}{\partial N_s^o}\frac{\partial N_s^o}{\partial p}-\left(\frac{\partial f_i^g}{\partial p}+\sum_{s=1}^{n_c}\frac{\partial f_i^g}{\partial N_s^g}\frac{\partial N_s^g}{\partial p}\right)=0, \tag{4.6.5}$$

$$\sum_{s=1}^{n_c}\frac{\partial f_i^o}{\partial N_s^o}\frac{\partial N_s^o}{\partial N_m}-\sum_{s=1}^{n_c}\frac{\partial f_i^g}{\partial N_s^g}\frac{\partial N_s^g}{\partial N_m}=0, \tag{4.6.6}$$

where

$$f_i^o=f\left(p,x_1,x_2,...,x_{nc}\right) \quad \Rightarrow \quad \left.\frac{\partial f_i^o}{\partial N_s^o}\right|_p=\sum_{k=1}^{n_c}\frac{\partial f_i^o}{\partial x_k}\frac{\partial x_k}{\partial N_s^o}. \tag{4.6.7}$$

Substituting Equations (4.6.3) and (4.6.4) into Equations (4.6.5) and (4.6.6) gives

$$\sum_{s=1}^{n_c}\left(\frac{\partial f_i^o}{\partial N_s^o}-\frac{\partial f_i^g}{\partial N_s^g}\right)\frac{\partial N_s^o}{\partial p}=\frac{\partial f_i^g}{\partial p}-\frac{\partial f_i^o}{\partial p} \quad i=1...n_c, \tag{4.6.8}$$

$$\sum_{s=1}^{n_c}\left(\frac{\partial f_i^o}{\partial N_s^o}-\frac{\partial f_i^g}{\partial N_s^g}\right)\frac{\partial N_s^o}{\partial N_m}=\frac{\partial f_i^g}{\partial N_m^g} \quad i,m=1...n_c. \tag{4.6.9}$$

Equation (4.6.8) is a system of n_c equations and Equation (4.6.9) is a group of n_c systems of n_c equations. After solving for $\frac{\partial N_s^o}{\partial p}$ and all of $\frac{\partial N_s^o}{\partial N_m}$, the derivatives of N^o and N^g can be calculated by the respective summations of all components. Furthermore, the derivatives of the component mole fractions can be calculated by Equations (4.6.10) and (4.6.11).

$$\left.\frac{\partial x_i}{\partial p}\right|_{N_r} = \sum_{s=1}^{n_c} \frac{\partial x_i}{\partial N_s^o} \frac{\partial N_s^o}{\partial p}, \tag{4.6.10}$$

$$\left.\frac{\partial x_i}{\partial N_m}\right|_{p,N_r} = \sum_{s=1}^{n_c} \frac{\partial x_i}{\partial N_s^o} \frac{\partial N_s^o}{\partial N_m}, \tag{4.6.11}$$

where

$$x_i = \frac{N_i^o}{N} \quad \Rightarrow \quad \left.\frac{\partial x_i}{\partial N_s^o}\right|_{N_r^o} = \frac{\left(\delta_{is} - x_i\right)}{N^o}. \tag{4.6.12}$$

Using this procedure, it is possible to completely decouple the flash calculation equations from the main Jacobian matrix in a fully implicit formulation.

4.4 BRANCO AND RODRIGUEZ FORMULATION (BRANCO AND RODRIGUEZ, 1996)

Branco and Rodriguez (1996) proposed a new IMPSAT formulation. They proposed to reduce the Coats formulation (1980) by calculating just pressure and two saturations as primary variables, implying a reduced degree of implicitness since the mole fractions are calculated explicitly. According to this procedure, the flux terms are calculated implicitly with respect to pressure and saturations, and explicitly with respect to mole fractions; also, a decoupling procedure is needed to decouple the mole fraction terms in the component material balance equations.

In this work, we use a similar procedure as proposed by Cao (2002) to decouple the primary equations. Considering that we need three equations for the IMPSAT formulation, Cao (2002) proposed to use the water material balance equation, which is not dependent on the component mole fractions, as one of the three. The summation of all component material balance equations also can be considered independent of the component mole fractions, if we consider density as function of pressure only. Finally, as

the third equation, Cao (2002) suggested to apply the decoupling procedure in the remaining $n_c - 1$ equations. This procedure has the advantage of a reduced computational effort, because it does not require the manipulation of all the n_c component material balance equations when density is also considered a function of mole fractions.

4.5 SEQUENTIAL IMPEC FORMULATION

A similar idea as proposed by Branco and Rodriguez (1996) can be used to generate a pressure equation for a semi-implicit IMPEC model. This idea was also applied by Lacroix et al. (2000) for a black-oil simulator.

Starting from the n_c+1 equations generated by Coats formulation (1980), we use a similar Gauss elimination scheme as in Branco and Rodriguez (1996) to reduce the system for just one pressure equation for each grid block. Thus, after solving for pressure, all the mole fractions and saturations are updated and a new Newton iteration is performed. The process is repeated until the convergence criteria are reached, that is, convergence on the primary variable and sufficiently low material balance error.

Chapter 5. Enhancements of Formulations with New Features

In this chapter, we present the enhancements of the formulations with new features not presented in the original publications, such as three-phase flash, dispersion, and unstructured grid. These enhancements serve to improve the modeling by adding some physical phenomena often ignored (four-phase flow in porous media and dispersion in miscible processes) or to improve the representation of the reservoir geometry (cases with complex geometries, such as faults, fractures, and anisotropies). Section 5.1 will present the three-phase flash algorithm, Section 5.2 will show the molecular diffusion and dispersivity tensor, and Section 5.3 will describe the unstructured grid formulation.

5.1 THREE-PHASE FLASH CALCULATION

For cases of CO_2 injection at high pressure and low temperature, a new liquid phase can appear in reservoir conditions. In such cases, a new flash calculation has to be implemented in order to identify the number and which phases are present; the terms corresponding to this new phase need to be included in the material balance equations; and the new set of fugacity equations needs to be included in the system of non-linear equations.

As presented in Chapter 3, our mathematical model is given by

$$V_b \frac{\partial}{\partial t}\left(\phi N_i\right) - V_b \vec{\nabla} \cdot \sum_{j=2}^{n_p} \left(\frac{\bar{\bar{k}} k_{rj}}{\mu_j} \xi_j x_{ij} \left(\nabla P_j - \gamma_j \nabla D \right) - \phi \xi_j S_j \bar{\bar{K}}_{ij} \nabla x_{ij} \right) - q_i = 0 , \tag{3.2.1}$$

$$V_b \frac{\partial}{\partial t}\left(\phi N_w\right) - V_b \vec{\nabla} \cdot \frac{\bar{\bar{k}} k_{rw}}{\mu_w} \xi_w \left(\nabla P_w - \gamma_w \nabla D \right) - q_w = 0 , \tag{3.2.3}$$

$$f_i^{\,2} - f_i^{\,j} = 0 \quad for\ j = 3...n_p , \tag{3.2.4}$$

$$\sum_{i=1}^{n_c} x_{ij} = 1 \quad for\ j = 2...n_p \,. \tag{3.2.5}$$

$$\sum_{j=1}^{n_p} \frac{N_j}{\xi_j} - 1 = 0 \text{ or } \sum_{j=1}^{n_p} S_j - 1 = 0 \,. \tag{3.2.6}$$

For this new situation, where a second hydrocarbon liquid phase may appear, n_p is equal to four. Therefore, we will have $2n_c$ fugacity equations, three mole fraction constraints, one volume constraint, and $n_c + 1$ material balance equations, which totals $3n_c + 5$ equations and $3n_c + 5$ variables.

We discretize the mathematical model in the same way as presented in Section 3.5 and we solve the system of non-linear equations by the Newton-Raphson method. Equation (5.1.1) shows one of the diagonal terms of the Jacobian with respect to the natural variables. From this equation, we can notice a new set of n_c fugacity equations is included, in addition to a new mole fraction constraint for the second liquid, and the new variables associated with this new phase (mole fractions and saturation of the second liquid).

$$
\begin{bmatrix}
\frac{\partial R_{m1}}{\partial S_o} & \frac{\partial R_{m1}}{\partial S_g} & \frac{\partial R_{m1}}{\partial S_{L2}} & \frac{\partial R_{m1}}{\partial y_4} & \cdots & \frac{\partial R_{m1}}{\partial y_{nc}} & \frac{\partial R_{m1}}{\partial p} \\
\frac{\partial R_{m2}}{\partial S_o} & \frac{\partial R_{m2}}{\partial S_g} & \frac{\partial R_{m2}}{\partial S_{L2}} & \frac{\partial R_{m2}}{\partial y_4} & \cdots & \frac{\partial R_{m2}}{\partial y_{nc}} & \frac{\partial R_{m2}}{\partial p} \\
\frac{\partial R_{m3}}{\partial S_o} & \frac{\partial R_{m3}}{\partial S_g} & \frac{\partial R_{m3}}{\partial S_{L2}} & \frac{\partial R_{m3}}{\partial y_4} & \cdots & \frac{\partial R_{m3}}{\partial y_{nc}} & \frac{\partial R_{m3}}{\partial p} \\
\vdots & \vdots & \vdots & \vdots & \cdots & \vdots & \vdots \\
\frac{\partial R_{mn_c}}{\partial S_o} & \frac{\partial R_{mn_c}}{\partial S_g} & \frac{\partial R_{mn_c}}{\partial S_{L2}} & \frac{\partial R_{mn_c}}{\partial y_4} & \cdots & \frac{\partial R_{mn_c}}{\partial y_{nc}} & \frac{\partial R_{mn_c}}{\partial p} \\
\frac{\partial R_w}{\partial S_o} & \frac{\partial R_w}{\partial S_g} & \frac{\partial R_w}{\partial S_{L2}} & \frac{\partial R_w}{\partial y_4} & \cdots & \frac{\partial R_w}{\partial y_{nc}} & \frac{\partial R_w}{\partial p}
\end{bmatrix}
\begin{bmatrix}
\frac{\partial R_{m1}}{\partial y_1} & \frac{\partial R_{m1}}{\partial y_2} & \frac{\partial R_{m1}}{\partial y_3} & \frac{\partial R_{m1}}{\partial x_{11}} & \cdots & \frac{\partial R_{m1}}{\partial x_{1n_c}} & \frac{\partial R_{m1}}{\partial x_{21}} & \cdots & \frac{\partial R_{m1}}{\partial x_{2n_c}} \\
\frac{\partial R_{m2}}{\partial y_1} & \frac{\partial R_{m2}}{\partial y_2} & \frac{\partial R_{m2}}{\partial y_3} & \frac{\partial R_{m2}}{\partial x_{11}} & \cdots & \frac{\partial R_{m2}}{\partial x_{1n_c}} & \frac{\partial R_{m2}}{\partial x_{21}} & \cdots & \frac{\partial R_{m2}}{\partial x_{2n_c}} \\
\frac{\partial R_{m3}}{\partial y_1} & \frac{\partial R_{m3}}{\partial y_1} & \frac{\partial R_{m3}}{\partial y_3} & \frac{\partial R_{m3}}{\partial x_{11}} & \cdots & \frac{\partial R_{m3}}{\partial x_{1n_c}} & \frac{\partial R_{m3}}{\partial x_{21}} & \cdots & \frac{\partial R_{m3}}{\partial x_{2n_c}} \\
\vdots & \vdots & \vdots & \vdots & \cdots & \vdots & \vdots & \cdots & \vdots \\
\frac{\partial R_{mn_c}}{\partial y_1} & \frac{\partial R_{mn_c}}{\partial y_2} & \frac{\partial R_{mn_c}}{\partial y_3} & \frac{\partial R_{mn_c}}{\partial x_{11}} & \cdots & \frac{\partial R_{mn_c}}{\partial x_{1n_c}} & \frac{\partial R_{mn_c}}{\partial x_1} & \cdots & \frac{\partial R_{mn_c}}{\partial x_{2n_c}} \\
\frac{\partial R_w}{\partial y_1} & \frac{\partial R_w}{\partial y_2} & \frac{\partial R_w}{\partial y_2} & \frac{\partial R_w}{\partial x_{11}} & \cdots & \frac{\partial R_w}{\partial x_{1n_c}} & \frac{\partial R_w}{\partial x_{21}} & \cdots & \frac{\partial R_w}{\partial x_{2n_c}}
\end{bmatrix}
$$

$$
\begin{bmatrix}
\frac{\partial R_{f11}}{\partial S_o} & \frac{\partial R_{f11}}{\partial S_g} & \frac{\partial R_{f11}}{\partial S_{L2}} & \frac{\partial R_{f11}}{\partial y_4} & \cdots & \frac{\partial R_{f11}}{\partial y_{nc}} & \frac{\partial R_{f11}}{\partial p} \\
\vdots & \vdots & \vdots & \vdots & \cdots & \vdots & \vdots \\
\frac{\partial R_{f1nc}}{\partial S_o} & \frac{\partial R_{f1nc}}{\partial S_g} & \frac{\partial R_{f1nc}}{\partial S_{L2}} & \frac{\partial R_{f1nc}}{\partial y_4} & \cdots & \frac{\partial R_{f1nc}}{\partial y_{nc}} & \frac{\partial R_{f1nc}}{\partial p} \\
\frac{\partial R_{f21}}{\partial S_o} & \frac{\partial R_{f21}}{\partial S_g} & \frac{\partial R_{f21}}{\partial S_{L2}} & \frac{\partial R_{f21}}{\partial y_4} & \cdots & \frac{\partial R_{f21}}{\partial y_{nc}} & \frac{\partial R_{f21}}{\partial p} \\
\vdots & \vdots & \vdots & \vdots & \cdots & \vdots & \vdots \\
\frac{\partial R_{f2nc}}{\partial S_o} & \frac{\partial R_{f2nc}}{\partial S_g} & \frac{\partial R_{f2nc}}{\partial S_{L2}} & \frac{\partial R_{f2nc}}{\partial y_4} & \cdots & \frac{\partial R_{f2nc}}{\partial y_{nc}} & \frac{\partial R_{f2nc}}{\partial p} \\
\frac{\partial R_{x1}}{\partial S_o} & \frac{\partial R_{x1}}{\partial S_g} & \frac{\partial R_{x1}}{\partial S_{L2}} & \frac{\partial R_{x1}}{\partial y_4} & \cdots & \frac{\partial R_{x1}}{\partial y_{nc}} & \frac{\partial R_{x1}}{\partial p} \\
\frac{\partial R_{x2}}{\partial S_o} & \frac{\partial R_{x2}}{\partial S_g} & \frac{\partial R_{x2}}{\partial S_{L2}} & \frac{\partial R_{x2}}{\partial y_4} & \cdots & \frac{\partial R_{x2}}{\partial y_{nc}} & \frac{\partial R_{x2}}{\partial p} \\
\frac{\partial R_y}{\partial S_o} & \frac{\partial R_y}{\partial S_g} & \frac{\partial R_y}{\partial S_{L2}} & \frac{\partial R_y}{\partial y_4} & \cdots & \frac{\partial R_y}{\partial y_{nc}} & \frac{\partial R_y}{\partial p}
\end{bmatrix}
\begin{bmatrix}
\frac{\partial R_{f11}}{\partial y_1} & \frac{\partial R_{f11}}{\partial y_2} & \frac{\partial R_{f11}}{\partial y_3} & \frac{\partial R_{f11}}{\partial x_{11}} & \cdots & \frac{\partial R_{f11}}{\partial x_{1n_c}} & \frac{\partial R_{f11}}{\partial x_{21}} & \cdots & \frac{\partial R_{f11}}{\partial x_{2n_c}} \\
\vdots & \vdots & \vdots & \vdots & \cdots & \vdots & \vdots & \cdots & \vdots \\
\frac{\partial R_{f1n_c}}{\partial y_1} & \frac{\partial R_{f1n_c}}{\partial y_2} & \frac{\partial R_{f1n_c}}{\partial y_3} & \frac{\partial R_{f1nc}}{\partial x_{11}} & \cdots & \frac{\partial R_{f1nc}}{\partial x_{1n_c}} & \frac{\partial R_{f1nc}}{\partial x_{21}} & \cdots & \frac{\partial R_{f1nc}}{\partial x_{2n_c}} \\
\frac{\partial R_{f11}}{\partial y_1} & \frac{\partial R_{f11}}{\partial y_2} & \frac{\partial R_{f11}}{\partial y_3} & \frac{\partial R_{f11}}{\partial x_{11}} & \cdots & \frac{\partial R_{f11}}{\partial x_{1n_c}} & \frac{\partial R_{f11}}{\partial x_{21}} & \cdots & \frac{\partial R_{f11}}{\partial x_{2n_c}} \\
\vdots & \vdots & \vdots & \vdots & \cdots & \vdots & \vdots & \cdots & \vdots \\
\frac{\partial R_{f1n_c}}{\partial y_1} & \frac{\partial R_{f1n_c}}{\partial y_1} & \frac{\partial R_{f1n_c}}{\partial y_3} & \frac{\partial R_{f1nc}}{\partial x_{11}} & \cdots & \frac{\partial R_{f1nc}}{\partial x_{1n_c}} & \frac{\partial R_{f1nc}}{\partial x_{21}} & \cdots & \frac{\partial R_{f1nc}}{\partial x_{2n_c}} \\
\frac{\partial R_{x1}}{\partial y_1} & \frac{\partial R_{x1}}{\partial y_2} & \frac{\partial R_{x1}}{\partial y_3} & \frac{\partial R_{x1}}{\partial x_{11}} & \cdots & \frac{\partial R_{x1}}{\partial x_{1n_c}} & \frac{\partial R_{x1}}{\partial x_{21}} & \cdots & \frac{\partial R_{x1}}{\partial x_{2n_c}} \\
\frac{\partial R_{x2}}{\partial y_1} & \frac{\partial R_{x2}}{\partial y_2} & \frac{\partial R_{x2}}{\partial y_3} & \frac{\partial R_{x2}}{\partial x_{11}} & \cdots & \frac{\partial R_{x2}}{\partial x_{1n_c}} & \frac{\partial R_{x2}}{\partial x_{21}} & \cdots & \frac{\partial R_{x2}}{\partial x_{2n_c}} \\
\frac{\partial R_y}{\partial y_1} & \frac{\partial R_y}{\partial y_2} & \frac{\partial R_y}{\partial y_3} & \frac{\partial R_y}{\partial x_{11}} & \cdots & \frac{\partial R_y}{\partial x_{1n_c}} & \frac{\partial R_y}{\partial x_{21}} & \cdots & \frac{\partial R_y}{\partial x_{2n_c}}
\end{bmatrix}
=
\begin{bmatrix}
R_{m1} \\ R_{m2} \\ R_{m3} \\ \vdots \\ R_{mn_c} \\ R_w
\end{bmatrix}
\begin{bmatrix}
R_{f11} \\ \vdots \\ R_{f1nc} \\ R_{f12} \\ \vdots \\ R_{f2nc} \\ R_{x1} \\ R_{x2} \\ R_y
\end{bmatrix}. \qquad (5.1.1)
$$

Using the same procedure as used for Coats (1980), the secondary variables (mole fractions of oil, mole fractions of the second liquid, and mole fractions of the first three components of gas), and the secondary equations (fugacity and constraint equations) can be eliminated to reduce the system of $3n_c + 5$ equations to just $n_c + 1$ equations.

The implementation of the three-phase flash for Branco and Rodriguez (1996) formulation and Sequential IMPEC formulation is straightforward. After the $n_c + 1$ equations for Coats (1980) formulation are obtained, we use the same procedure as that used for the two-phase flash implementation to eliminate the other secondary equations.

It is important to mention that in considering a three phase flash, we need to perform a stability test for all the grid blocks in each Newton-Raphson iteration. The only exception is the case when the three hydrocarbon phases are present. In this case, the phase disappearance criterion discussed in Section 4.2 is used.

5.2 MOLECULAR DIFFUSION AND MECHANICAL DISPERSIVITY TENSOR

Although the integration of the second term on the right hand side of Equation (3.5.9) is made in a similar fashion as in Equation (3.5.10), the dispersion tensor cannot be approximated by a diagonal tensor. The expansion for the phase *j* is given in Equation (5.2.1) and the expressions for each direction are given in Equations (5.2.2a), (5.2.2b), and (5.2.2c).

$$\int_A \left(\phi\xi_j S_j \bar{\bar{K}}_{ij} \cdot \nabla x_{ij}\right) \cdot d\bar{A} = \int_{A_x} \left(\phi\xi_j S_j \bar{\bar{K}}_{ij} \cdot \nabla x_{ij}\right) \cdot d\bar{A}_x + \int_{A_y} \left(\phi\xi_j S_j \bar{\bar{K}}_{ij} \cdot \nabla x_{ij}\right) \cdot d\bar{A}_y + \int_{A_z} \left(\phi\xi_j S_j \bar{\bar{K}}_{ij} \cdot \nabla x_{ij}\right) \cdot d\bar{A}_z, \tag{5.2.1}$$

$$\int_{A_x}\left(\phi\xi_j S_j \bar{\bar{K}}_{ij}\cdot\nabla x_{ij}\right)\cdot d\bar{A}_x =$$

$$\left(\phi\xi_j S_j K_{ij\,xx}\right)_{x+\frac{1}{2}}\left(\frac{\partial x_{ij}}{\partial x}\right)_{x+\frac{1}{2}}\left(\Delta y\Delta z\right)_{x+\frac{1}{2}}-\left(\phi\xi_j S_j K_{ij\,xx}\right)_{x-\frac{1}{2}}\left(\frac{\partial x_{ij}}{\partial x}\right)_{x-\frac{1}{2}}\left(\Delta y\Delta z\right)_{x-\frac{1}{2}}+$$

$$\left(\phi\xi_j S_j K_{ij\,xy}\right)_{x+\frac{1}{2}}\left(\frac{\partial x_{ij}}{\partial y}\right)_{x+\frac{1}{2}}\left(\Delta y\Delta z\right)_{x+\frac{1}{2}}-\left(\phi\xi_j S_j K_{ij\,xy}\right)_{x-\frac{1}{2}}\left(\frac{\partial x_{ij}}{\partial y}\right)_{x-\frac{1}{2}}\left(\Delta y\Delta z\right)_{x-\frac{1}{2}}+ \qquad (5.2.2a)$$

$$\left(\phi\xi_j S_j K_{ij\,xz}\right)_{x+\frac{1}{2}}\left(\frac{\partial x_{ij}}{\partial z}\right)_{x+\frac{1}{2}}\left(\Delta y\Delta z\right)_{x+\frac{1}{2}}-\left(\phi\xi_j S_j K_{ij\,xz}\right)_{x-\frac{1}{2}}\left(\frac{\partial x_{ij}}{\partial z}\right)_{x-\frac{1}{2}}\left(\Delta y\Delta z\right)_{x-\frac{1}{2}},$$

$$\int_{A_y}\left(\phi\xi_j S_j \bar{\bar{K}}_{ij}\cdot\nabla x_{ij}\right)\cdot d\bar{A}_y =$$

$$\left(\phi\xi_j S_j K_{ij\,yy}\right)_{y+\frac{1}{2}}\left(\frac{\partial x_{ij}}{\partial y}\right)_{y+\frac{1}{2}}\left(\Delta x\Delta z\right)_{y+\frac{1}{2}}-\left(\phi\xi_j S_j K_{ij\,yy}\right)_{y-\frac{1}{2}}\left(\frac{\partial x_{ij}}{\partial y}\right)_{y-\frac{1}{2}}\left(\Delta x\Delta z\right)_{y-\frac{1}{2}}+$$

$$\left(\phi\xi_j S_j K_{ij\,yx}\right)_{y+\frac{1}{2}}\left(\frac{\partial x_{ij}}{\partial x}\right)_{y+\frac{1}{2}}\left(\Delta x\Delta z\right)_{y+\frac{1}{2}}-\left(\phi\xi_j S_j K_{ij\,yx}\right)_{y-\frac{1}{2}}\left(\frac{\partial x_{ij}}{\partial x}\right)_{y-\frac{1}{2}}\left(\Delta x\Delta z\right)_{y-\frac{1}{2}}+ \qquad (5.2.2b)$$

$$\left(\phi\xi_j S_j K_{ij\,yz}\right)_{y+\frac{1}{2}}\left(\frac{\partial x_{ij}}{\partial z}\right)_{y+\frac{1}{2}}\left(\Delta x\Delta z\right)_{y+\frac{1}{2}}-\left(\phi\xi_j S_j K_{ij\,yz}\right)_{y-\frac{1}{2}}\left(\frac{\partial x_{ij}}{\partial z}\right)_{y-\frac{1}{2}}\left(\Delta x\Delta z\right)_{y-\frac{1}{2}},$$

$$\int_{A_z}\left(\phi\xi_j S_j \bar{\bar{K}}_{ij}\cdot\nabla x_{ij}\right)\cdot d\bar{A}_z =$$

$$\left(\phi\xi_j S_j K_{ij\,zz}\right)_{z+\frac{1}{2}}\left(\frac{\partial x_{ij}}{\partial z}\right)_{z+\frac{1}{2}}\left(\Delta x\Delta y\right)_{z+\frac{1}{2}}-\left(\phi\xi_j S_j K_{ij\,zz}\right)_{z-\frac{1}{2}}\left(\frac{\partial x_{ij}}{\partial z}\right)_{z-\frac{1}{2}}\left(\Delta x\Delta y\right)_{z-\frac{1}{2}}+$$

$$\left(\phi\xi_j S_j K_{ij\,zx}\right)_{z+\frac{1}{2}}\left(\frac{\partial x_{ij}}{\partial x}\right)_{z+\frac{1}{2}}\left(\Delta x\Delta y\right)_{z+\frac{1}{2}}-\left(\phi\xi_j S_j K_{ij\,zx}\right)_{z-\frac{1}{2}}\left(\frac{\partial x_{ij}}{\partial x}\right)_{z-\frac{1}{2}}\left(\Delta x\Delta y\right)_{z-\frac{1}{2}}+ \qquad (5.2.2c)$$

$$\left(\phi\xi_j S_j K_{ij\,zy}\right)_{z+\frac{1}{2}}\left(\frac{\partial x_{ij}}{\partial y}\right)_{z+\frac{1}{2}}\left(\Delta x\Delta y\right)_{z+\frac{1}{2}}-\left(\phi\xi_j S_j K_{ij\,zy}\right)_{z-\frac{1}{2}}\left(\frac{\partial x_{ij}}{\partial y}\right)_{z-\frac{1}{2}}\left(\Delta x\Delta y\right)_{z-\frac{1}{2}}.$$

From Equations (5.2.2a) through (5.2.2c), we can see that some of the mole fraction derivatives are taken at the interfaces perpendicular to the derivative direction and others on the interfaces parallel to the derivative direction. In the case of the

derivative taken in the perpendicular interface of the derivative direction, the approximation is made in the same way as we did for the pressure derivatives in Section 3.5, i.e.

$$\left(\frac{\partial x_{ij}}{\partial x}\right)_{x+\frac{1}{2}} \simeq 2\frac{x_{ij_{x+1}} - x_{ij_x}}{\Delta x_{x+1} - \Delta x_x}, \tag{5.2.3a}$$

$$\left(\frac{\partial x_{ij}}{\partial y}\right)_{y+\frac{1}{2}} \simeq 2\frac{x_{ij_{y+1}} - x_{ij_y}}{\Delta y_{y+1} - \Delta y_y}, \tag{5.2.3b}$$

$$\left(\frac{\partial x_{ij}}{\partial z}\right)_{z+\frac{1}{2}} \simeq 2\frac{x_{ij_{z+1}} - x_{ij_z}}{\Delta z_{z+1} - \Delta z_z}. \tag{5.2.3c}$$

In the case of the derivative taken in the parallel interface of the derivative direction, the upwind scheme has to be used to decide which control volumes are to be used for the approximation of the derivative, i.e.

$$\left(\frac{\partial x_{ij}}{\partial x}\right)_{y+\frac{1}{2}} \simeq \frac{x_{ij_{y(x+1)}} - x_{ij_{y(x-1)}}}{\Delta x_x + 0.5\left(\Delta x_{x+1} + \Delta x_{x-1}\right)} \quad if\ \Phi_{xy} \geq \Phi_{x(y+1)}, \tag{5.2.4a}$$

$$\left(\frac{\partial x_{ij}}{\partial x}\right)_{y+\frac{1}{2}} \simeq \frac{x_{ij_{(y+1)(x+1)}} - x_{ij_{(y+1)(x-1)}}}{\Delta x_x + 0.5\left(\Delta x_{x+1} + \Delta x_{x-1}\right)} \quad if\ \Phi_{xy} < \Phi_{x(y+1)}, \tag{5.2.4b}$$

Evaluating the dispersion coefficient in Equations (5.2.2a) through (5.2.2c) also requires a special treatment. This is a result of the definition of the velocities in the direction perpendicular to each of the interfaces. Therefore, if we need a velocity in a direction parallel to the interface, the upwind scheme is used, i.e.

$$\left(u_{yj}\right)_{\left(x\pm\frac{1}{2}\right)yz} \simeq \frac{1}{2}\left[\left(u_{yj}\right)_{x\left(y+\frac{1}{2}\right)z} + \left(u_{yj}\right)_{x\left(y-\frac{1}{2}\right)z}\right] \quad if\ \Phi_{xyz} \geq \Phi_{(x\pm1)yz}, \tag{5.2.5a}$$

$$\left(u_{yj}\right)_{\left(x\pm\frac{1}{2}\right)yz} \simeq \frac{1}{2}\left[\left(u_{yj}\right)_{(x\pm1)\left(y+\frac{1}{2}\right)z} + \left(u_{yj}\right)_{(x\pm1)\left(y-\frac{1}{2}\right)z}\right] \quad if\ \Phi_{xyz} < \Phi_{(x\pm1)yz}\,. \tag{5.2.5b}$$

5.3 UNSTRUCTURED GRID

For most real situations, complexities such as faults, fractures, and anisotropies complicate the task of generating a grid. In such situations, unstructured grids present many advantages because of the flexibility of using many different elements to conform to complicated geometries.

As presented in Chapter 2, many researchers have been working using different formulations to adapt for reservoir simulation. Among those formulations are the Element based Finite Volume Method (EbFVM) presented by Cordazzo et al. (2005; 2004a; 2004b) for a two-phase black-oil simulator, procedures by Marcondes and Sepehnoori (2007; 2010) for a two-dimensional compositional simulation, and Marcondes et al. (2013) for a three-dimensional compositional simulation. In this section, the EbFVM methodology is presented.

In the EbFVM, each element is divided into sub-elements. These sub-elements will be called sub-control volumes. The conservation equation, Equation (3.2.1), needs to be integrated for each one of these sub-control volumes. **Figure 5.3.1** presents the four elements employed and the sub-control volumes associated with each element. it shows that except for the pyramid, each element has three quadrilateral integration surfaces associated with each sub-control volume. For the pyramid element, the sub-control volumes associated with the base have two triangular integration surfaces and one quadrangular integration surface. The sub-control volume associated with the apex has four quadrilateral integration surfaces. It is worthwhile to mention that in general, due to the shape functions, the hexahedron element should be used throughout most parts of the reservoir. For areas needing a local grid refinement, tetrahedron element is more suitable.

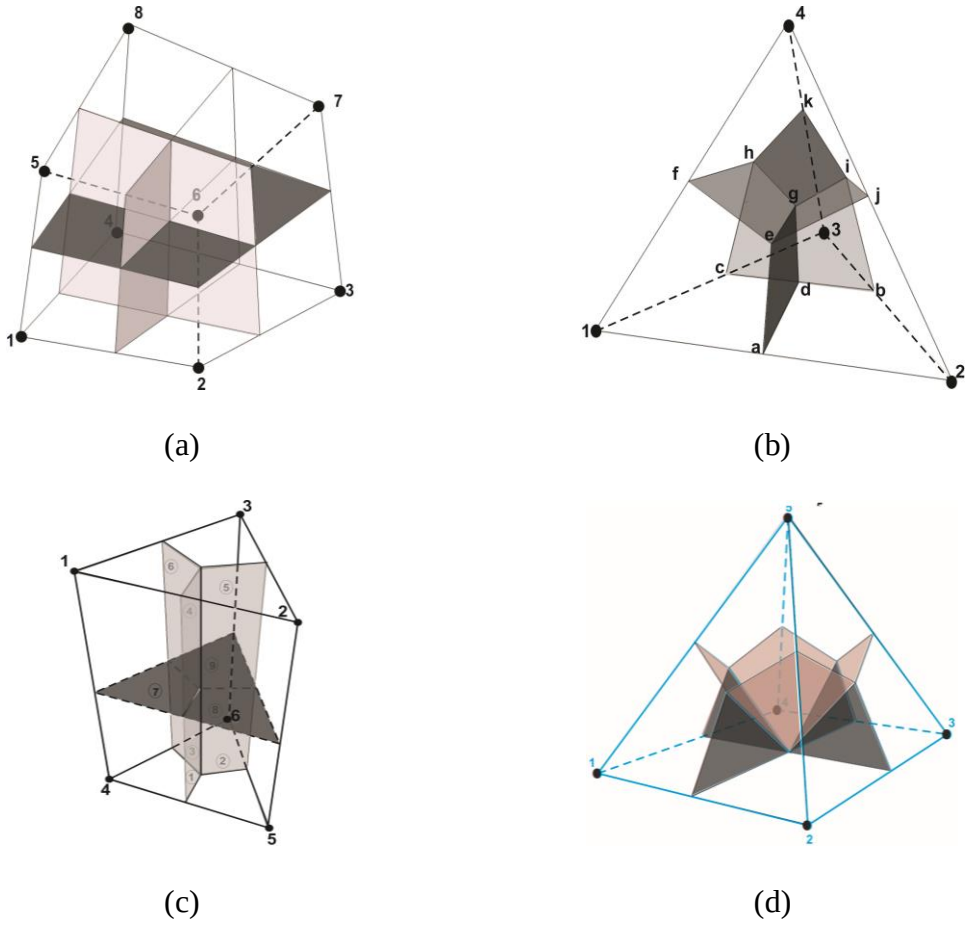

Figure 5.3.1. 3D elements and their respective sub-control volumes. a) Hexahedron b) Tetrahedron c) Prism d) Pyramid

For areas between hexahedron and tetrahedron elements, transition elements like pyramids or prisms are necessary in order to match the triangular surfaces of tetrahedron and quadrilateral surfaces of the hexahedrons. By integrating Equation (3.2.1) in time and for each one of the sub-control volumes and applying the Gauss theorem for the convective and dispersive terms we obtain

$$\int_V \frac{\partial}{\partial t}\left(\phi N_i\right) dV - \int_A \sum_{j=2}^{n_p} \left(\frac{k_{rj}}{\mu_j} \xi_j x_{ij} \bar{\bar{k}} \cdot \left(\nabla P_j - \gamma_j \nabla D \right) - \phi \xi_j S_j \bar{\bar{K}}_{ij} \cdot \nabla x_{ij} \right) \cdot d\bar{A} - \int_V \frac{q_i}{V_b} dV = 0 , \quad (5.6.1)$$

$$\int_V \frac{\partial}{\partial t}\left(\phi N_w\right)dV - \int_A \frac{k_{rw}}{\mu_w}\xi_w \bar{\bar{k}}\cdot\left(\nabla P_w - \gamma_w \nabla D\right)\cdot d\bar{A} - \int_V \frac{q_w}{V_b}dV = 0\,. \tag{5.6.2}$$

Integration of first two terms of Equations (5.6.1) and (5.6.2) is done by using the shape functions, which in 2D are given by

$$N_1(s,t) = 1 - s - t\,, \tag{5.6.3a}$$

$$N_2(s,t) = s\,, \text{ and} \tag{5.6.3b}$$

$$N_3(s,t) = t\,. \tag{5.6.3c}$$

for the triangular element and

$$N_1(s,t) = \frac{1}{4}\left(1-s\right)\left(1-t\right), \tag{5.6.4a}$$

$$N_2(s,t) = \frac{1}{4}\left(1+s\right)\left(1-t\right), \tag{5.6.4b}$$

$$N_3(s,t) = \frac{1}{4}\left(1+s\right)\left(1+t\right), \text{ and} \tag{5.6.4c}$$

$$N_4(s,t) = \frac{1}{4}\left(1-s\right)\left(1+t\right) \tag{5.6.4d}$$

for the quadrangular element.

In 3D, the shape functions are given by

$$N_1(s,t,p) = \frac{(1+s)(1-t)(1+p)}{8}\,, \tag{5.6.5a}$$

$$N_2(s,t,p) = \frac{(1+s)(1-t)(1-p)}{8}, \tag{5.6.5b}$$

$$N_3(s,t,p) = \frac{(1-s)(1-t)(1-p)}{8}, \tag{5.6.5c}$$

$$N_4(s,t,p)=\frac{(1-s)(1-t)(1+p)}{8}, \tag{5.6.5d}$$

$$N_5(s,t,p)=\frac{(1+s)(1+t)(1+p)}{8}, \tag{5.6.5e}$$

$$N_6(s,t,p)=\frac{(1+s)(1+t)(1-p)}{8}, \tag{5.6.5f}$$

$$N_7(s,t,p)=\frac{(1-s)(1+t)(1-p)}{8}, \text{ and} \tag{5.6.5g}$$

$$N_8(s,t,p)=\frac{(1-s)(1+t)(1+p)}{8} \tag{5.6.5h}$$

for the hexahedron element;

$$N_1(s,t,p)=1-s-t-p, \tag{5.6.6a}$$

$$N_2(s,t,p)=s, \tag{5.6.6b}$$

$$N_3(s,t,p)=t, \text{ and} \tag{5.6.6c}$$

$$N_4(s,t,p)=p \tag{5.6.6d}$$

for the tetrahedron element;

$$N_1(s,t,p)=(1-s-t)(1-p), \tag{5.6.7a}$$

$$N_2(s,t,p)=s(1-p), \tag{5.6.7b}$$

$$N_3(s,t,p)=t(1-p), \tag{5.6.7c}$$

$$N_4(s,t,p)=p(1-s-t), \tag{5.6.7d}$$

$$N_5(s,t,p)=s.p, \text{ and} \tag{5.6.7e}$$

$$N_6(s,t,p)=t.p \tag{5.6.7f}$$

for the prism element; and

$$N_1(s,t,p)=\frac{1}{4}\left[(1-s)(1-t)-p+\frac{s\cdot t\cdot p}{(1-p)}\right], \tag{5.6.8a}$$

$$N_2(s,t,p)=\frac{1}{4}\left[(1+s)(1-t)-p-\frac{s\cdot t\cdot p}{(1-p)}\right], \tag{5.6.8b}$$

$$N_3(s,t,p)=\frac{1}{4}\left[(1+s)(1+t)-p-\frac{s\cdot t\cdot p}{(1-p)}\right], \tag{5.6.8c}$$

$$N_4(s,t,p)=(1-s)(1+t)-p-\frac{s\cdot t\cdot p}{(1-p)}\text{, and} \tag{5.6.8d}$$

$$N_5(s,t,p)=p \tag{5.6.8e}$$

for the pyramid element.

Using the shape functions, it is possible to calculate any property inside the control volume by

$$\Phi(s,t)=\sum_i N_i\Phi_i\,, \tag{5.6.9}$$

as well as the global coordinates can be calculated by

$$x(s,t)=\sum_i N_i x_i\,, \tag{5.6.10a}$$

$$y(s,t)=\sum_i N_i y_i\,. \tag{5.6.10b}$$

A important advantage of shape functions is that they constitute the easiest way by which derivatives with respect to the global coordinates can be calculated and therefore the associated gradients. These derivatives are presented below:

$$\frac{\partial \Phi}{\partial x} = \sum_i \frac{\partial N_i}{\partial x} \Phi_i \,, \tag{5.6.11a}$$

$$\frac{\partial \Phi}{\partial y} = \sum_i \frac{\partial N_i}{\partial y} \Phi_i \,. \tag{5.6.11b}$$

As we can see in Equations (5.6.11a) and (5.6.11b), it is necessary to calculate the derivatives of the shape functions with respect to the global variables, which can be done by

$$\frac{\partial N_i}{\partial s} = \frac{\partial N_i}{\partial x}\frac{\partial x}{\partial s} + \frac{\partial N_i}{\partial y}\frac{\partial y}{\partial s}, \tag{5.6.12a}$$

$$\frac{\partial N_i}{\partial t} = \frac{\partial N_i}{\partial x}\frac{\partial x}{\partial t} + \frac{\partial N_i}{\partial y}\frac{\partial y}{\partial t}. \tag{5.6.12b}$$

In matrix form, the Equations (5.6.12a) and (5.6.12b) can be written as

$$\begin{bmatrix} \frac{\partial N_1}{\partial t} & \cdots & \frac{\partial N_{n_v}}{\partial t} \\ \frac{\partial N_1}{\partial s} & \cdots & \frac{\partial N_{n_v}}{\partial s} \end{bmatrix} = \begin{bmatrix} \frac{\partial x}{\partial t} & \frac{\partial y}{\partial t} \\ \frac{\partial x}{\partial s} & \frac{\partial y}{\partial s} \end{bmatrix} \begin{bmatrix} \frac{\partial N_1}{\partial x} & \cdots & \frac{\partial N_{n_v}}{\partial x} \\ \frac{\partial N_1}{\partial y} & \cdots & \frac{\partial N_{n_v}}{\partial y} \end{bmatrix}, \tag{5.6.13a}$$

or

$$\begin{bmatrix} \frac{\partial N_1}{\partial x} & \cdots & \frac{\partial N_{n_v}}{\partial x} \\ \frac{\partial N_1}{\partial y} & \cdots & \frac{\partial N_{n_v}}{\partial y} \end{bmatrix} = \begin{bmatrix} \frac{\partial x}{\partial t} & \frac{\partial y}{\partial t} \\ \frac{\partial x}{\partial s} & \frac{\partial y}{\partial s} \end{bmatrix}^{-1} \begin{bmatrix} \frac{\partial N_1}{\partial t} & \cdots & \frac{\partial N_{n_v}}{\partial t} \\ \frac{\partial N_1}{\partial s} & \cdots & \frac{\partial N_{n_v}}{\partial s} \end{bmatrix} \tag{5.6.13b}$$

in 2D and

$$\begin{bmatrix} \frac{\partial N_1}{\partial t} & \cdots & \frac{\partial N_{n_v}}{\partial t} \\ \frac{\partial N_1}{\partial s} & \cdots & \frac{\partial N_{n_v}}{\partial s} \\ \frac{\partial N_1}{\partial p} & \cdots & \frac{\partial N_{n_v}}{\partial p} \end{bmatrix} = \begin{bmatrix} \frac{\partial x}{\partial t} & \frac{\partial y}{\partial t} & \frac{\partial z}{\partial t} \\ \frac{\partial x}{\partial s} & \frac{\partial y}{\partial s} & \frac{\partial z}{\partial s} \\ \frac{\partial x}{\partial p} & \frac{\partial y}{\partial p} & \frac{\partial z}{\partial p} \end{bmatrix} \begin{bmatrix} \frac{\partial N_1}{\partial x} & \cdots & \frac{\partial N_{n_v}}{\partial x} \\ \frac{\partial N_1}{\partial y} & \cdots & \frac{\partial N_{n_v}}{\partial y} \\ \frac{\partial N_1}{\partial z} & \cdots & \frac{\partial N_{n_v}}{\partial z} \end{bmatrix}, \tag{5.6.14a}$$

or

$$\begin{bmatrix} \frac{\partial N_1}{\partial x} & \cdots & \frac{\partial N_{n_v}}{\partial x} \\ \frac{\partial N_1}{\partial y} & \cdots & \frac{\partial N_{n_v}}{\partial y} \\ \frac{\partial N_1}{\partial z} & \cdots & \frac{\partial N_{n_v}}{\partial z} \end{bmatrix} = \begin{bmatrix} \frac{\partial x}{\partial t} & \frac{\partial y}{\partial t} & \frac{\partial z}{\partial t} \\ \frac{\partial x}{\partial s} & \frac{\partial y}{\partial s} & \frac{\partial z}{\partial s} \\ \frac{\partial x}{\partial p} & \frac{\partial y}{\partial p} & \frac{\partial z}{\partial p} \end{bmatrix}^{-1} \begin{bmatrix} \frac{\partial N_1}{\partial t} & \cdots & \frac{\partial N_{n_v}}{\partial t} \\ \frac{\partial N_1}{\partial s} & \cdots & \frac{\partial N_{n_v}}{\partial s} \\ \frac{\partial N_1}{\partial p} & \cdots & \frac{\partial N_{n_v}}{\partial p} \end{bmatrix} \tag{5.6.14b}$$

in 3D, where n_v is the number of vertices.

To perform the integration of Equations (5.6.1) and (5.6.2), it is necessary to define the volumes of each sub-control volume and the area of each interface.

In 2D, the volumes of each sub-control volume for the triangles and quadrilaterals are given by

$$Vscv_i = \frac{\det(J_t)\Delta s \Delta t}{h} \tag{5.6.15}$$

$$Vscv_i = \det(J_t) h \Delta s \Delta t \tag{5.6.16}$$

In 3D, the volumes of each sub-control volume for hexahedron, tetrahedron, prism, and pyramid elements are given by

$$Vscv_i = \det(J_t), \tag{5.6.17}$$

$$Vscv_i = \det(J_t)/6, \tag{5.6.18}$$

$$Vscv_i = \det(J_t)/12, \text{ and} \tag{5.6.19}$$

$$Vscv_i = \begin{cases} 2\det(J_t)/9 & for \quad i = 1,4 \ (base) \\ 4\det(J_t)/9 & for \quad i = 5 \ (apex) \end{cases} \tag{5.6.20}$$

where

$$\det(J_t) = \left(\frac{\partial x}{\partial s}\frac{\partial y}{\partial t} - \frac{\partial x}{\partial t}\frac{\partial y}{\partial s} \right) \text{ in 2D} \tag{5.6.21}$$

and

$$\det(J_t) = \frac{\partial x}{\partial s}\left(\frac{\partial y}{\partial t}\frac{\partial z}{\partial p} - \frac{\partial y}{\partial p}\frac{\partial z}{\partial t} \right) - \frac{\partial y}{\partial s}\left(\frac{\partial x}{\partial t}\frac{\partial z}{\partial p} - \frac{\partial x}{\partial p}\frac{\partial z}{\partial t} \right) + \frac{\partial z}{\partial s}\left(\frac{\partial x}{\partial t}\frac{\partial y}{\partial p} - \frac{\partial x}{\partial p}\frac{\partial y}{\partial t} \right) \text{ in 3D} \tag{5.6.22}$$

It is important to mention that $\det(J_t)$ needs to be evaluated at the center of each sub-control volume.

The area of each interface in 2D is evaluated by

$$d\vec{A} = hdy\vec{i} - hdx\vec{j} \tag{5.6.23}$$

The area of each interface for the hexahedron element is evaluated by

$$\begin{aligned} d\vec{A} = &\left(\frac{\partial y}{\partial m}\frac{\partial z}{\partial n} - \frac{\partial y}{\partial n}\frac{\partial z}{\partial m} \right) dm\,dn\,\vec{i} - \left(\frac{\partial x}{\partial n}\frac{\partial z}{\partial m} - \frac{\partial x}{\partial m}\frac{\partial z}{\partial n} \right) dm\,dn\,\vec{j} + \\ &\left(\frac{\partial x}{\partial m}\frac{\partial y}{\partial n} - \frac{\partial x}{\partial n}\frac{\partial y}{\partial m} \right) dm\,dn\,\vec{k}, \end{aligned} \tag{5.6.24}$$

where m and n denote the local system s, t, or p. For the other elements, the interfaces can be evaluated using a similar procedure. We just need to define the local vectors for each interface.

Substituting Equations (5.6.15) through (5.6.20) for the accumulation term; and Equations (5.6.23), or (5.6.24) for the convective and dispersive fluxes into Equations (5.6.1) and (5.6.2). And evaluating the fluid properties through a fully implicit procedure, we obtain the following equations for the two mentioned terms:

$$Acc_{m,i} = Vscv_{m,i}\left(\left(\frac{\phi N_m}{\Delta t}\right)_i - \left(\frac{\phi N_m}{\Delta t}\right)_i^o\right) \quad ; \quad m=1,N_v \; ; \; i=1,..,n_c,n_w \tag{5.6.25}$$

and

$$\begin{aligned}
F_{m,i} &= \int_A \sum_{j=1}^{n_p} (\xi_j \, x_{ij} \, \lambda_j \overline{\overline{K}} \bullet \nabla \Phi_j + \phi \xi_j S_j \vec{\vec{K}}_{ij} \bullet \nabla x_{ij}) \bullet \overrightarrow{dA} \\
&= \int_{A_1} \sum_{j=1}^{N_p} \left(\varepsilon_j x_{ij} \lambda_j\right)_{ip_1} \left(K_{11} \frac{\partial \Phi_j}{\partial x} + K_{12} \frac{\partial \Phi_j}{\partial y} + K_{13} \frac{\partial \Phi_j}{\partial z} \right) dA_1 + \\
&\int_{A_2} \sum_{j=1}^{N_p} \left(\varepsilon_j x_{ij} \lambda_j\right)_{ip_2} \left(K_{12} \frac{\partial \Phi_j}{\partial x} + K_{22} \frac{\partial \Phi_j}{\partial y} + K_{23} \frac{\partial \Phi_j}{\partial z} \right) dA_2 + \\
&\int_{A_3} \sum_{j=1}^{N_p} \left(\varepsilon_j x_{ij} \lambda_j\right)_{ip_3} \left(K_{13} \frac{\partial \Phi_j}{\partial x} + K_{23} \frac{\partial \Phi_j}{\partial y} + K_{33} \frac{\partial \Phi_j}{\partial z} \right) dA_3 \\
&+ \int_{A_1} \sum_{j=1}^{N_p} \left(\phi \xi_j S_j\right)_{ip_1} \left(k_{ij,11} \frac{\partial x_{ij}}{\partial x} + k_{ij,12} \frac{\partial x_{ij}}{\partial y} + k_{ij,13} \frac{\partial x_{ij}}{\partial z} \right) dA_1 + \\
&\int_{A_2} \sum_{j=1}^{N_p} \left(\phi \xi_j S_j\right)_{ip_2} \left(k_{ij,12} \frac{\partial x_{ij}}{\partial x} + k_{ij,22} \frac{\partial x_{ij}}{\partial y} + k_{ij,23} \frac{\partial x_{ij}}{\partial z} \right) dA_2 + \\
&\int_{A_3} \sum_{j=1}^{N_p} \left(\varepsilon_j x_{ij} \lambda_j\right)_{ip_3} \left(k_{ij,13} \frac{\partial x_{ij}}{\partial x} + k_{ij,23} \frac{\partial x_{ij}}{\partial y} + k_{ij,33} \frac{\partial x_{ij}}{\partial z} \right) dA_3 \; ; \\
&m=1,n_v \; ; \; i=1,..,n_c+1.
\end{aligned} \tag{5.6.26}$$

By inspecting Equation (5.6.26), it can be inferred that it is necessary to evaluate molar densities, molar fraction and mobilities in three interfaces of each sub-control volume. To evaluate these properties, an upwind scheme based on Cordazzo *et al.* (2004)

will be used. The mobilities and other fluid properties are evaluated at the integration point 1 of **Figure 5.3.1**, for instance, by

$$\begin{aligned} &\lambda_{j1} = \lambda_{j2} \quad if \quad \overline{\overline{K}}.\nabla\Phi_j.\overrightarrow{dA}\Big|_{ip1} \leq 0, \\ &\lambda_{j1} = \lambda_{j1} \quad if \quad \overline{\overline{K}}.\nabla\Phi_j.\overrightarrow{dA}\Big|_{ip1} > 0. \end{aligned} \tag{5.6.27}$$

Inserting Equations (5.6.25) and (5.6.27) into Equation (5.6.1), the following equation for each element is obtained:

$$Acc_{m,i} + F_{m,i} + q_i = 0 \;\; ; \quad m = 1, N_v \; ; \; i = 1, n_c + 1 . \tag{5.6.28}$$

Equation (5.6.28) denotes the conservation for each sub-control volume of each element. Now, it is necessary to assemble the equation of each control volume obtaining the contribution of each sub-control volume that shares the same vertex. This process is similar to assembling of the stiffness global matrix in the finite element method. Further details can be found in Cordazzo (2004a; 2004b), Marcondes and Sepehrnoori (2010), Marcondes et al. (2013), and Santos et al. (2013). Finalizing this section, it is important to mention that each element may have different permeabilities and porosities, thus allowing the simulation of highly anisotropic reservoirs.

Chapter 6. Comparison of the Formulations Implemented for Different Scenarios

In this chapter, we will present six different test cases used for comparing the different implemented formulations: a water flooding problem, an immiscible gas injection problem, a miscible gas injection problem, a condensate gas problem, a dry gas problem, and an immiscible gas injection in heterogeneous reservoir problem. For all cases, we used pressure, saturations, and mole fractions as the convergence criteria. Following the presentation of case studies, we will present a discussion about the results.

6.1 WATER FLOODING

The first case study is a water flooding problem with two components. The reservoir model is heterogeneous (Dykstra-Parsons coefficient equals 0.72) and anisotropic. It has *50* x *50* x *5* grid blocks, one injector and one producer well in a quarter of five-spot configuration. **Table 6.1.1** presents the physical properties and initial conditions for this case. For the relative permeability model, we used the parameters given in **Table 6.1.2** for the Corey's model (Equation 6.1.1). **Figure 6.1.1** presents the horizontal absolute permeability for this case. The vertical absolute permeability was taken to be ten percent of the horizontal permeability.

$$K_{rj} = K_{rj}^{0} S_j^{n_j} \;;\; \bar{S}_j = \frac{S_j - S_j^{0}}{1 - \sum_{i=1}^{np} S_i^{0}}, \tag{6.1.1}$$

where S_j^0 denotes the residual saturation of the j-th phase, and the others parameters are defined in **Table 6.1.2**.

Table 6.1.1. Physical properties for Case 1

Grid blocks dimension in x, y, and z directions	50 x 50 x 5	
Length (m)	609.6	
Width (m)	609.6	
Thickness (m)	61.0	
Porosity (fraction)	0.3	
Rock compressibility (kPa^{-1})	$5.80x10^{-7}$	
Reservoir temperature (^oC)	18.33	
Permeability in x direction (m^2)	Figure 6.1.1	
Permeability in y direction (m^2)	Figure 6.1.1	
Permeability in z direction (m^2)	0.1 K_x	
Water viscosity (Pa.s)	$8x10^{-4}$	
Water density (mol/m^3)	$55.55x10^3$	
Water compressibility (kPa^{-1})	$4.35x10^{-7}$	
Initial water saturation (fraction)	0.25	
Initial reservoir pressure (MPa)	20.68	
Water injection rate (m^3/s)	$9.2x10^{-3}$	
Producer bottom hole pressure (MPa)	20.68	
Reservoir fluid initial composition	C1	0.1
	NC16	0.9

Table 6.1.2. Corey's model rel. perm. data for Case 1, Case 3, and Case 5

	Water	Oil	Gas
End point relative permeability	0.3	0.75	0.9
Residual saturation	0.25	0.2	0.0
Exponent of relative permeability	2.0	2.0	2.0

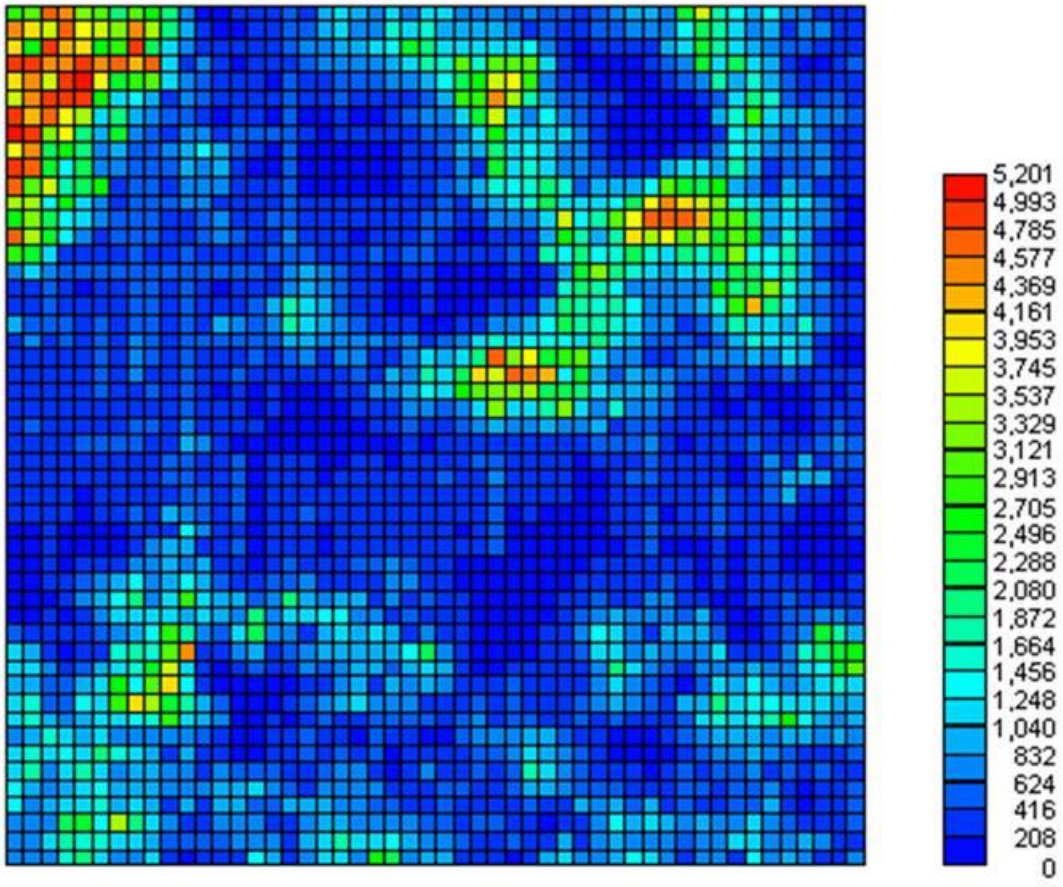

Figure 6.1.1. Horizontal absolute permeability for Case 3 (units in *md* : 1 *md*=10^{-15} m^2).

Figures 6.1.2 and **6.1.3** present the volumetric oil and water rate versus time for all formulations in Case 1. As can be seen in **Figures 6.1.2** and **6.1.3**, all formulations produced similar results. For this case, Wang et al. (1997) and Collins et al. (1992) formulations are the same since there are no fugacity equations to be solved. Originally, the problem has just two components (C_1 and C_{16}), but we split the second component (C_{16}) into two equal components ($C_{16(1)}$ and $C_{16(2)}$) for all the formulations to have a total of three components. This was done to include Branco and Rodriguez (1996) in this comparison. With just two components, we would have just three equations, i.e. one material balance equation for each component, and one material balance equation for

water. Therefore, Branco and Rodriguez formulation (1996) would be the same as Coats formulation (1980).

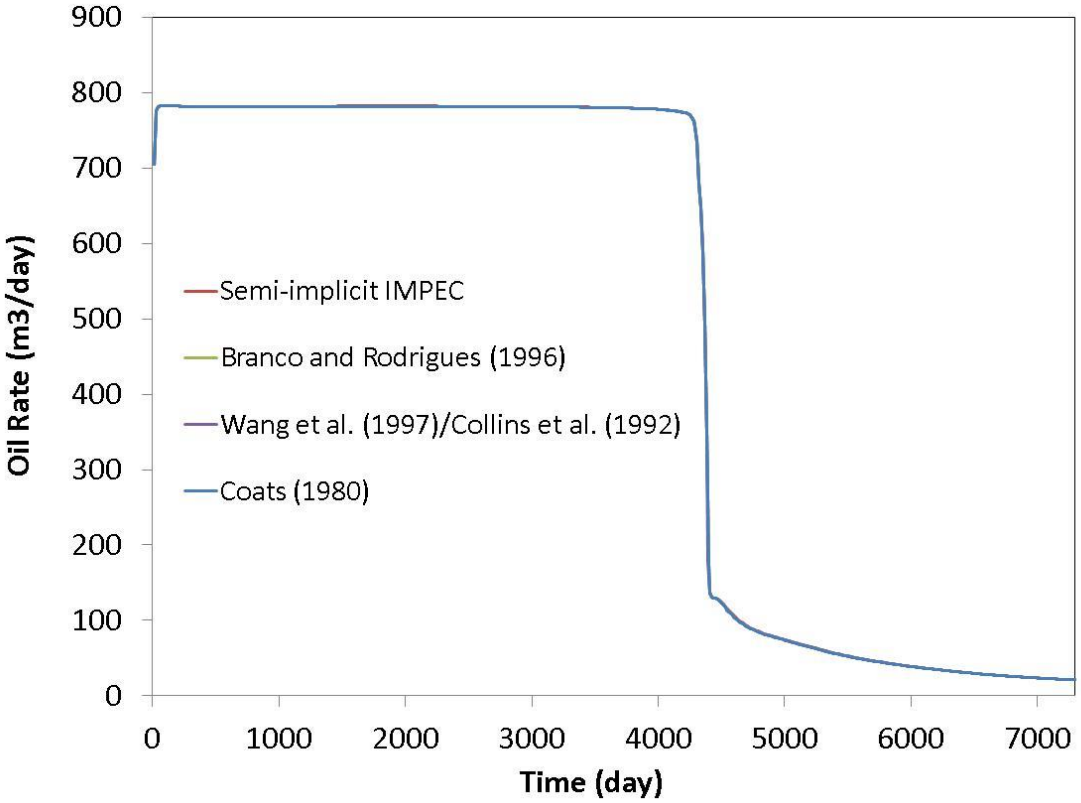

Figure 6.1.2. Volumetric oil rate versus time comparison for all formulations for Case 1.

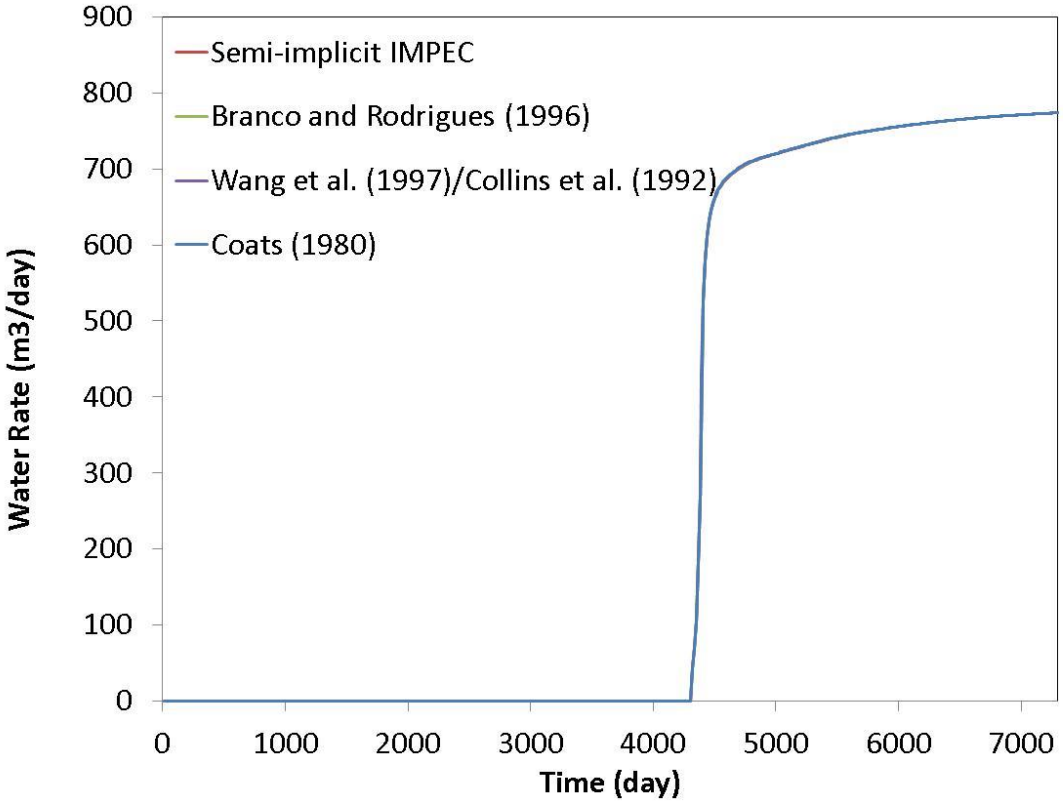

Figure 6.1.3. Volumetric water rate versus time comparison for all formulations for Case 1.

Figure 6.1.4 shows the material balance error for all formulations for Case 1. As can be seen, all the formulations maintained low material balance errors (less than 10^{-3}) during simulation. Branco and Rodriguez (1996), Coats (1980), and Wang et al. (1997) formulations completed the simulation with a material balance error close to 10^{-5}. The material balance error was calculated using Equation (6.1.2).

$$MB_{error} = \frac{\sum_{k=1}^{n_b}\left(N_i^{n+1} - N_i^n\right)_k - \sum_{k=1}^{n_w}\left(q_i\right)_k}{\sum_{k=1}^{n_w}\left(q_i\right)_k}, \qquad (6.1.2)$$

where n_b is the number of grid blocks, n_w is the number of wells, N_i is the number of moles of component i, q_i is the source/sink term, and the superscript n indicates the time level.

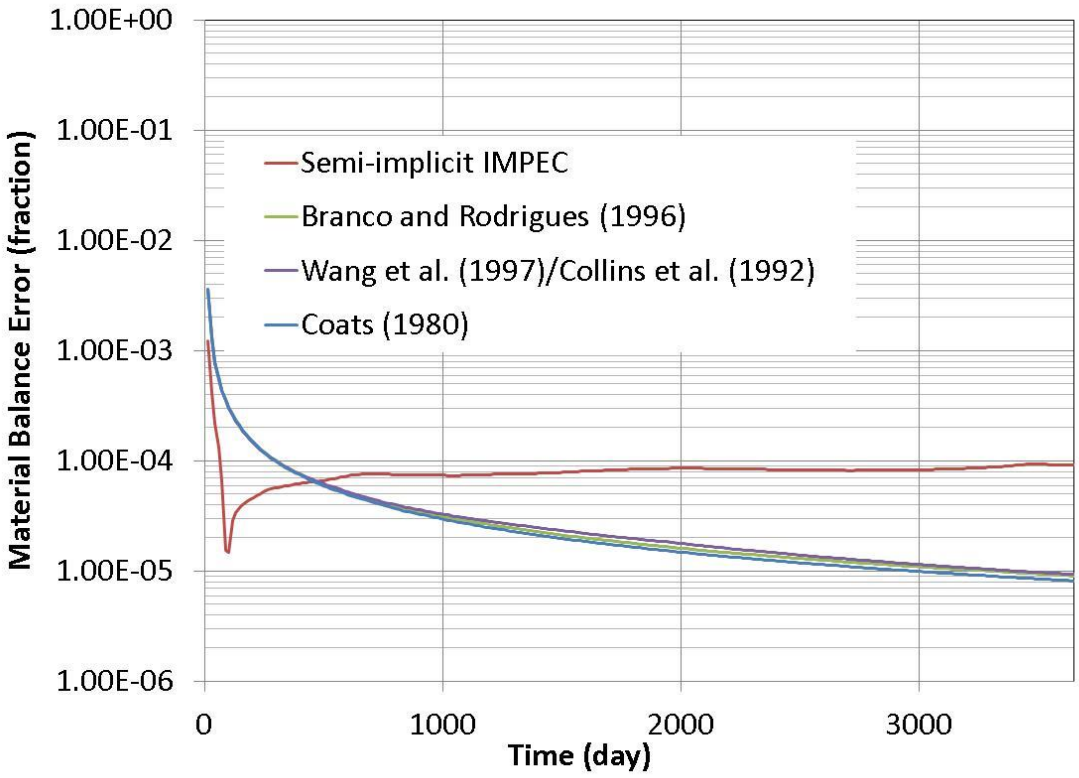

Figure 6.1.4. Material balance error for all the formulations for Case 3.

Table 6.1.3 presents the total number of Newton iterations for all formulations for Case 1. Wang et al. (1997) and Collins et al. (1992) formulations ran with a lower number of Newton iterations than all the other formulations. Coats (1980) and Branco and Rodriguez (1996) formulations ran with a similar number of Newton iterations. Since there are no fugacity equations to be solved for this problem, Coats (1980) and Branco and Rodriguez (1996) formulations differ only by just elimination of one equation (one

material balance equation for one of the components), which explains the similar performance.

Table 6.1.3. Number of Newton iterations for Case 1

Formulations	Total number of Newton iterations
Semi-implicit IMPEC	6741
Branco and Rodriguez (1996)	5954
Wang et al. (1997)	3888
Collins et al. (1992)	3888
Coats (1980)	5259

6.2 IMMISCIBLE GAS INJECTION

The second case study is an immiscible gas injection in a quarter of five-spot with simultaneous flow of gas and oil. **Table 6.2.1** shows the fluid model with six components, the reservoir properties, and the initial conditions. As we can see in **Table 6.2.1**, this is a homogeneous and isotropic reservoir. The relative permeability was modeled using Corey's correlation. All the parameters used to model the relative permeability are listed in **Table 6.2.2**. To discretize the model, we used *30* x *30* x *7* gridblocks.

Table 6.2.1. Physical properties for Case 2

Grid blocks dimension in x, y, and z directions	30 x 30 x 7	
Length (m)	170.7	
Width (m)	170.7	
Thickness (m)	30.5	
Porosity (fraction)	0.35	
Rock compressibility (kPa^{-1})	$1.45x10^{-7}$	
Reservoir temperature (^oC)	71.1	
Permeability in x direction (m^2)	$1x10^{-14}$	
Permeability in y direction (m^2)	$1x10^{-14}$	
Permeability in z direction (m^2)	$1x10^{-14}$	
Water viscosity (Pa.s)	$1x10^{-3}$	
Water density (mol/m^3)	$55.55x10^3$	
Water compressibility (kPa^{-1})	$4.35x10^{-7}$	
Initial water saturation (fraction)	0.17	
Initial reservoir pressure (MPa)	10.34	
Gas injection rate (m^3/s)	0.3277	
Producer bottom hole pressure (MPa)	8.96	
Reservoir fluid initial composition	C1	0.5
	C3	0.03
	C6	0.07
	C10	0.2
	C15	0.15
	C20	0.05

Table 6.2.1 – Continued. Physical properties for Case 2

Injected fluid composition	C1	0.77
	C3	0.2
	C6	0.01
	C10	0.01
	C15	0.005
	C20	0.005

Table 6.2.2. Corey's model relative permeability data for Case 1

	Water	Oil	Gas
End point relative permeability	0.4	0.9	0.9
Residual saturation	0.3	0.1	0.0
Exponent of relative permeability	3.0	2.0	2.0

Figures 6.2.1 and **6.2.2** present the volumetric oil and gas flow rate versus time results for all the formulations of Case 1. As can be seen, the results for all formulations are in good agreement. **Figure 6.2.3** presents the material balance error versus time for all the formulations. From **Figure 6.2.3**, we can see that the material balance error was maintained below 10^{-3} for all the formulations and close to 10^{-4} at the end of simulations.

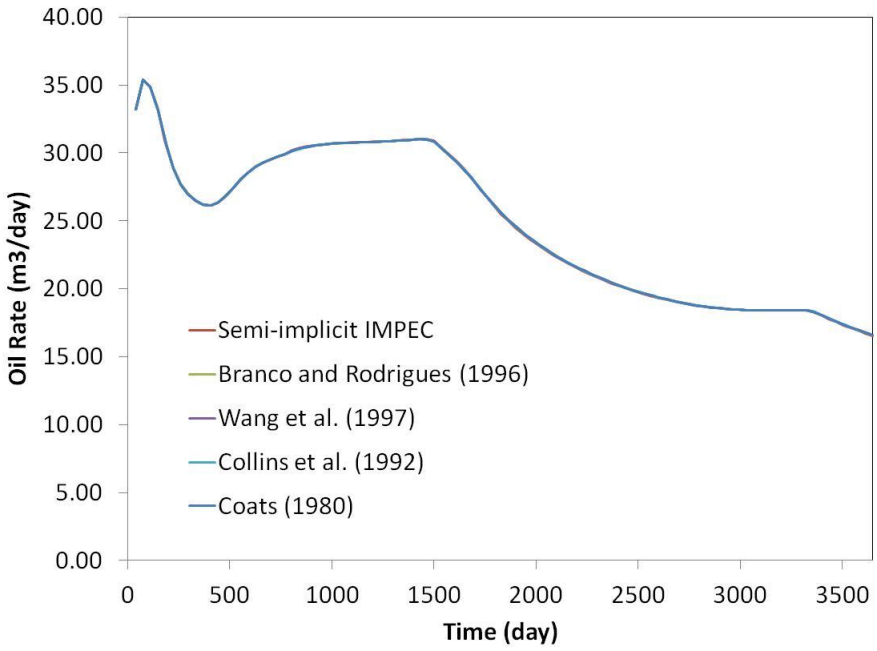

Figure 6.2.1. Volumetric oil rate versus time comparison for all formulations for Case 2.

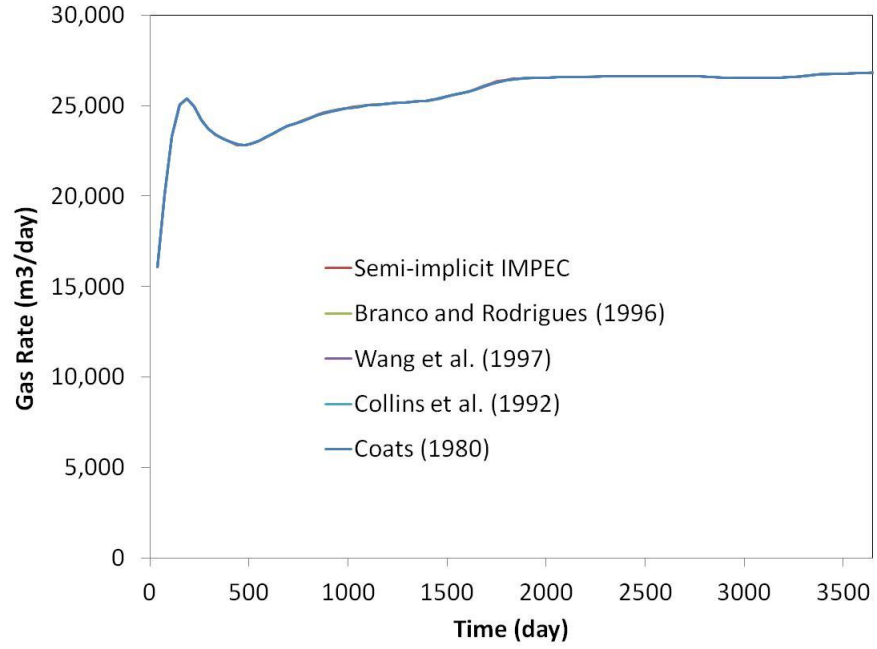

Figure 6.2.2. Volumetric gas rate versus time comparison for all formulations for Case 2.

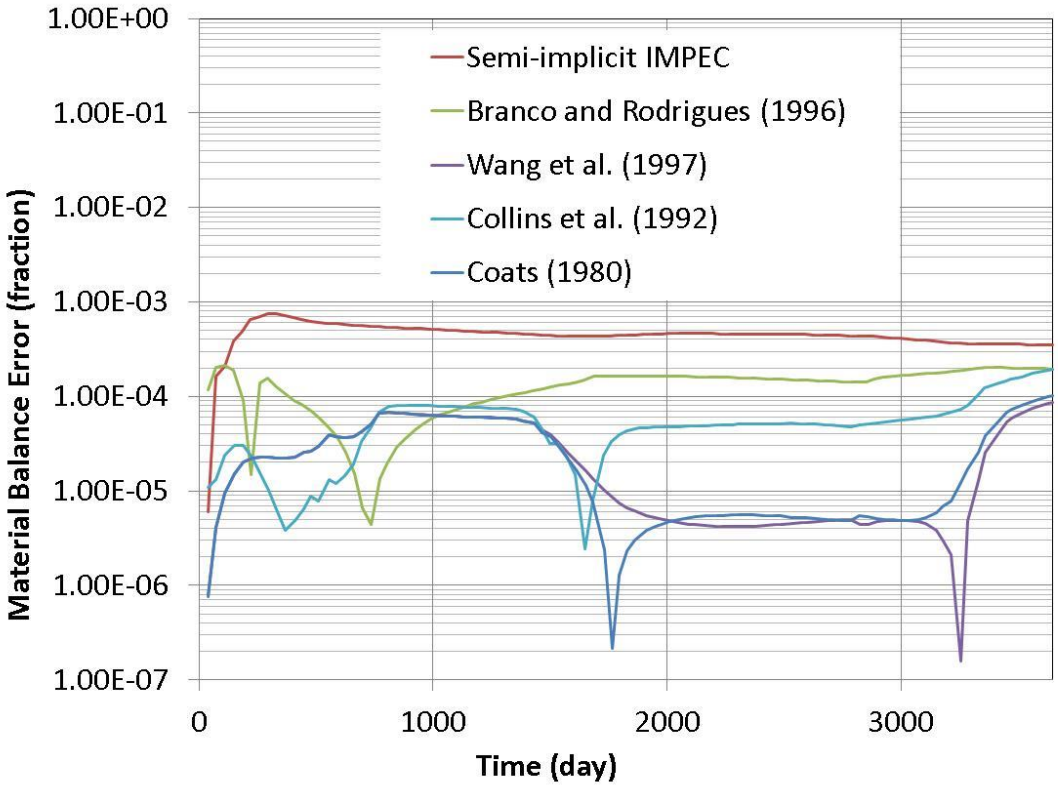

Figure 6.2.3. Material balance error for all formulations for Case 2.

Table 6.2.3 presents the total number of Newton iterations performed by each formulation for Case 2. As can be seen, all three fully implicit formulations have a much lower number of Newton iterations. Although the Branco and Rodriguez (1996) and the Semi-implicit IMPEC are sequential implicit formulations (all the variables are updated in each Newton iteration), they require a higher number of iterations because of the explicit evaluations of the convection terms in each iteration (no dependence on the neighboring gridblocks mole fractions in case of Branco and Rodriguez formulation (1996) and no dependence on the neighboring gridblocks mole fractions and saturations in case of Semi-implicit IMPEC formulation). In this case, Coats (1980) has a slightly lower number of Newton iterations compared to that of other fully implicit formulations.

Table 6.2.3. Number of Newton iterations for Case 2

Formulations	Total number of Newton iterations
Semi-implicit IMPEC	6714
Branco and Rodriguez (1996)	3211
Wang et al. (1997)	768
Collins et al. (1992)	780
Coats (1980)	766

6.3 MISCIBLE GAS INJECTION

The third case study is a homogeneous and isotropic quarter of five-spot saturated with oil. For this case, we simulate a CO_2 injection using three components for the fluid model and *20* x *20* x *4* grid blocks to discretize the reservoir model. **Table 6.3.1** presents all the physical properties and initial conditions for this case. We used Corey's correlation for the relative permeability model. All the parameters for the Corey's correlation are listed on **Table 6.3.2**.

Table 6.3.1. Physical properties for Case 3

Grid blocks dimension in x, y, and z directions	20 x 20 x 4	
Length (m)	121.9	
Width (m)	121.9	
Thickness (m)	36.6	
Porosity (fraction)	0.30	
Rock compressibility (kPa^{-1})	$5.8x10^{-7}$	
Reservoir temperature (^oC)	18.33	
Permeability in x direction (m^2)	$1x10^{-13}$	
Permeability in y direction (m^2)	$1x10^{-13}$	
Permeability in z direction (m^2)	$1x10^{-13}$	
Water viscosity (Pa.s)	$8x10^{-4}$	
Water density (mol/m^3)	$55.55x10^3$	
Water compressibility (kPa^{-1})	$4.35x10^{-7}$	
Initial water saturation (fraction)	0.25	
Initial reservoir pressure (MPa)	20.68	
Gas injection rate (m^3/s)	0.3277	
Producer bottom hole pressure (MPa)	20.68	
Reservoir fluid initial composition	CO_2	0.01
	C1	0.19
	NC16	0.80
Injected fluid initial composition	CO_2	0.95
	C1	0.04
	NC16	0.01

Table 6.3.2. Corey's model relative permeability data for Case 3

	Water	Oil	Gas
End point relative permeability	0.3	0.75	0.75
Residual saturation	0.25	0.2	0.0
Exponent of relative permeability	2.0	2.0	2.0

Figures 6.3.1 and **6.3.2** present the volumetric oil and gas rate for Case 3, respectively. As can be seen in the figures, the results for all formulations are in good agreement with the exception of Wang et al. (1997) formulation. Although all formulations share the same routines for the stability test, flash calculation, and phase identification, the Jacobian is different for the various formulations. Therefore, the convergence rate and the robustness of the formulations may vary.

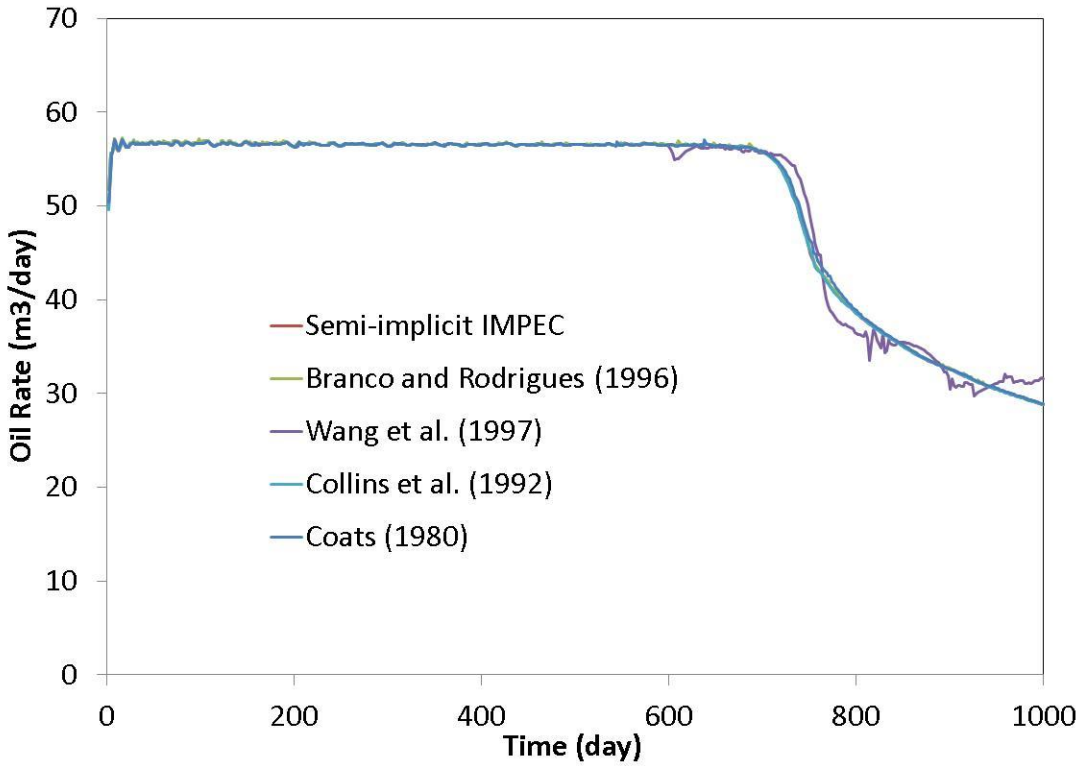

Figure 6.3.1. Volumetric oil rate versus time comparison for all formulations for Case 3.

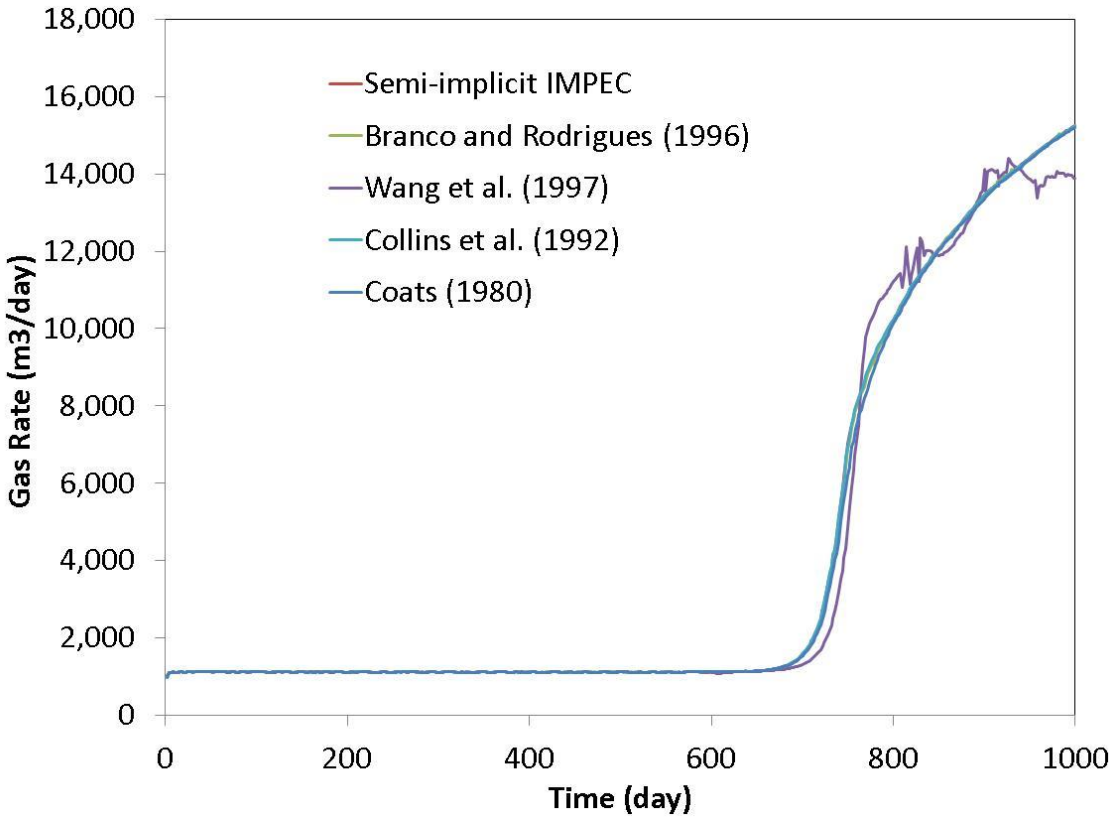

Figure 6.3.2. Volumetric gas rate versus time comparison for all formulations for Case 3.

Figure 6.3.3 presents the material balance error for all formulations. The error remained lower than 10^{-3} for all formulations during the simulation period, except for Collins et al. (1992) and Wang et al. (1997) formulations at the beginning of the simulation.

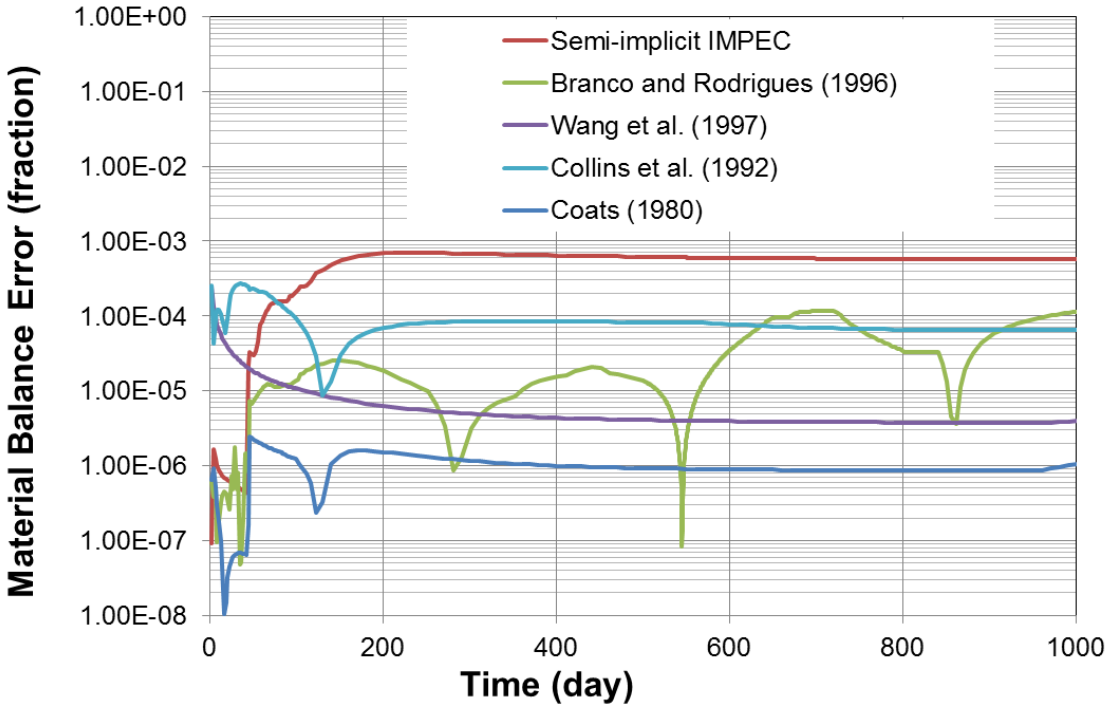

Figure 6.3.3. Material balance error for all formulations for Case 3.

Table 6.3.3 presents the total number of Newton iterations for all formulations for Case 3. For this case, Coats (1980) formulation had the lowest number of Newton iterations. We can also see that Wang et al. (1997) formulation performed worse than the other fully implicit formulations (higher number of Newton iterations). Although Collins et al. (1992) formulation shares the same primary variables as Wang et al. (1997) formulation, the phase behavior decoupling was beneficial to improve the robustness of the system as a whole. This occurs because the convergence problems associated with the fugacity equations do not affect the Jacobian in a decoupled system.

Table 6.3.3. Number of Newton iterations for Case 3

Formulations	Total number of Newton iterations
Semi-implicit IMPEC	83658
Branco and Rodriguez (1996)	46954
Wang et al. (1997)	22133
Collins et al. (1992)	11047
Coats (1980)	7416

6.4 CONDENSATE GAS PRODUCTION

The fourth case study is a condensate gas reservoir with one producer well in the center. The reservoir model has *21* x *21* x *5* grid blocks and the fluid model has five components. **Table 6.4.1** presents the reservoir physical properties and the initial conditions. The parameters for the relative permeability curve are listed in **Table 6.4.2**.

Table 6.4.1. Physical properties for Case 4

Grid blocks dimension in x, y, and z directions	21 x 21 x 5	
Length (m)	512.1	
Width (m)	512.1	
Thickness (m)	45.7	
Porosity (fraction)	0.3	
Rock compressibility (kPa^{-1})	$5.8x10^{-7}$	
Reservoir temperature (^oC)	132.2	
Permeability in x direction (m^2)	$1x10^{-14}$	
Permeability in y direction (m^2)	$1x10^{-14}$	
Permeability in z direction (m^2)	$1x10^{-14}$	
Water viscosity (Pa.s)	$8x10^{-4}$	
Water density (mol/m^3)	$55.55x10^3$	
Water compressibility (kPa^{-1})	$4.35x10^{-7}$	
Initial water saturation (fraction)	0.25	
Initial reservoir pressure (MPa)	20.68	
Producer bottom hole pressure (MPa)	6.89	
Reservoir fluid initial composition	C1	0.7
	C3	0.1
	C4	0.05
	C6	0.02
	C7	0.13

Table 6.4.2. Corey's model relative permeability data for Case 4

	Water	Oil	Gas
End point relative permeability	0.3	0.75	0.75
Residual saturation	0.25	0.2	0.0
Exponent of relative permeability	2.0	2.0	2.0

Figures 6.4.1 and **6.4.2** present the volumetric oil and gas rate, respectively. As we can see, all the formulations produced similar results. **Figure 6.4.3** presents the material balance error for this case. All the formulations ran with a material balance error lower than 10^{-3}.

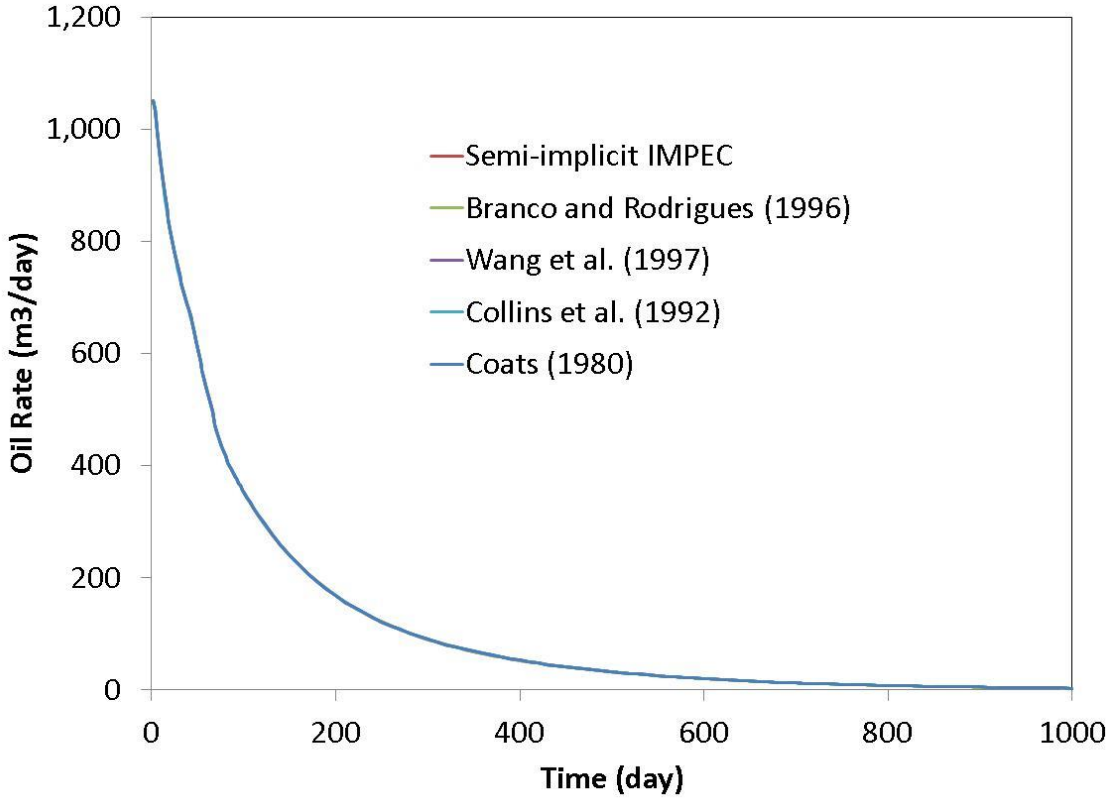

Figure 6.4.1. Volumetric oil rate versus time comparison for all formulations for Case 4.

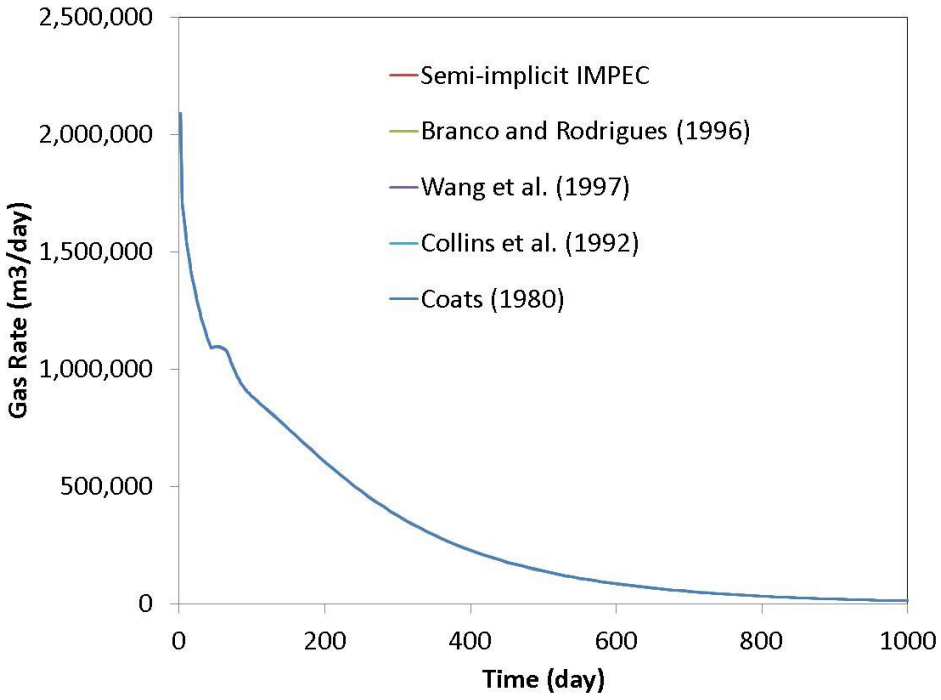

Figure 6.4.2. Volumetric gas rate versus time comparison for all formulations for Case 4.

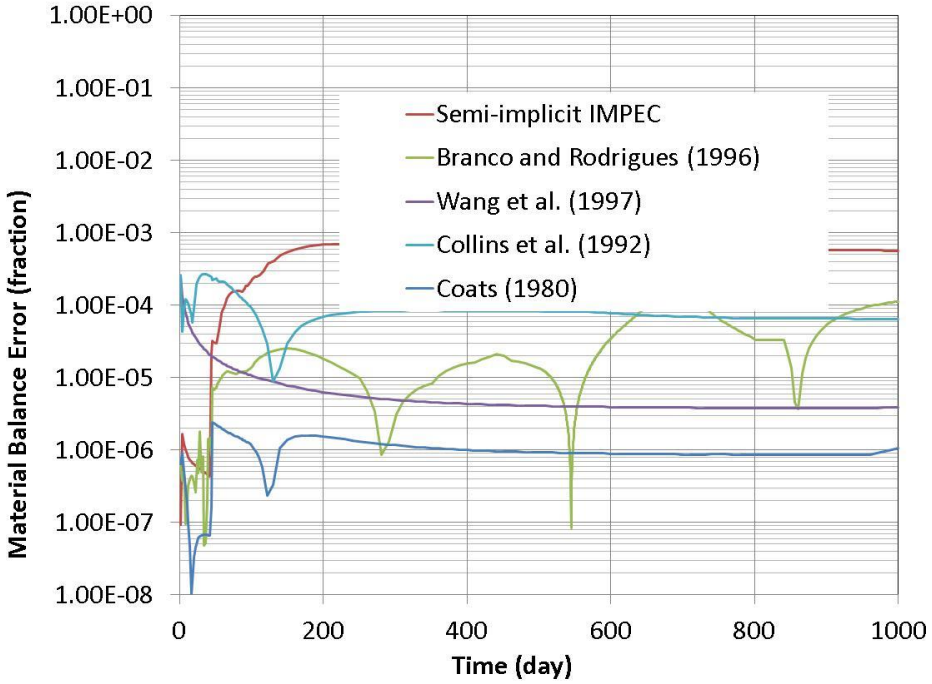

Figure 6.4.3. Material balance error for all the formulations for Case 4.

Table 6.4.3 presents total number of Newton iterations for all formulations for Case 4. Coats (1980) formulation performed better than the other fully implicit formulations. For this problem, we also observed a much larger number of Newton iterations for the semi-implicit formulations (Branco and Rodriguez, 1996, and semi-implicit IMPEC).

Table 6.4.3. Number of Newton iterations for Case 4

Formulations	Total number of Newton iterations
Semi-implicit IMPEC	2740
Branco and Rodriguez (1996)	1736
Wang et al. (1997)	668
Collins et al. (1992)	736
Coats (1980)	587

6.5 DRY GAS PRODUCTION

The fifth case study refers to a dry gas production problem in a homogeneous square reservoir with one well in the center. The discretization of the problem was performed with *11 x 11 x 5* grid blocks and the fluid model has five components. **Table 6.5.1** presents the reservoir physical properties and the initial conditions. The parameters for the relative permeability curve are the same as in the fourth case study and are listed in **Table 6.4.2**.

Table 6.5.1. Physical properties for Case 5

Grid blocks dimension in x, y, and z directions	11 x 11 x 5	
Length (m)	512.1	
Width (m)	512.1	
Thickness (m)	45.7	
Porosity (fraction)	0.3	
Rock compressibility (kPa^{-1})	$5.8x10^{-7}$	
Reservoir temperature (^oC)	176.7	
Permeability in x direction (m^2)	$1x10^{-14}$	
Permeability in y direction (m^2)	$1x10^{-14}$	
Permeability in z direction (m^2)	$1x10^{-14}$	
Water viscosity (Pa.s)	$8x10^{-4}$	
Water density (mol/m^3)	$55.55x10^3$	
Water compressibility (kPa^{-1})	$4.35x10^{-7}$	
Initial water saturation (fraction)	0.25	
Initial reservoir pressure (MPa)	27.58	
Producer bottom hole pressure (MPa)	10.34	
Reservoir fluid initial composition	C1	0.8
	C3	0.1
	C4	0.05
	C6	0.02
	C7	0.03

Figures 6.5.1 presents the volumetric gas rate. As we can see, all the formulations produced similar results. **Figure 6.5.2** presents the material balance error for this case. All the formulations ran with a material balance error lower than 10^{-3}.

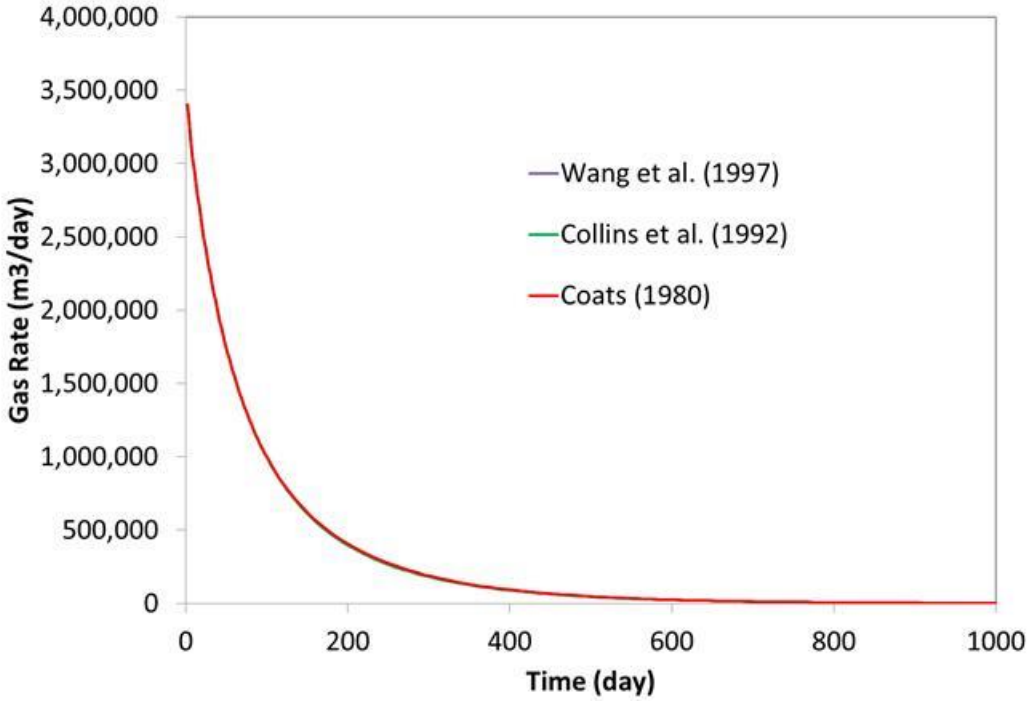

Figure 6.5.1. Volumetric gas rate versus time comparison for all formulations for Case 5.

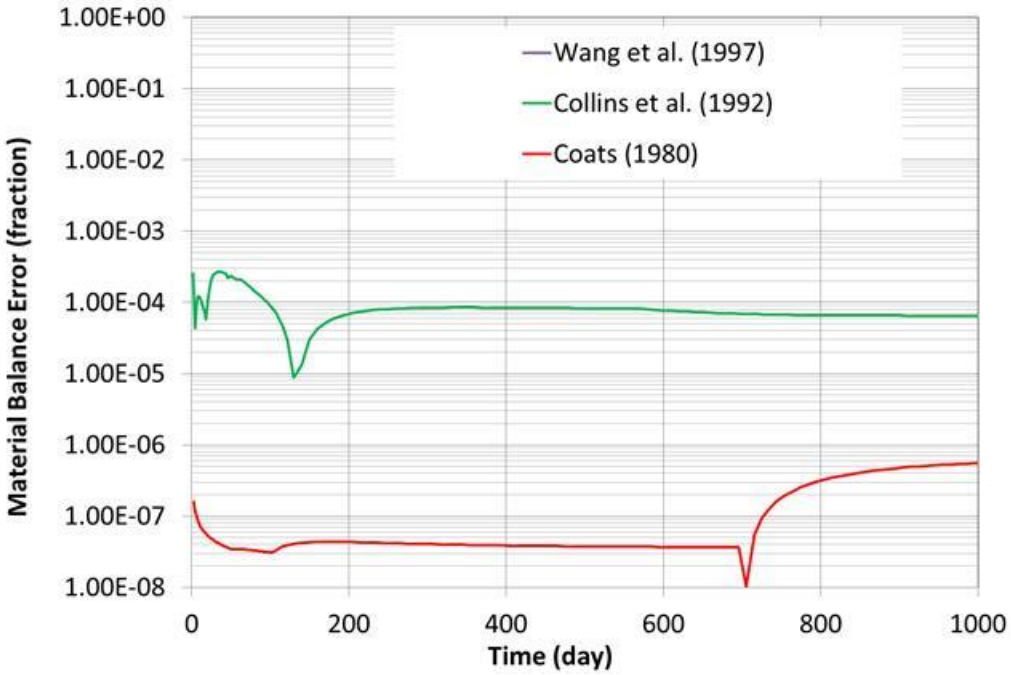

Figure 6.5.2. Material balance error for all the formulations for Case 5.

Table 6.5.2. Number of Newton iterations for Case 5

Formulations	Total number of Newton iterations
Wang et al. (1997)	478
Collins et al. (1992)	478
Coats (1980)	320

6.6 IMMISCIBLE GAS INJECTION IN A HETEROGENEOUS LARGE RESERVOIR

The last case study refers to an immiscible gas injection in a heterogeneous and anisotropic reservoir. This case was simulated using Coats (1980) formulation, Wang et al. (1997) formulation, and Collins et al. (1992) formulation. The results were also compared with CMG-GEM simulator. The case was modeled using *80* x *80* x *10* grid blocks and 113 wells (49 producers and 64 injectors). **Table 6.6.1** presents the physical properties used to simulate this case. **Figures 6.6.1** and **6.6.2** present the absolute horizontal permeability and porosity fields, respectively.

Table 6.6.1. Physical properties for Case 6

Grid blocks dimension in x, y, and z directions	80 x 80 x 10	
Length (m)	7315.2	
Width (m)	7315.2	
Thickness (m)	91.44	
Porosity (fraction)	Figure 6.6.2	
Rock compressibility (kPa^{-1})	0.0	
Reservoir temperature (^oC)	71.1	
Permeability in x direction (m^2)	Figure 6.6.1	
Permeability in y direction (m^2)	Figure 6.6.1	
Permeability in z direction (m^2)	$0.1K_{xx}$	
Water viscosity (Pa.s)	$5x10^{-4}$	
Water density (mol/m^3)	$55.55x10^3$	
Water compressibility (kPa^{-1})	0.0	
Initial water saturation (fraction)	0.25	
Initial reservoir pressure (MPa)	10.34	
Producers bottom hole pressure (MPa)	8.96	
Injection gas rate – each well (m^3/s)	3.28	
Reservoir fluid initial composition	C1	0.5
	C3	0.03
	C6	0.07
	C10	0.2
	C15	0.15
	C20	0.05

Table 6.6.1 – Continued. Physical properties for Case 6

Injected fluid composition	C1	0.77
	C3	0.2
	C6	0.01
	C10	0.01
	C15	0.005
	C20	0.005

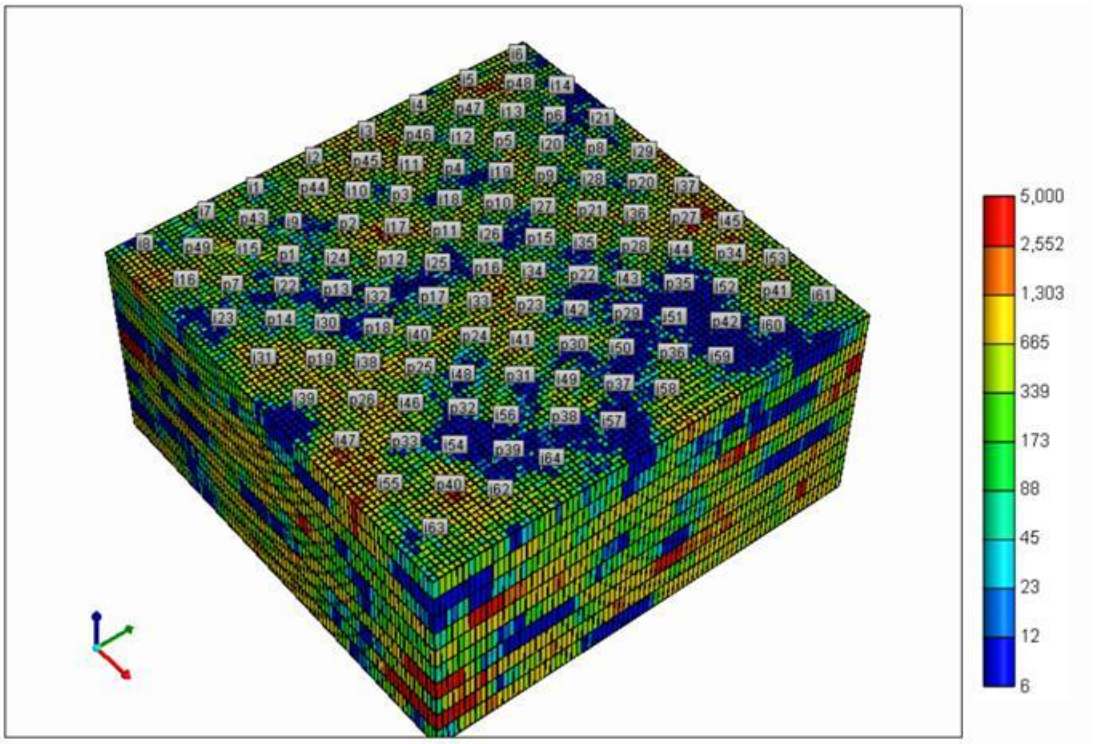

Figure 6.6.1. Absolute horizontal permeability field for Case 6 (units in *md* : 1 *md*=10^{-15} m^2).

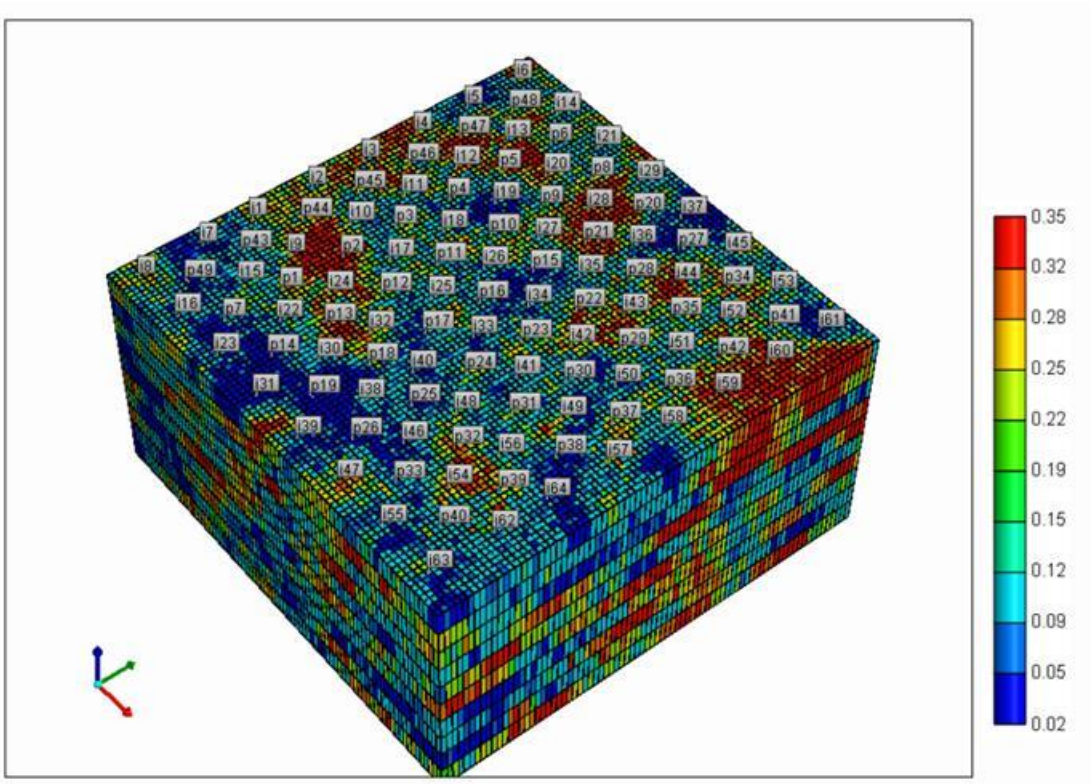

Figure 6.6.2. Porosity field for Case 6.

This case was simulated using Coats (1980) and Collins et al. (1992) formulations implemented in GPAS. The results were also compared with CMG-GEM simulator. **Figures 6.6.3** and **6.6.4** show the gas saturation field using Coats (1980) formulation and CMG-GEM, respectively. From these figures, we can see that the results of GPAS and CMG-GEM are similar. **Figure 6.6.5** presents the volumetric oil rate for Coats (1980) and Collins et al. (1992) formulations. In order to validate GPAS, we included other various cases in Appendix A comparing GPAS, UTCOMP, CMG-GEM, and the analytical solution, if it exists. The cases in Appendix A are part of Xue Li thesis (Li, 2012).

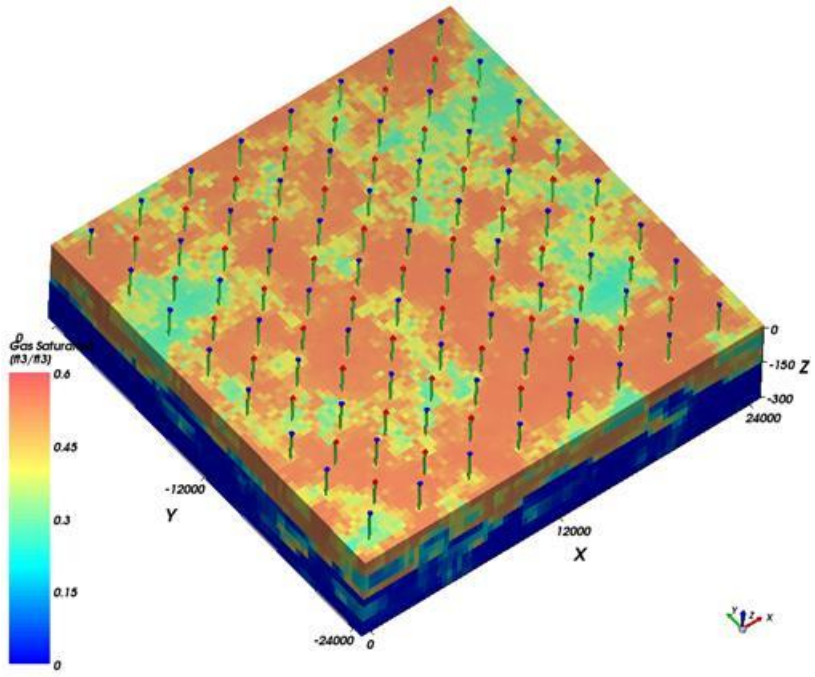

Figure 6.6.3. Gas saturation field at 500 days using Coats (1980) formulation.

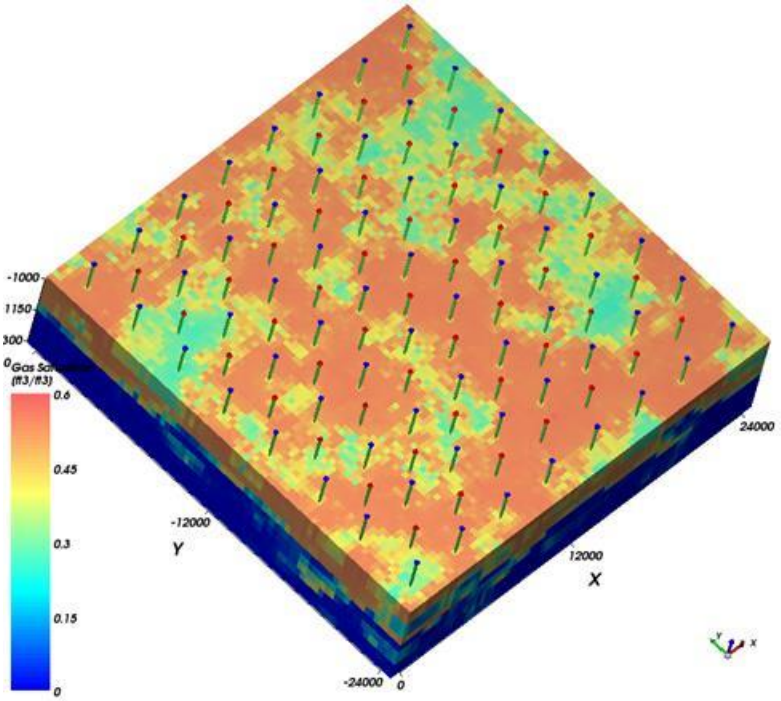

Figure 6.6.4. Gas saturation field at 500 days using CMG-GEM.

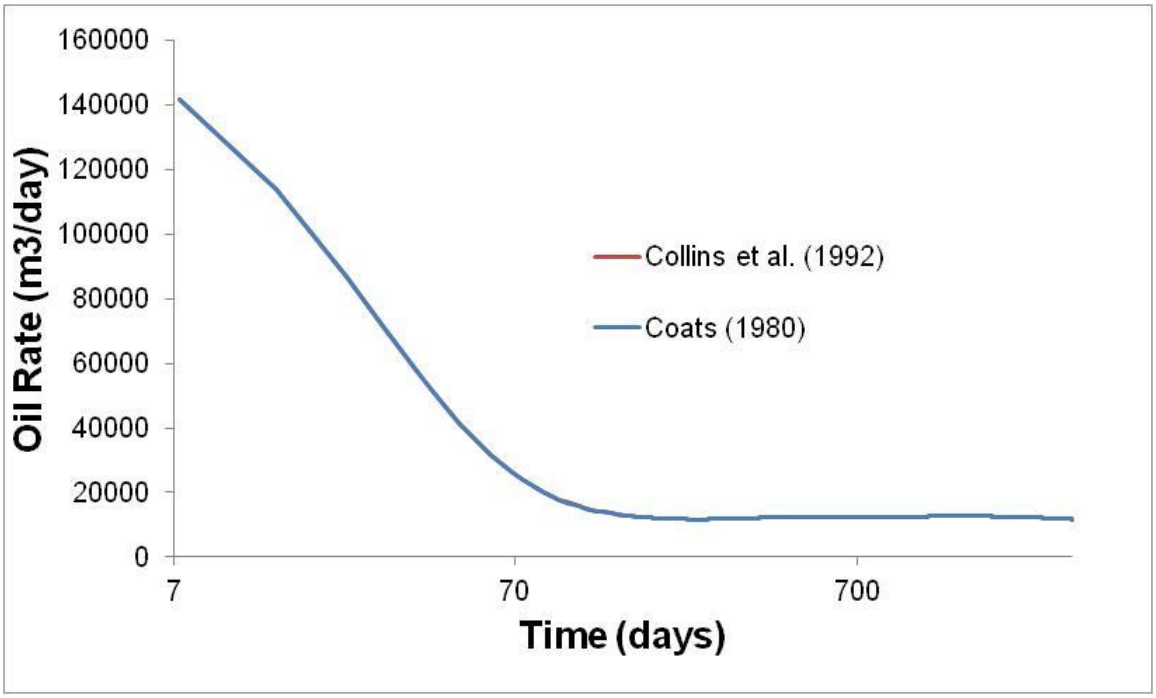

Figure 6.6.5. Volumetric oil rate for Coats (1980) and Collins et al. (1992) formulations for Case 6.

Figure 6.6.6 presents the results of the material balance error for Coats (1980) and Collins et al. (1992) formulations. From this figure, we can see that Collins et al. (1992) performed better in terms of material balance error. Wang et al. (1997) formulation does not appear in this figure because it failed to run this case. CMG-GEM performed similarly with a final material balance error equal to 1.8×10^{-5}.

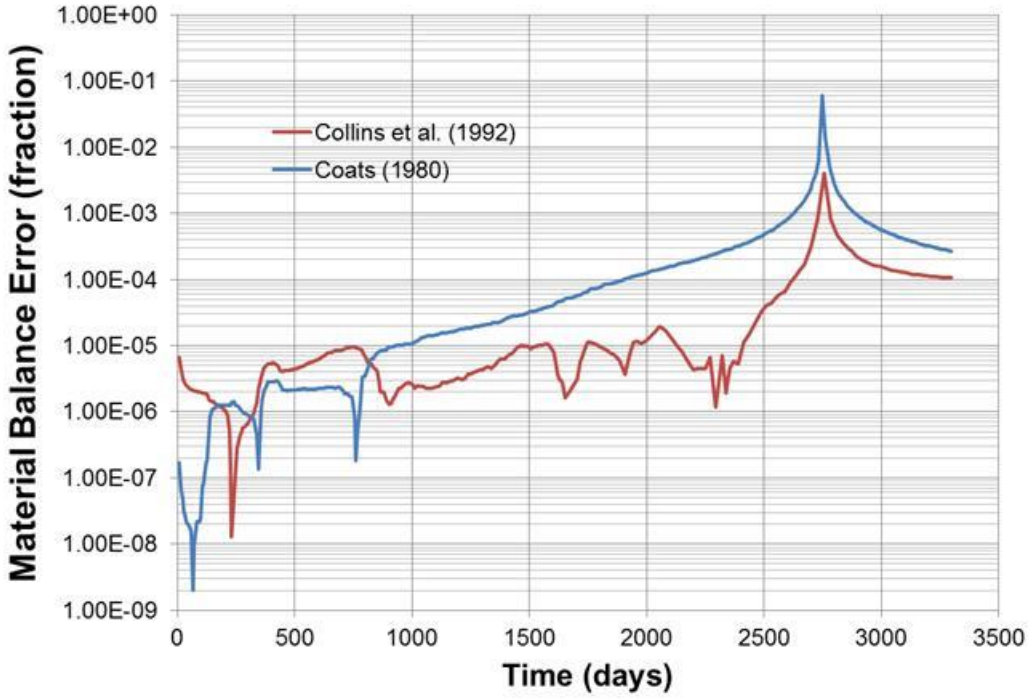

Figure 6.6.6. Material balance error for Coats (1980) and Collins et al. (1992) formulations for Case 6.

Table 6.6.2 present the total number of Newton iterations performed by Coats (1980), Collins et al. (1992) and CMG-GEM. From this table, we can see that Collins et al. (1992) performed better than Coats (1980) in terms of total Newton iterations. We can also see that CMG-GEM performed worse than Collins et al. (1992), but this result is highly influenced by the convergence criteria used by both simulators, which are not the same.

Table 6.6.2. Number of Newton iterations for Case 6

Formulations	Total number of Newton iterations
CMG-GEM	2839
Collins et al. (1992)	1037
Coats (1980)	1452

6.7 DISCUSSION

Results presented in the previous sections, show that using different primary variables changes the number of non-linear iterations. Therefore, the final performance is affected.

As discussed by Cao (2002), changing the primary variables can be done by a transformation matrix. This operation is done for each grid block using the chain rule. As an example, see Equation 6.7.1,

$$J=\begin{bmatrix} \frac{\partial R_1}{\partial x_1} & \frac{\partial R_1}{\partial x_2} & \frac{\partial R_1}{\partial x_3} \\ \frac{\partial R_2}{\partial x_1} & \frac{\partial R_2}{\partial x_2} & \frac{\partial R_2}{\partial x_3} \\ \frac{\partial R_3}{\partial x_1} & \frac{\partial R_3}{\partial x_2} & \frac{\partial R_3}{\partial x_3} \end{bmatrix} = \begin{bmatrix} \frac{\partial R_1}{\partial y_1} & \frac{\partial R_1}{\partial y_2} & \frac{\partial R_1}{\partial y_3} \\ \frac{\partial R_2}{\partial y_1} & \frac{\partial R_2}{\partial y_2} & \frac{\partial R_2}{\partial y_3} \\ \frac{\partial R_3}{\partial y_1} & \frac{\partial R_3}{\partial y_2} & \frac{\partial R_3}{\partial y_3} \end{bmatrix} \begin{bmatrix} \frac{\partial y_1}{\partial x_1} & 0 & 0 \\ 0 & \frac{\partial y_2}{\partial x_2} & 0 \\ 0 & 0 & \frac{\partial y_3}{\partial x_3} \end{bmatrix}. \tag{6.7.1}$$

The operation performed in Equation (6.7.1) can be written for the whole system as

$$A\cdot\delta y=(AM)\cdot\left(M^{-1}\delta y\right)=(AM)\cdot\delta x=B, \tag{6.7.2}$$

where δy is one set of primary variables, δx is another set of primary variables, and M is a transformation matrix.

Matrix M in Equation (6.7.2) can be also interpreted as a preconditioner for matrix A. Therefore, the new matrix AM has a different condition number than matrix A, which will obviously influence the linear solver performance.

Drexler (1998) proved that equations closer to linearity converge faster using Newton-Raphson's method. Drexler analyzed polynomial equations and proved that the rate of convergence can be calculated by Equation (6.7.3):

$$r\left(p_{\max}\right)=\left(\frac{p_{\max}-1}{p_{\max}}\right)^{p_{\max}}, \tag{6.7.3}$$

where $p_{\max}$ is the degree of the non-linear system of equations.

Cao (2002) demonstrated that changing the primary variables also changes the linearity of the primary equations; thus the non-linear solver performance is affected. As an example, Cao (2002) presented the case where the non-linear function solved is given by $F=X^2-2=0$. Using Newton's method and the initial estimate $X=1$, the next iteration is given by $X^{\nu+1}=X^{\nu}-\frac{F}{F'}=1.5$. But, if we switch the primary variable for $Y=X^2$, then $Y^{\nu+1}=Y^{\nu}-\frac{F}{F'}=2$ and $X^{\nu+1}=\sqrt{2}$, which is the exact solution. From this example, we can see that switching the primary variables changes the non-linear convergence performance and, as proved by Drexler (1998), equations closer to the linearity converges faster.

Let us now analyze the primary variables compared in this dissertation for a compositional reservoir simulation case. As presented in Chapter 3, considering the

assumptions elaborated in Section 3.1, the mathematical model for a compositional reservoir simulation problem is given by

$$V_b \frac{\partial}{\partial t}\left(\phi \sum_{j=2}^{n_p} \xi_j S_j x_{ij} \right) - V_b \vec{\nabla} \cdot \sum_{j=2}^{n_p} \left(\frac{\bar{\bar{k}}k_{rj}}{\mu_j} \xi_j x_{ij} \left(\nabla P_j - \gamma_j \nabla D \right) - \phi \xi_j S_j \bar{\bar{K}}_{ij} \nabla x_{ij} \right) - q_i = 0, \qquad (3.2.1)$$

$$V_b \frac{\partial}{\partial t}\left(\phi N_w \right) - V_b \vec{\nabla} \cdot \frac{\bar{\bar{k}}k_{rw}}{\mu_w} \xi_w \left(\nabla P_w - \gamma_w \nabla D \right) - q_w = 0, \qquad (3.2.3)$$

$$f_i^{\,2} - f_i^{\,j} = 0 \quad for\ j = 3...n_p, \qquad (3.2.4)$$

$$\sum_{i=1}^{n_c} x_{ij} = 1 \quad for\ j = 2...n_p, \text{ and} \qquad (3.2.5)$$

$$\sum_{j=1}^{n_p} \frac{N_j}{\xi_j} - 1 = 0 \text{ or } \sum_{j=1}^{n_p} S_j - 1 = 0. \qquad (3.2.6)$$

In case of two hydrocarbon phases, Equations (3.2.1) through (3.2.6) form a system of $2n_c + 4$ equations and $2n_c + 4$ variables, but just $n_c + 1$ equations need to be solved in a fully implicit formulation. These $n_c + 1$ equations are called primary equations and, for all the formulations analyzed in this dissertation, the primary equations are the material balance equations (Equation 3.2.1 and 3.2.3). It is also important to mention that although just $n_c + 1$ equations need to be solved, some manipulation needs to be performed in order to eliminate the $n_c + 3$ secondary variables and this manipulation uses the secondary equations. Therefore, making of secondary equations more linear also improves the non-linear solver convergence.

In this dissertation, we compared three groups of fully implicit primary variables. The first group, called natural variables (Coats, 1980), is formed by x_{ij}, P, S_o, and S_g; the second group is formed by N_i, $\ln(K_i)$, N_w, and P (Wang et al., 1997); and the third group

is formed by N_i, N_w, and P (Collins et al., 1992). For the analysis of these three groups, the second and the third groups (Wang et al. and Collins et al. formulations) make the accumulation term in the material balance equations linear. On the other hand, they make the convective term and the well terms more non-linear than the natural variables. For the volume constraint equation, the natural variables group makes it linear, which does not occur with the other two groups of primary variables. Finally, for the fugacity equations, the behavior is very much dependent on the problem, but in general they are the most non-linear equations; therefore they will define the non-linear convergence rate as proved by Drexley (1998).

Collins et al. (1992) formulation is expected to always have a larger number of Newton iterations compared to the Wang et al. (1997) formulation, except in case of failure (as in Case 3), or in the case of a single hydrocarbon phase (as in Cases 1 and 6). This conclusion can be explained using the fugacity equations (Equation 3.2.4). For Wang et al. (1997) formulation, this equation is rewritten as in Equation (6.7.4):

$$\ln \phi_i^o - \ln \phi_i^g - \ln K_i = 0 . \qquad (6.7.4)$$

In the Collins et al. (1992) formulation, Equation (6.7.4) is incorporated into the material balance equations by solving the $n_c + 1$ systems of linear equations formed by Equations (4.6.8) and (4.6.9). These systems are solved after the flash calculation is performed and the calculated derivatives are used in the material balance equations:

$$\sum_{s=1}^{n_c} \left(\frac{\partial f_i^o}{\partial N_s^o} - \frac{\partial f_i^g}{\partial N_s^g} \right) \frac{\partial N_s^o}{\partial p} = \frac{\partial f_i^g}{\partial p} - \frac{\partial f_i^o}{\partial p} \quad i = 1 \ldots n_c , \qquad (4.6.8)$$

$$\sum_{s=1}^{n_c} \left(\frac{\partial f_i^o}{\partial N_s^o} - \frac{\partial f_i^g}{\partial N_s^g} \right) \frac{\partial N_s^o}{\partial N_m} = \frac{\partial f_i^g}{\partial N_m^g} \quad i, m = 1 \ldots n_c . \qquad (4.6.9)$$

This process brings the advantage of a complete decoupling of the fugacity equations from the non-linear system of equations, but it is less efficient because it increases the nonlinearity of the system. It is easier to see this effect with the following example:

Original system of equations:

$$x_1^3 + x_2 = 0$$
$$x_1 + x_2^3 - 5 = 0$$

Using the Newton-Raphson method with the initial guesses $x_1^0 = -2$ and $x_2^0 = 8$ we obtain

$$\begin{bmatrix} 12 & 1 \\ 1 & 192 \end{bmatrix} \begin{bmatrix} \delta x_1 \\ \delta x_2 \end{bmatrix} = \begin{bmatrix} 0 \\ -505 \end{bmatrix}.$$

Therefore, $x_1^1 = -1.7807$ and $x_2^1 = 5.3687$. Thus, the new iteration is given by

$$\begin{bmatrix} 9.513 & 1 \\ 1 & 86.467 \end{bmatrix} \begin{bmatrix} \delta x_1 \\ \delta x_2 \end{bmatrix} = \begin{bmatrix} 0.2780 \\ -147.98 \end{bmatrix},$$

resulting in $x_1^2 = -1.5714$ and $x_2^2 = 3.6551$. For a convergence criterion of $R \leq 10^{-6}$, where *R* is higher residual from the system of equations, this system converges in eight iterations.

This system can be replaced by

$$F = x_1 - x_1^9 - 5 = 0.$$

For the same initial guess, $x_1^0 = -2$, we get

$$x_1^{\nu+1} = x_1^{\nu} - \frac{x_1 - x_1^9 - 5}{-9x_1^8 + 1} = -2 - \frac{-505}{-2303} = -1.7807.$$

Therefore, the next iteration is given by

$$x_1^2 = -1.7807 - \frac{-173.26}{-908.93} = -1.5901.$$

Using the same convergence criterion, this equation converges in nine iterations.

Comparing these two solutions, we can observe that in the first iteration, the first solution reduced the highest residual from *-505* to *-147.96*, while the second solution reduced the residual from *-505* to *-173.26*. Applying Equation (6.7.3) proposed by Drexley (1998) to calculate the rate of convergence, we obtain

For the first solution:

$$r(p_{\max}) = \left(\frac{p_{\max} - 1}{p_{\max}}\right)^{p_{\max}} = \left(\frac{2}{3}\right)^3 = 0.296$$

For the second solution:

$$r(p_{\max}) = \left(\frac{p_{\max} - 1}{p_{\max}}\right)^{p_{\max}} = \left(\frac{8}{9}\right)^9 = 0.346$$

which is close enough to the results we obtained from our example. For the first solution $r = \frac{-147.96}{-505} = 0.293$ and for the second $r = \frac{-173.26}{-505} = 0.343$.

These results can be understood as a price to pay for the decoupling of the system of equations and, except for cases where the equations are linear, we always increase the degree of the system by performing this kind of decoupling. This conclusion was also in agreement with our numerical experiments performed in Sections 6.1 through 6.6. Thus, Collins et al. (1992) formulation will always require a higher number of Newton-Raphson iterations when compared to Wang et al. (1997). Besides this disadvantage, solving the $n_c + 1$ systems of n_c equations in order to decouple the fugacity equations is

computationally more expensive than just solving the full Jacobian. Therefore, decoupling the system of equations as performed by Collins et al. (1992) can be worthwhile because of the flexibility of having the flash calculation completely independent from the material balance equations.

Unfortunately, it is more complicated to determine a general rule to compare Wang et al. (1997) formulation and Coats (1980) formulation, especially because of the strong non-linear behavior of the fugacity equations. Otherwise, we can affirm that the Jacobian calculation is cheaper as cited by Cao (2002). In general, it converges faster as demonstrated in our numerical experiments and has a better condition number as shown in **Table 6.7.1**. Therefore, our results indicate that Coats (1980) formulation is the most efficient formulation among the three fully implicit formulations analyzed in this dissertation. This conclusion is supported by the normalized CPU times presented in **Table 6.7.2**.

Table 6.7.1. Condition Number for the Implemented Fully Implicit Formulations

Case	Condition Number		
	Coats (1980)	Wang et al. (1997)	Collins et al. (1992)
Case 1 (Water flooding)	1.66E+09	2.44E+07	2.44E+07
Case 2 (Immiscible gas injection)	2.44E+06	2.99E+12	2.44E+12
Case 3 (Miscible gas injection)	5.42E+04	4.43E+11	4.43E+11
Case 4 (Condensate gas production)	2.34E+06	3.61E+09	3.79E+10
Case 5 (Dry gas production)	5.65E+04	4.96E+11	4.96E+11

Table 6.7.2. Normalized CPU Times for Various Case Studies using all Formulations

	Wang et al. (1997)	Coats (1980)	Collins et al. (1992)	Branco and Rodriguez (1996)	Sequential IMPEC
Case 1	1.00	1.24	1.00	0.99	0.82
Case 2	1.00	0.61	0.78	3.46	4.87
Case 3	1.00	0.14	3.48	0.74	1.21
Case 4	1.00	0.44	0.98	1.07	3.76
Case 5	1.00	0.30	1.00	**	**
Case 6	*	1.00	1.46	**	**

* Fail

** Not tested

Chapter 7. Application and Model Validation of the Enhanced Formulations

In this chapter, we present different applications of the enhancements implemented into various formulations. Enhancements are in the implementation of a three-phase flash algorithm, in the implementation of the physical dispersion term in the material balance equations, and in the implementation of the Element based Finite Volume Method (EbFVM) for unstructured mesh.

7.1 THREE-PHASE FLASH APPLICATIONS

In this first section of this chapter, we present two applications of the three-phase flash capability implemented into GPAS for Coats (1980) formulation, Branco and Rodriguez (1996) formulation, and sequential IMPEC formulation. The first application is a three-dimensional CO_2 injection at low temperature and pressure conditions. Therefore, three hydrocarbon phases coexist in this case (oil, gas, and a second liquid phase rich in CO_2). The second application is also a three-dimensional CO_2 injection using a fluid model proposed by Khan (1992) with seven components. This same fluid model was used by Okuno et al. (2011) to study cases of high displacement when the third hydrocarbon phase appears.

7.1.1 Three-dimensional CO_2 injection

The first case study refers to a quarter of five-spot at low temperature conditions. Low temperature provides the necessary conditions for the coexistence of all three hydrocarbon phases when CO_2 is injected. Also, the water phase is present; thus, we have three-phase flash and four-phase flow in this case. **Table 7.1.1.1** presents the input data used for this case. **Table 7.1.1.2** presents the Corey's parameters used for the relative permeability model.

Table 7.1.1.1. Input data for Case 1

Grid blocks dimension in x, y, and z directions	10 x 10 x 3	
Length (m)	121.9	
Width (m)	121.9	
Thickness (m)	36.58	
Porosity (fraction)	0.3	
Rock compressibility (kPa^{-1})	$5.8x10^{-7}$	
Reservoir temperature (^oC)	18.33	
Permeability in x direction (m^2)	$10x10^{-13}$	
Permeability in y direction (m^2)	$10x10^{-13}$	
Permeability in z direction (m^2)	$10x10^{-13}$	
Water viscosity (Pa.s)	$8x10^{-4}$	
Water density (mol/m^3)	$55.55x10^3$	
Water compressibility (kPa^{-1})	$4.4x10^{-7}$	
Initial water saturation (fraction)	0.25	
Initial reservoir pressure (MPa)	6.21	
Producer bottom hole pressure (MPa)	6.21	
Gas injection rate (m^3/s)	0.328 m^3/s	
Reservoir fluid initial composition	CO_2	0.01
	C1	0.19
	C16	0.80
Injected fluid composition	CO_2	0.95
	C1	0.05
	C16	0.00

Table 7.1.1.2. Corey's model relative permeability data

	Water	Oil	Gas	Second Liquid
End point relative permeability	0.3	0.75	0.9	0.9
Residual saturation	0.25	0.2	0.0	0.0
Exponent of relative permeability	2.0	2.0	2.0	2.0

Figures 7.1.1.1 and **7.1.1.2** present the results for the volumetric oil rate and the volumetric gas rate, respectively. From these figures, we can compare the results of UTCOMP, Coats (1980) formulation, Branco and Rodriguez (1996) formulation, and sequential IMPEC formulation. Comparing the results of the formulations implemented in GPAS and UTCOMP, we can see that they are similar, but UTCOMP predicts a higher gas rate after the breakthrough. This difference is caused by the UTCOMP's relative permeability model which is slightly different from the one in GPAS.

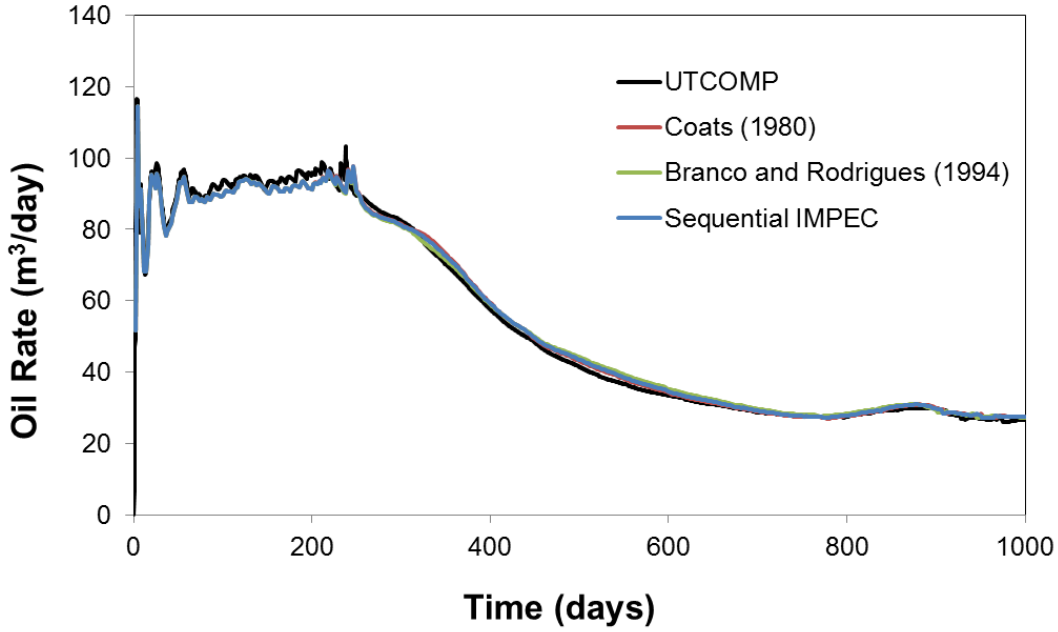

Figure 7.1.1.1. Volumetric oil rate versus time for Case 1.

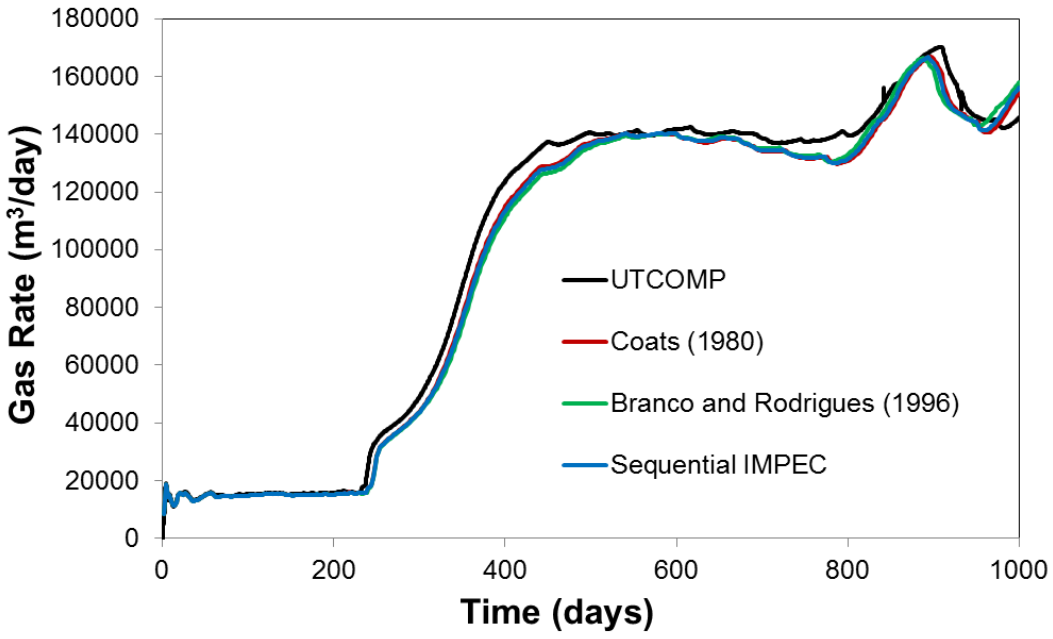

Figure 7.1.1.2. Volumetric gas rate versus time for Case 1.

7.1.2 Case Study Using the Bob Slaughter Block Oil

The second case study refers to a three-dimensional CO_2 injection using the seven-component Bob Slaughter Block (BSB) oil in west Texas. This fluid model was created by Khan (1992) to study cases of three hydrocarbon phases flowing. It was also used by Okuno et al. (2011) to study cases of high displacement when the third hydrocarbon phase appears. The properties used to run this case are similar to those used to run the first case study, except for the fluid model. **Table 7.1.1.1** presents the input data used for this case with the exception of the fluid composition and the fluid model which are presented in **Table 7.1.2.1** and **Table 7.1.2.2**, respectively. **Table 7.1.1.2** presents the Corey's parameters used for the relative permeability model.

Table 7.1.2.1. Reservoir fluid composition for case 2

Reservoir fluid initial composition	CO_2	0.034
	C1	0.086
	C2-C3	0.15
	C4-C6	0.167
	C7-C15	0.331
	C16-C27	0.161
	C28+	0.071
Injected fluid composition	CO_2	0.9
	C1	0.08
	C2-C3	0.015
	C4-C6	0.003
	C7-C15	0.0005
	C16-C27	0.0005
	C28+	0.001

Table 7.1.2.2. Reservoir fluid model for case study 2

Component	MW	T_c (^oR)	P_c (psia)	Accentric Factor	V_c (ft^3/lbmol)	BIC
CO_2	44.01	547.56	1069.87	0.23	1.51	-
C1	16.04	288.00	667.20	0.01	1.59	0.055
C2-C3	37.20	619.57	652.56	0.13	2.90	0.055
C4-C6	69.50	833.80	493.07	0.24	4.91	0.055
C7-C15	140.96	1090.35	315.44	0.62	9.00	0.105
C16-C27	280.99	1351.83	239.90	0.96	17.10	0.105
C28+	519.92	1696.46	238.12	1.27	32.50	0.105

In **Table 7.1.2.1** MW refers to molecular weight, T_c refers to critical temperature, P_c refers to critical pressure, V_c refers to critical volume, and BIC refers to binary interaction coefficients between CO_2 and each hydrocarbon pseudo-component. All the other binary interaction coefficients were set to zero.

Figures 7.1.2.1 and **7.1.2.2** present a comparison of predictions of the volumetric oil rate versus time and the volumetric gas rate versus time of UTCOMP and Coats (1980) formulation for the second case study. Although the predictions are similar, we can see that UTCOMP predicts an earlier breakthrough than GPAS. This difference appears because of the different relative permeability models implemented in GPAS and in UTCOMP. Both of them use Corey's model as indicated in **Table 7.1.1.2**, but UTCOMP has a three-phase interpolation procedure which is not implemented in GPAS. **Figures 7.1.2.3** and **7.1.2.4** present the gas saturation field and the second hydrocarbon liquid field saturation for Case 1 at 500 days.

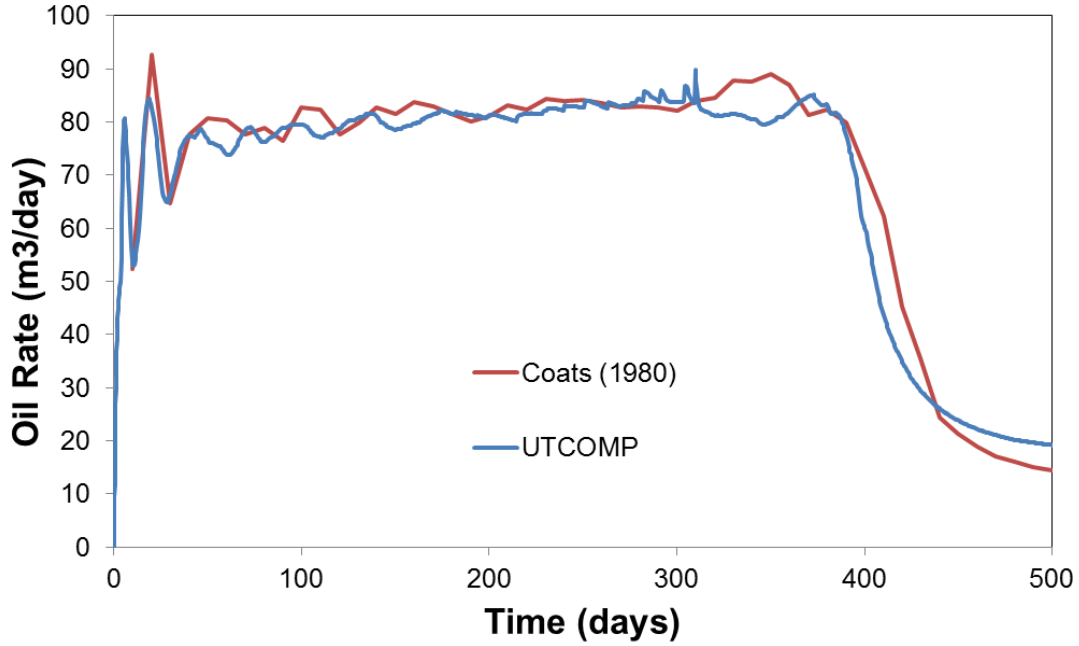

Figure 7.1.2.1. Volumetric oil rate versus time for Case 2.

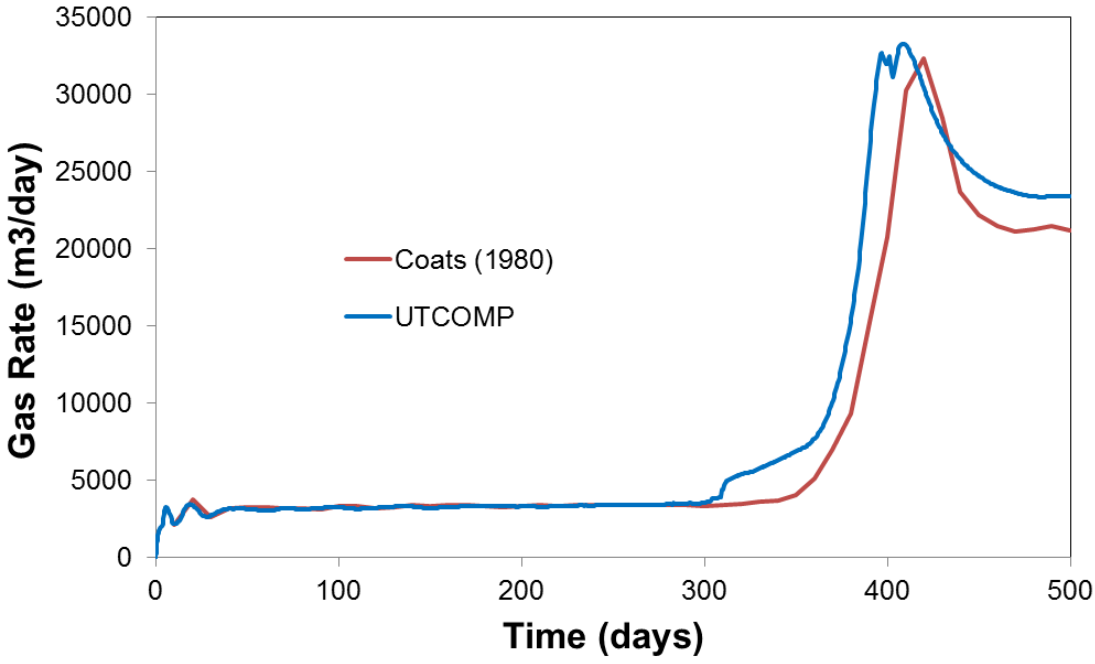

Figure 7.1.2.2. Volumetric gas rate versus time for Case 2.

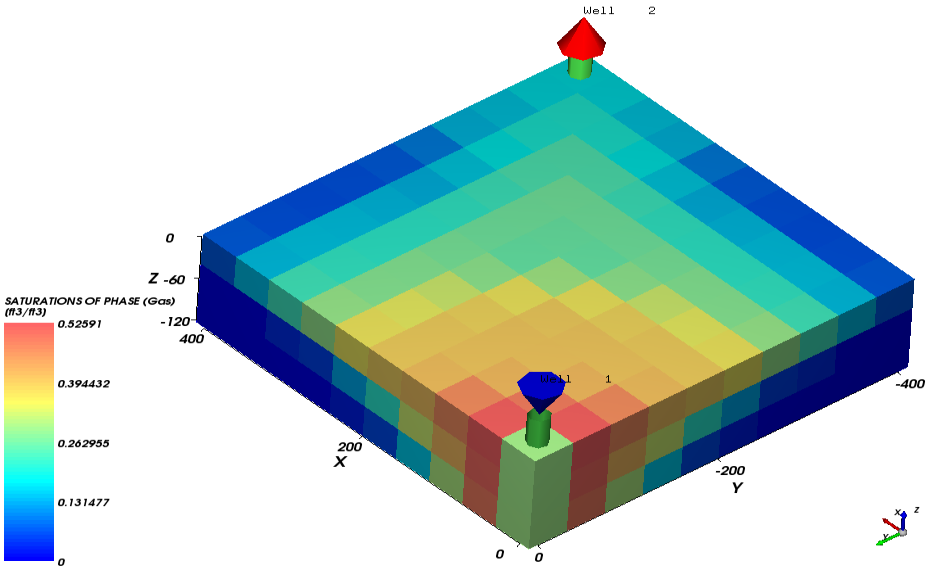

Figure 7.1.2.3. Gas saturation field for Case 2 at 500 days.

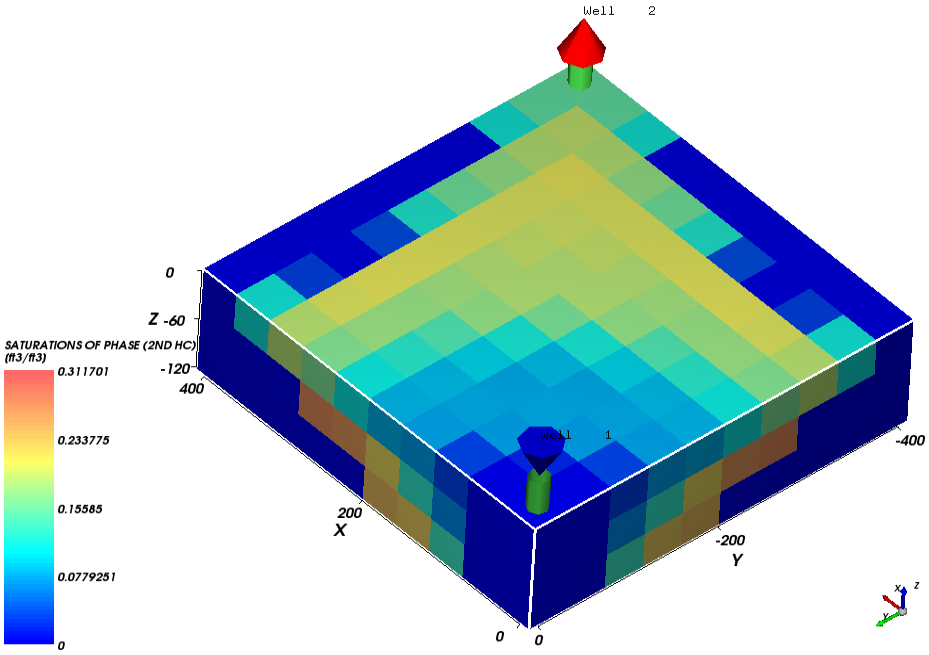

Figure 7.1.2.4. Second hydrocarbon liquid field saturation for Case 2 at 500 days.

7.2 DISPERSIVITY TENSOR APPLICATIONS

As discussed before, Coats (1980) formulation was enhanced with the implementation of the physical dispersion term. This section presents four simulation case studies for the investigation of the dispersion tensor effect in conjunction with the EbFVM approach.

7.2.1 One dimensional tracer injection

The first case study refers to simulation of a tracer injected into a one-dimensional isotropic and homogeneous reservoir saturated with water. **Figure 7.2.1.1** shows a schematic view of this case and **Table 7.2.1.1** presents the fluid and physical properties.

Because GPAS does not have a tracer component, we mimic tracer flooding using two components with same parameters. Also, we had to hard code a constant density value to guarantee an incompressible fluid flow.

Figure 7.2.1.1. Schematic view of Case 1.

Table 7.2.1.1. Input data for Case 1

Grid blocks dimension in x, y, and z directions	1000 x 1 x 1
Length (m)	12.19
Width (m)	0.03048
Thickness (m)	0.03048
Porosity (fraction)	0.2
Rock compressibility (kPa^{-1})	0.0
Reservoir temperature (^oC)	83.3
Permeability in x direction (m^2)	$5x10^{-13}$
Water viscosity (Pa.s)	$1.0x10^{-3}$
Water density (mol/m^3)	$39.77x10^3$
Water compressibility (kPa^{-1})	0.0
Initial water saturation (fraction)	1.0
Initial reservoir pressure (MPa)	13.79
Producer bottom hole pressure (MPa)	13.79
Tracer injection rate (m^3/s)	$1.31x10^{-8}$
Peclet Number	200
Tracer mole fraction	1.0

Figure 7.2.1.2 presents results of the dimensionless concentration of tracer versus the dimensionless length of the reservoir for case 1. The results of this simulation using the GPAS simulator in conjunction with Cartesian grid are also shown and both are compared with the analytical solution. **Figure 7.2.1.2** shows that the results of the present work using a hexahedron element (500 elements; 2004 vertices) and the Cartesian (1000 grid blocks) mesh match the analytical solution. It is important to mention that the number of vertices of the EbFVM approach is equal to the number of control volumes. Also, a 3D formulation is used to run this case. Therefore, for the discretization of the

problem, we have 501 control volumes in the flux direction. Thus, we can verify that the number of control volumes for the coarse Cartesian mesh is about twice as larger than that of the hexahedron grid.

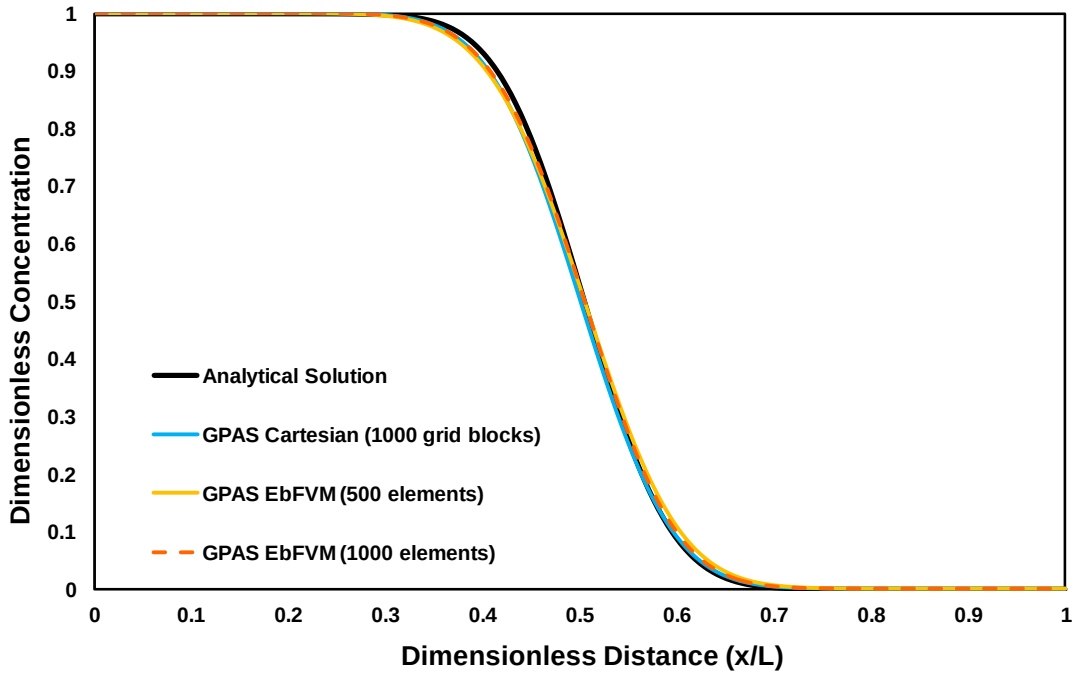

Figure 7.2.1.2. Dimensionless concentration versus dimensionless distance after 0.5 pore volume of tracer injection for Case 1.

7.2.2 Two dimensional tracer slug injection

The second case study refers to a two-dimensional simulation in a quarter-of-five spot of a tracer injection in a homogeneous and isotropic saturated reservoir. The fluid and physical properties are given in **Table 7.2.2.1**.

Table 7.2.2.1. Input data for Case 2

Grid blocks dimension in x, y, and z directions	100 x 100 x 1
Length (m)	502.92
Width (m)	502.92
Thickness (m)	0.3048
Porosity (fraction)	0.2
Rock compressibility (kPa^{-1})	0.0
Reservoir temperature (^oC)	83.3
Permeability in x direction (m^2)	$5x10^{-13}$
Permeability in y direction (m^2)	$5x10^{-13}$
Water viscosity (Pa.s)	$1x10^{-3}$
Water density (mol/m^3)	$39.77x10^3$
Water compressibility (kPa^{-1})	0.0
Initial water saturation (fraction)	1.0
Initial reservoir pressure (MPa)	0.689
Producer bottom hole pressure (MPa)	0.689
Injector well rate (m^3/s)	$5.12x10^{-3}$
Longitudinal dispersivity (m)	2.01
Transversal dispersivity (m)	0.201
Slug size (pore volume)	0.02
Tracer mole fraction	1.0

The results in terms of normalized effluent tracer concentration obtained for Case 2 are shown in **Figure 7.2.2.1**. This figure compares several hexahedron grids in conjunction with the EbFVM approach and Cartesian meshes and the analytical solution given by Abbaszadeh-Dehghani and Brigham (1984). From this comparison, we can see that a good match for the breakthrough time was obtained with the 100x100x1 EbFVM mesh, but the same was not true for the same level of refinement of the Cartesian mesh.

Also, it can be observed that for all the three levels of grid refinement investigated (30x30, 50x50, and 100x100), the EbFVM approach always produced concentration curves with less numerical dispersion compared to the original GPAS approach using Cartesian grids. It is also important to note that an upwind scheme was used for both formulations (EbFVM and Cartesian).

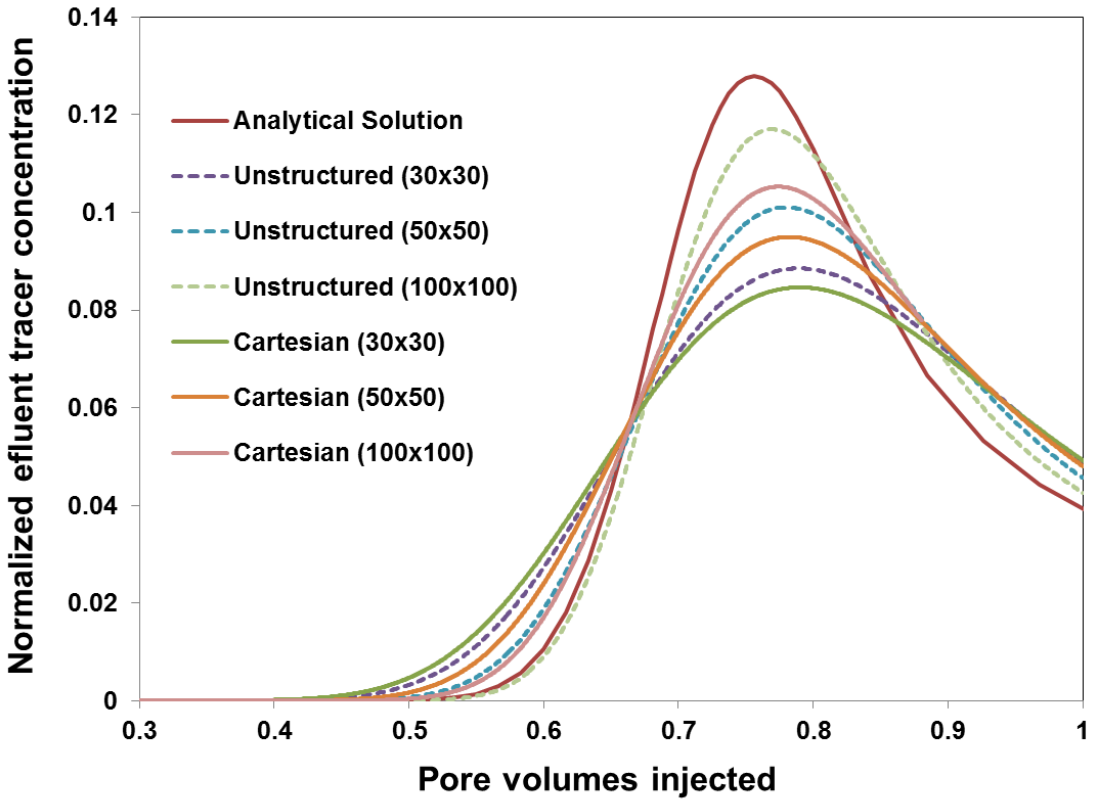

Figure 7.2.2.1. Normalized effluent tracer concentration versus pore volumes injected.

Figures 7.2.2.2 and **7.2.2.3** present the mole fraction of tracer at 15 days of simulation for the 100x100 Cartesian mesh and the 100x100 EbFVM mesh, respectively. Comparing these figures, we can see that the EbFVM formulation results in sharper

fronts as a result of less numerical dispersion. Therefore, with the same number of elements, the EbFVM approach better represents the modeled phenomenon.

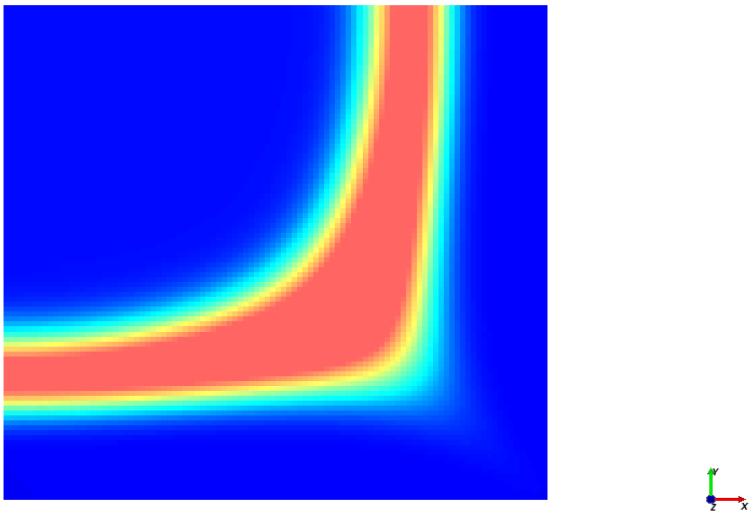

Figure 7.2.2.2. Mole fraction of tracer at 15 days for the 100x100 Cartesian mesh.

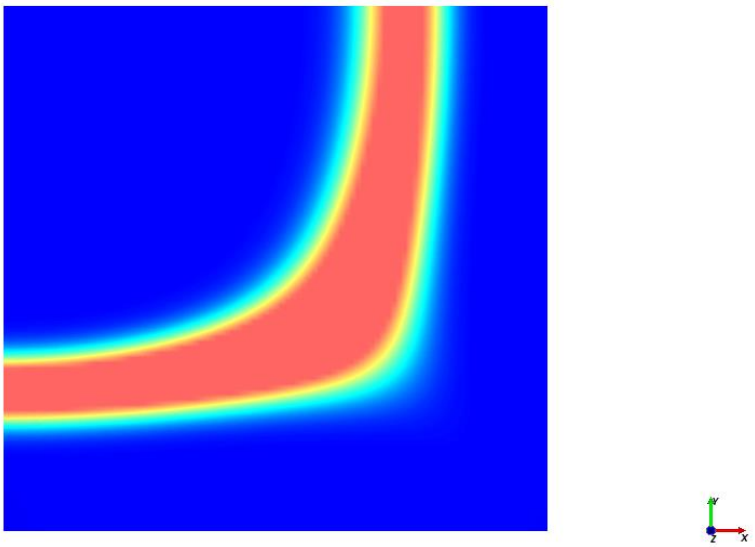

Figure 7.2.2.3. Mole fraction of tracer at 15 days for the 100x100 EbFVM mesh.

7.2.3 Three dimensional solvent injection

The third case study refers to solvent injection in a quarter-of-five spot, but a heterogeneous reservoir has been considered and a 3D variation of fluid and rock properties has been taken into account. **Tables 7.2.3.1** and **7.2.3.2** present the fluid and physical properties and Corey's model coefficients, respectively. The horizontal absolute permeability field is shown in **Figure 7.2.3.1**. For each grid block, the same value of K_{xx} was used for $K_{yy,}$ and the value of K_{zz} was set to one tenth of the K_{xx} component. The other components of the absolute permeability tensor were set to zero.

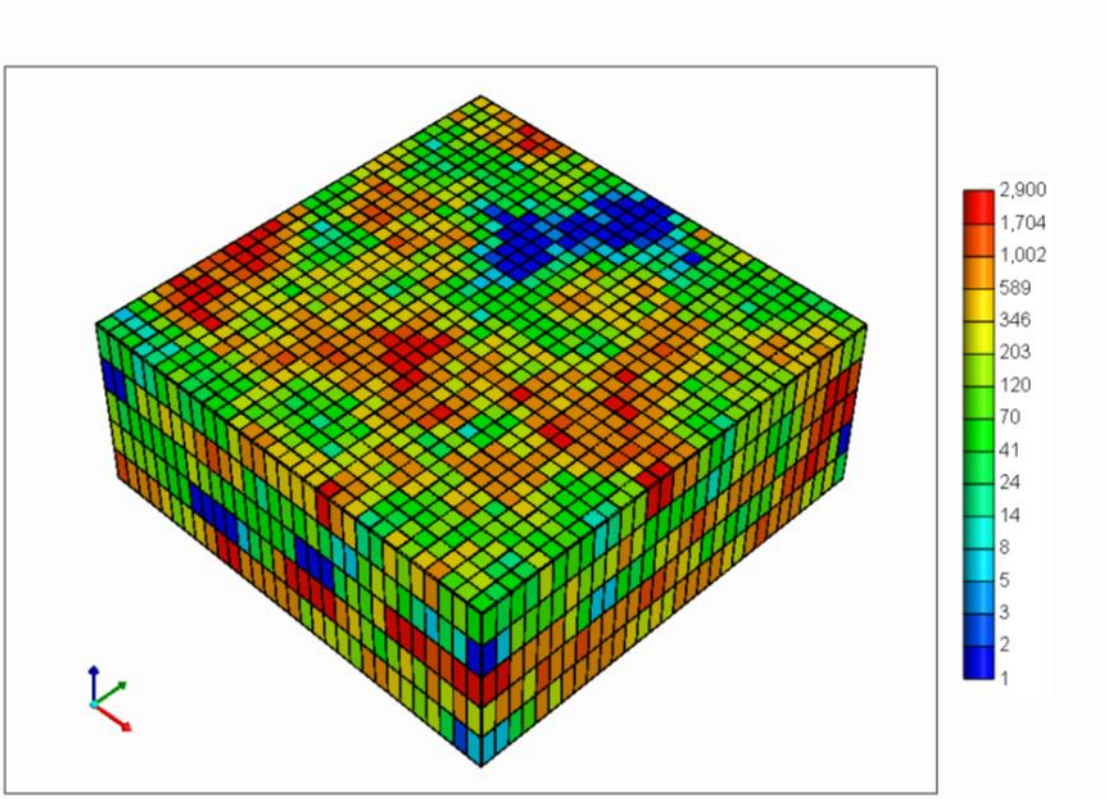

Figure 7.2.3.1. Horizontal absolute permeability field for Case 3.

Table 7.2.3.1. Input data for Case 3

Grid blocks dimension in x, y, and z directions	30 x 30 x 5	
Length (m)	609.6	
Width (m)	609.6	
Thickness (m)	60.96	
Porosity (fraction)	0.3	
Rock compressibility (kPa^{-1})	$5.8x10^{-7}$	
Reservoir temperature (^oC)	37.7	
Permeability in x direction (m^2)	Figure 7.2.3.1	
Permeability in y direction (m^2)	Figure 7.2.3.1	
Permeability in z direction (m^2)	0.1 K_{xx}	
Water viscosity (Pa.s)	$8x10^{-4}$	
Water density (mol/m^3)	$55.55x10^3$	
Water compressibility (kPa^{-1})	$4.35x10^{-7}$	
Initial water saturation (fraction)	0.25	
Initial reservoir pressure (MPa)	13.79	
Producer bottom hole pressure (MPa)	13.10	
Gas injection rate (m^3/s)	3.28 m^3/s	
Longitudinal dispersivity (m)	2.01	
Transversal dispersivity (m)	0.201	
Tracer mole fraction	1.0	
Reservoir fluid initial composition	CO_2	0.01
	C1	0.20
	C3	0.30
	C6	0.05
	C10	0.025
	C15	0.025
	C20	0.39

Table 7.2.3.1 – Continued. Input data for Case 3

Injected fluid composition	CO_2	0.7
	C1	0.2
	C3	0.065
	C6	0.02
	C10	0.01
	C15	0.004
	C20	0.001

Table 7.2.3.2. Corey's model relative permeability data for Case 3

	Water	Oil	Gas	Second oil
End point relative permeability	0.3	0.75	0.9	0.9
Residual saturation	0.25	0.2	0.0	0.0
Exponent of relative permeability	2.0	2.0	2.0	2.0

The results for Case 3, in terms of volumetric rates at standard conditions of oil and gas, obtained in conjunction with hexahedron element and Cartesian grid are shown in **Figures 7.2.3.2** and **7.2.3.3**. From these figures, we can observe that the volumetric rates by the hexahedron mesh are similar to the ones obtained by the Cartesian mesh. Spikes in the curves are due to phase changes in the reservoir associated with phase composition and pressure changes. Comparing both curves, we can see that the breakthrough in the EbFVM mesh occurred later than in the Cartesian one. **Figures 7.2.3.4** and **7.2.3.5** present CO_2 concentration fields at 2500 days for both EbFVM and Cartesian grids, respectively. From these figures, we can see that although the fronts are similar, the EbFVM mesh presents sharper fronts, since the numerical dispersion is lower for this approach.

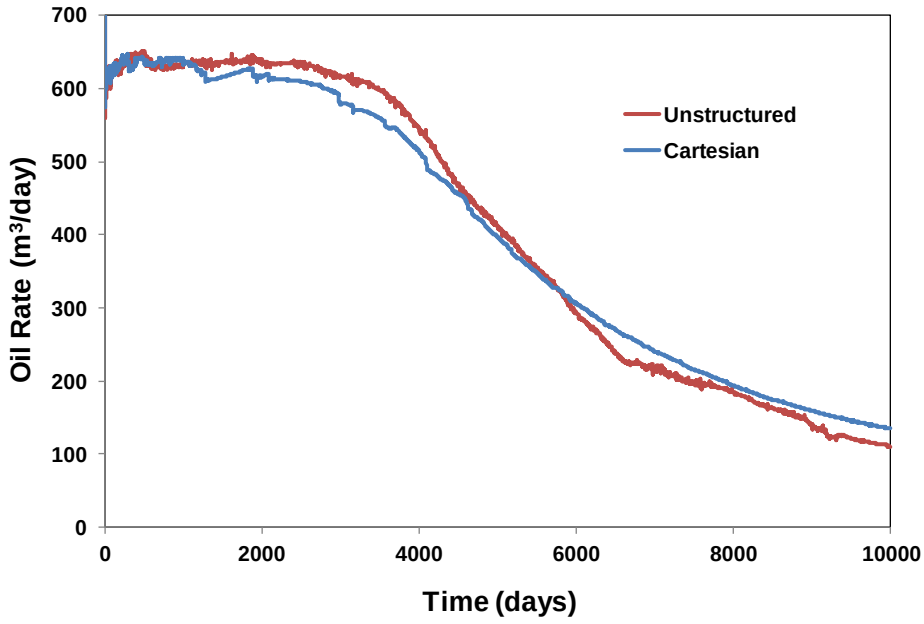

Figure 7.2.3.2. Oil production rate vs. time for Case 3.

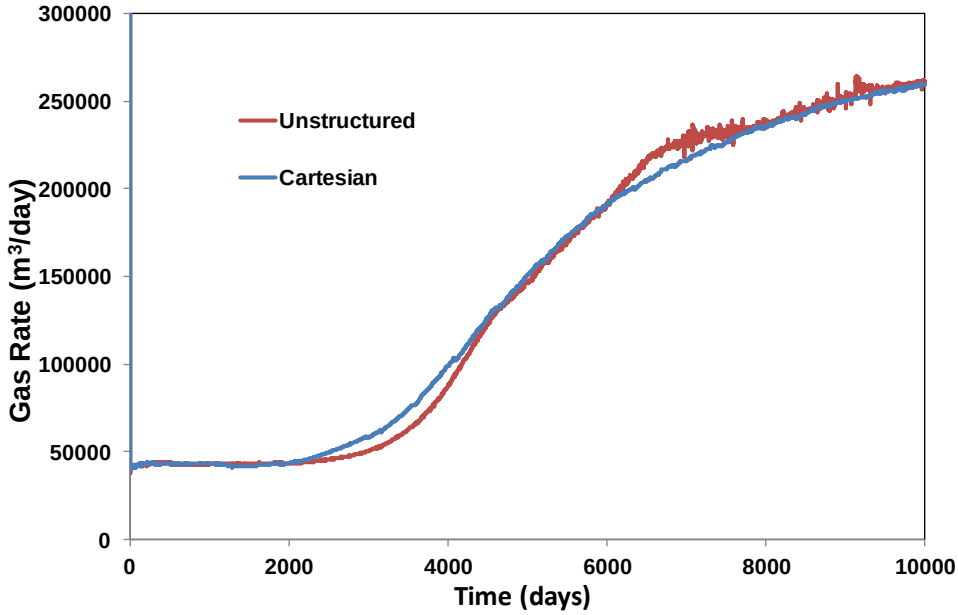

Figure 7.2.3.3. Gas production rate vs. time for Case 3.

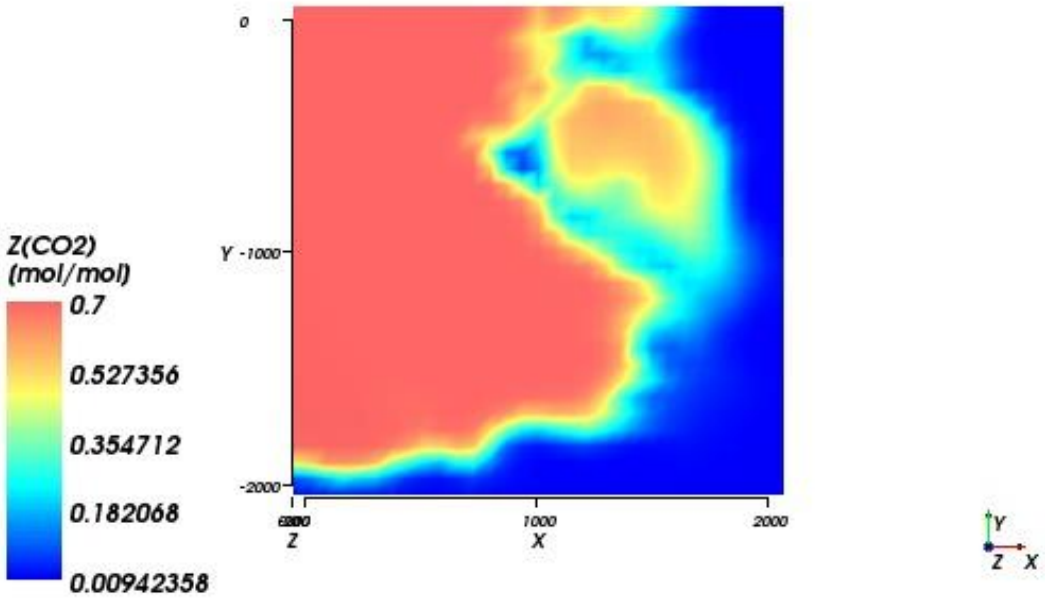

Figure 7.2.3.4. EbFVM CO_2 mole fraction field at 2500 days for Case 3.

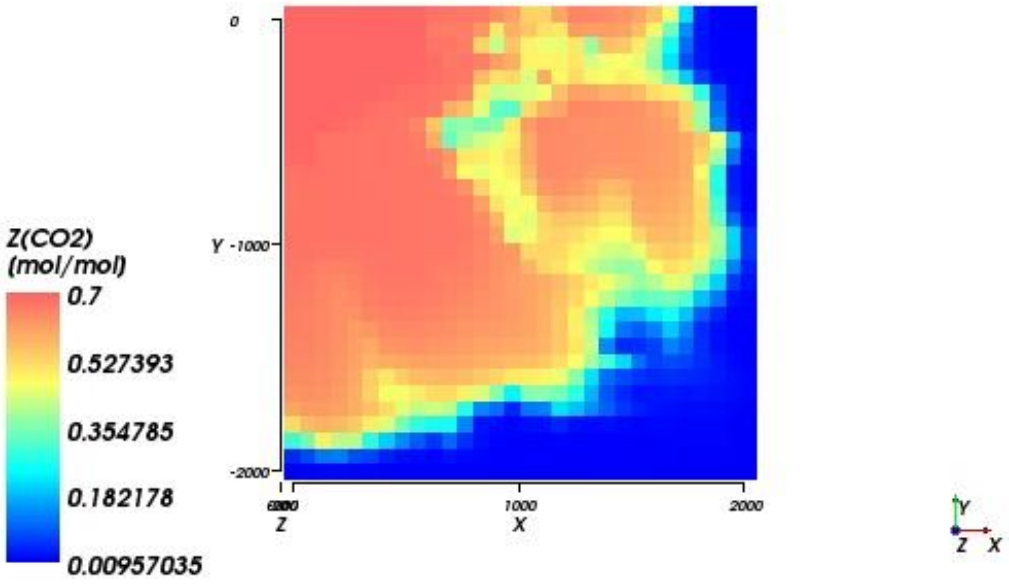

Figure 7.2.3.5 Cartesian CO_2 mole fraction field at 2500 days for Case 3.

7.2.4 Three dimensional solvent injection

The last case study is simulation of solvent injection into an irregular shaped reservoir. Except for the reservoir dimensions and the absolute permeabilities, we used the same properties shown in **Tables 7.2.3.1** and **7.2.3.2**. **Figures 7.2.4.1** and **7.2.4.2** show two grid-configurations employed for this reservoir. The first mesh, **Figure 7.2.4.1**, is composed only of hexahedrons, while the other one, **Figure 7.2.4.2**, is a hybrid mesh composed of tetrahedron, pyramid and hexahedron elements. In **Figures 7.2.4.1** and **7.2.4.2**, we show the reservoir top and bottom topologies, respectively. From these figures, we can see that this reservoir is irregularly shaped in x, y, and z directions. The absolute permeabilities in x and y directions are $5.0x10^{-13}$ m^2 (500 mD), and the absolute permeability in z direction is $5.0x10^{-14}$ m^2 (50 mD). For each injection well, we used the volumetric rate given in **Table 7.2.3.1**.

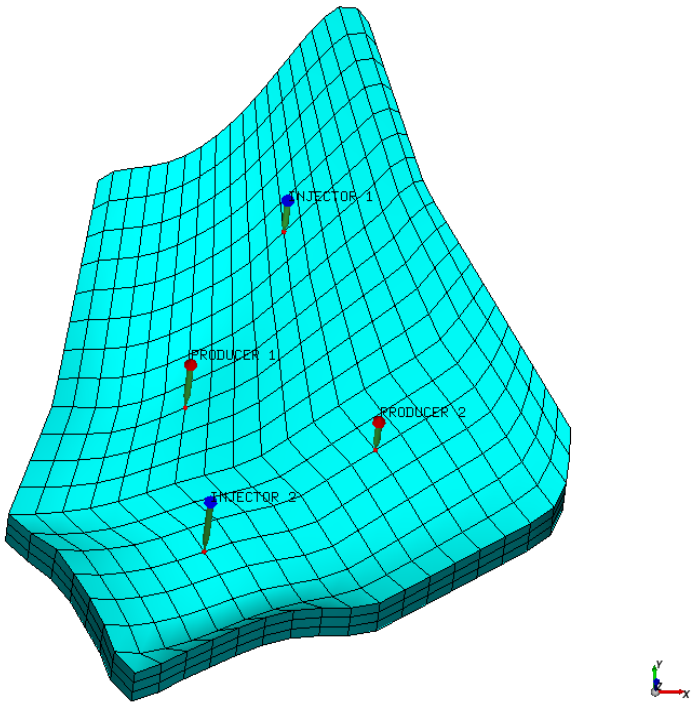

Figure 7.2.4.1. Reservoir and grid-configurations used for Case 4 (top view).

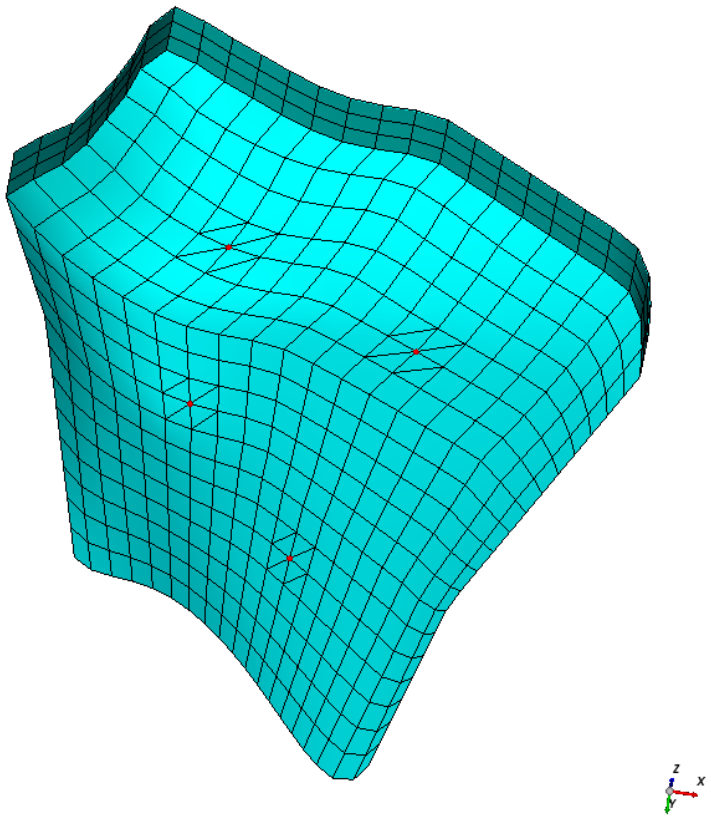

Figure 7.2.4.2. Reservoir and grid-configurations used for Case 4 (Bottom view).

Figures 7.2.4.3 and **7.2.4.4** present the results, in terms of oil and gas volumetric rates at standard condition, respectively, for the last case study in conjunction with the two meshes shown in **Figures 7.2.4.1** and **7.2.4.2**. Although the two grid configurations are different, the results in terms of oil and gas rates for both grids are in good agreement. The CO_2 mole fraction for two simulation times is shown in **Figures 7.2.4.5** through **7.2.4.8** for the two grid configurations. From these figures, it can be seen that a good agreement between results using two different grid configurations has been obtained.

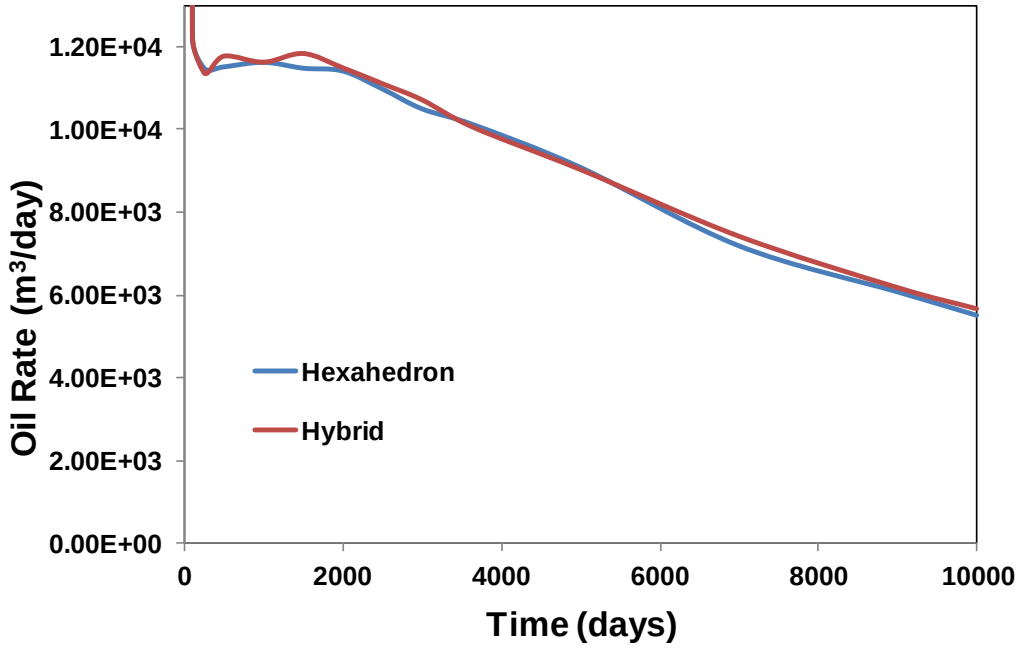

Figure 7.2.4.3. Oil production rate vs. time for Case 4.

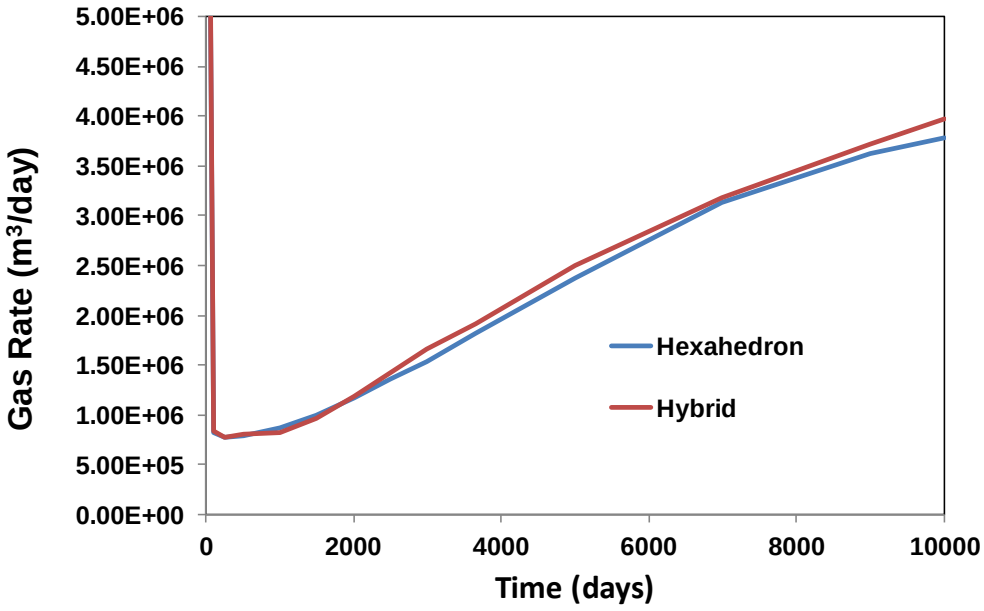

Figure 7.2.4.4. Gas production rate vs. time for Case 4.

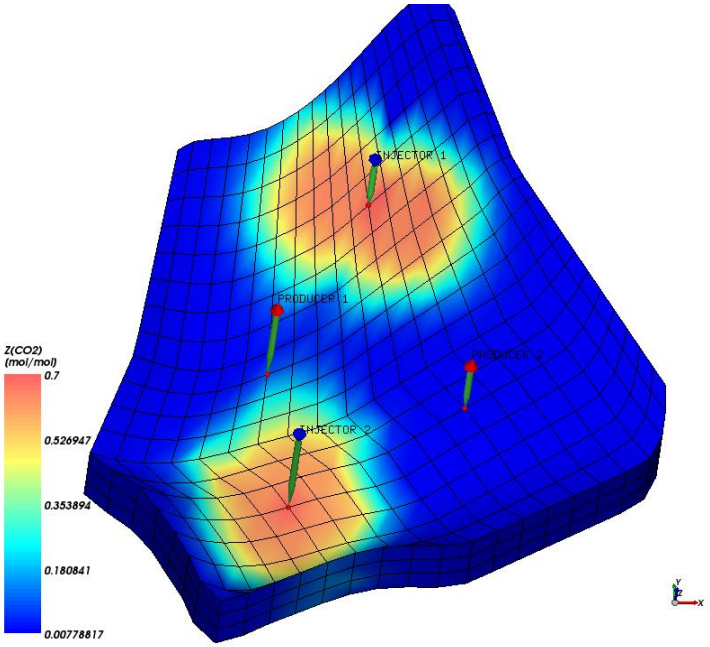

Figure 7.2.4.5. CO_2 mole fraction field in conjunction with hexahedron meshes at 1500 days for Case 4.

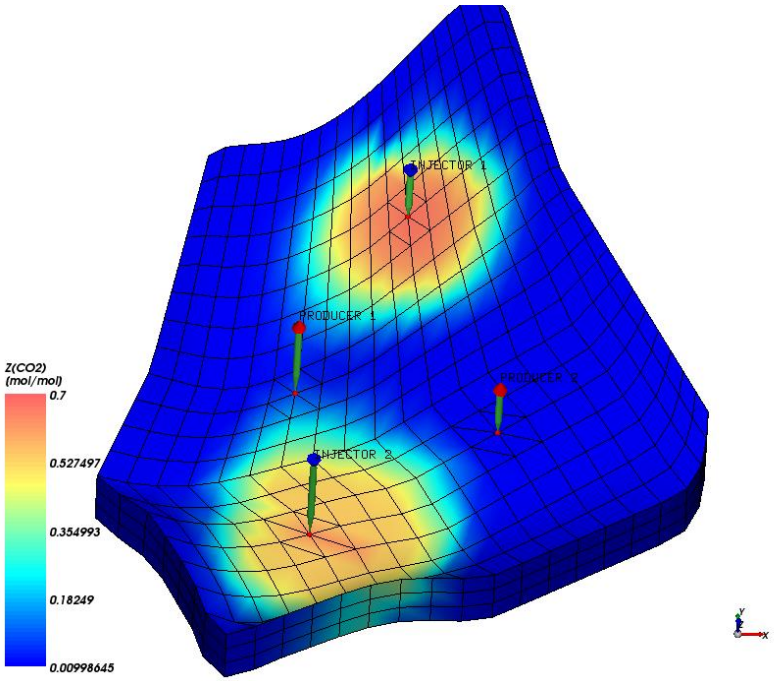

Figure 7.2.4.6. CO_2 mole fraction field in conjunction with hybrid meshes at 1500 days for Case 4.

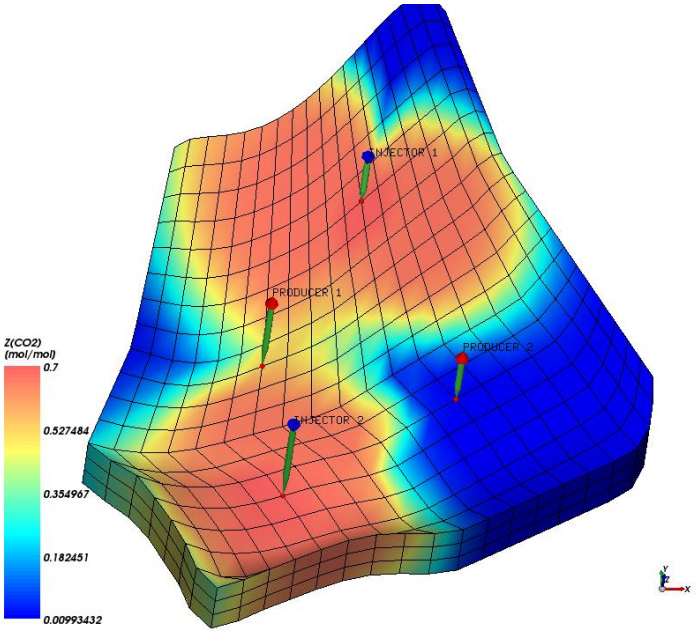

Figure 7.2.4.7. CO_2 mole fraction field in conjunction with hexahedron meshes at 7000 days for Case 4.

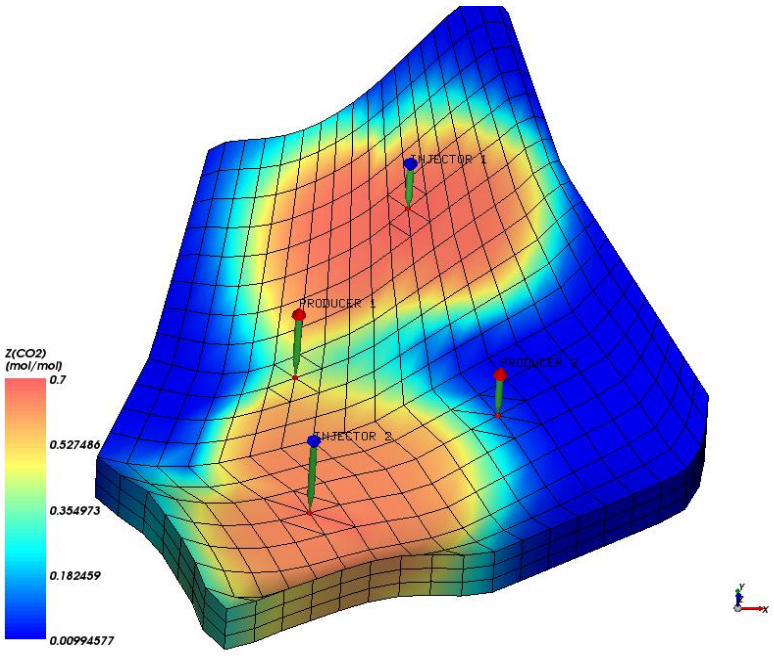

Figure 7.2.4.8. CO_2 mole fraction field in conjunction with hybrid meshes at 7000 days for Case 4.

7.3 UNSTRUCTURED GRID APPLICATIONS

In this section, the unstructured grid applications are presented. First, we present one two-dimensional application using Coats (1980) in conjunction with unstructured mesh of quadrilaterals and triangles in Subsection 7.3.1. Then, we present several three-dimensional applications in conjunction with unstructured mesh of hexahedrons, prisms, pyramids, and tetrahedrons.

7.3.1 Two-dimensional Application

In this subsection, one two-dimensional application of unstructured grid in conjunction with quadrilaterals and triangles is presented. The case study refers to a quarter of five-spot using six components for the fluid model. Five simulations are compared. Two Cartesian meshes of 25x25 and 50x50 grid blocks, one mesh of quadrilaterals, one mesh of triangles, and one hybrid mesh of triangles and quadrilaterals. **Table 7.3.1.1** presents the physical properties and initial conditions for this case.

Table 7.3.1.1. Physical properties for the two-dimensional unstructured grid application

Length (m)	170.7	
Width (m)	170.7	
Thickness (m)	30.5	
Porosity (fraction)	0.35	
Rock compressibility (kPa^{-1})	$1.45x10^{-7}$	
Reservoir temperature (^oC)	71.1	
Permeability in x direction (m^2)	$1x10^{-14}$	
Permeability in y direction (m^2)	$1x10^{-14}$	
Permeability in z direction (m^2)	$1x10^{-14}$	
Water viscosity (Pa.s)	$1x10^{-3}$	
Water density (mol/m^3)	$55.55x10^3$	
Water compressibility (kPa^{-1})	$4.35x10^{-7}$	
Initial water saturation (fraction)	0.17	
Initial reservoir pressure (MPa)	10.34	
Gas injection rate (m^3/s)	0.3277	
Producer bottom hole pressure (MPa)	8.96	
Reservoir fluid initial composition	C1	0.5
	C3	0.03
	C6	0.07
	C10	0.2
	C15	0.15
	C20	0.05

Table 7.3.1.1 – Continued. Physical properties for the two-dimensional unstructured grid application

Injected fluid composition	C1	0.77
	C3	0.2
	C6	0.01
	C10	0.01
	C15	0.005
	C20	0.005

Table 7.3.1.2. Corey's model relative permeability data for the two-dimensional unstructured grid application

	Water	Oil	Gas
End point relative permeability	0.4	0.9	0.9
Residual saturation	0.3	0.1	0.0
Exponent of relative permeability	3.0	2.0	2.0

Figures 7.3.1.1 and **7.3.1.**2 present the oil production rate versus time and the gas production rate versus time, respectively, for the five simulations performed for this case study. From these figures, we can see that all the five simulations had similar results. It is also important to notice from these figures that a significant larger number of grid blocks were required to simulate the Cartesian cases.

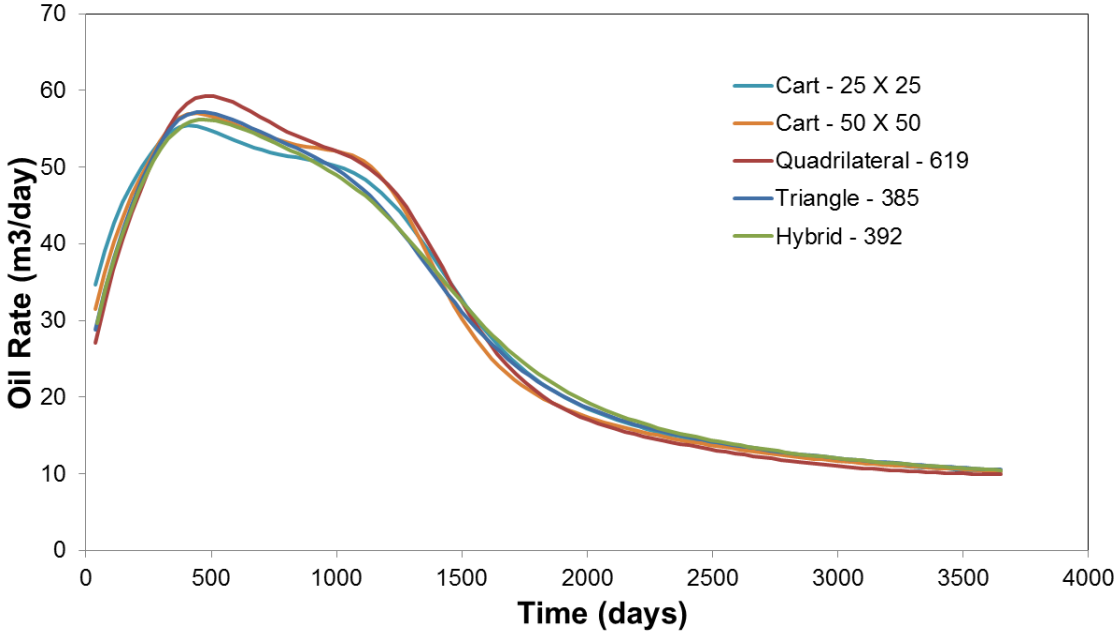

Figure 7.3.1.1. Results for the two-dimensional unstructured grid application in terms of oil production rate vs. time.

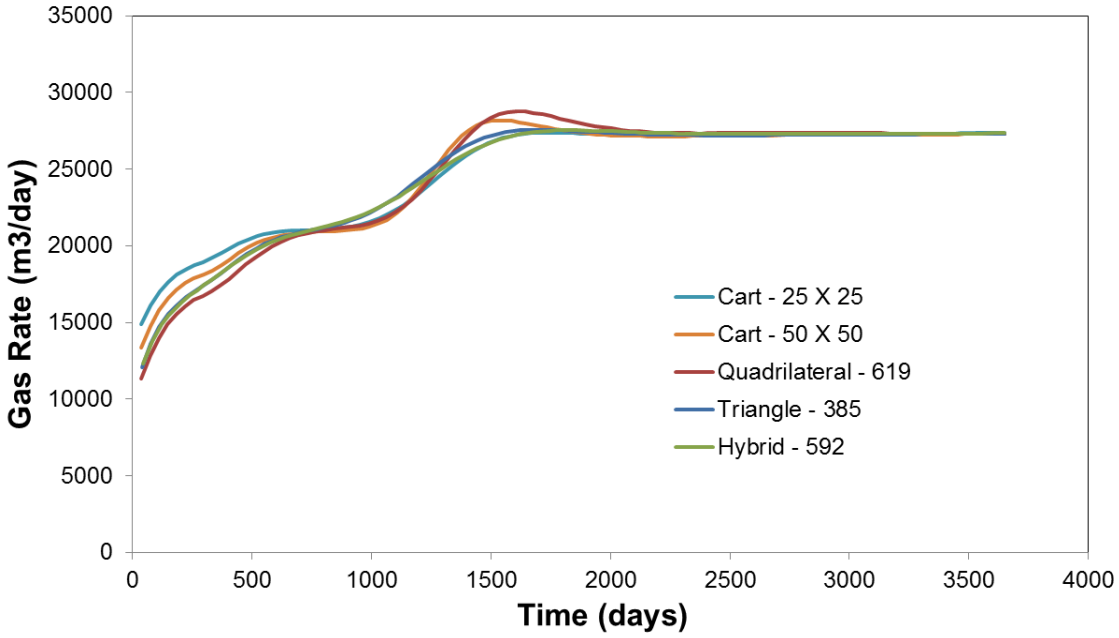

Figure 7.3.1.2. Results for the two-dimensional unstructured grid application in terms of gas production rate vs. time.

Figures 7.3.1.3 and **7.3.1.4** present the gas saturation field for the triangle elements mesh and the hybrid elements mesh. From these figures, we can see that using elements of triangles and both elements of triangles and quadrilaterals gave us similar results.

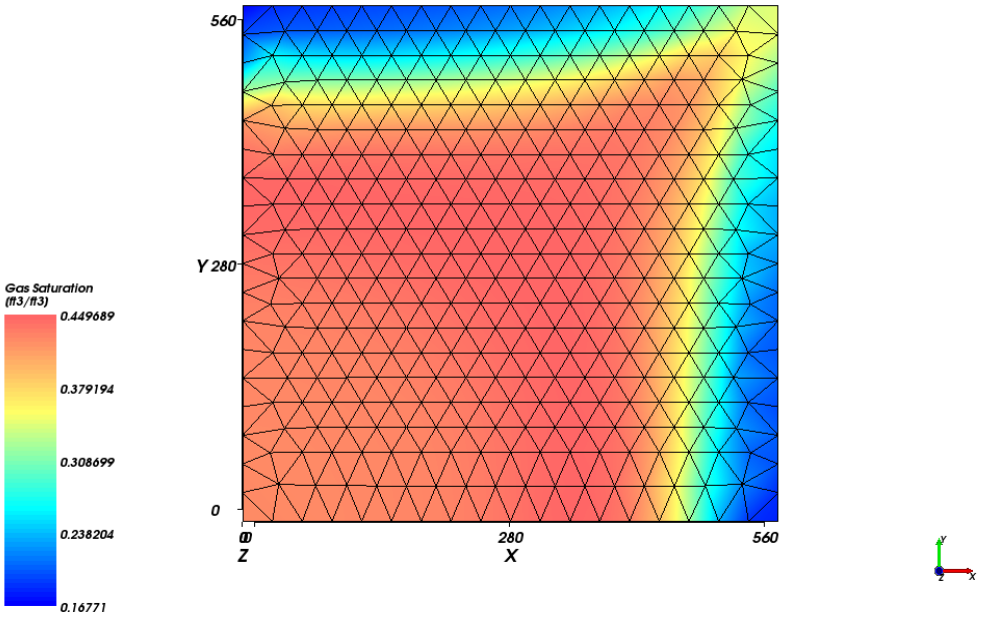

Figure 7.3.1.3. Gas saturation field for the two-dimensional unstructured grid application in conjunction with triangle elements.

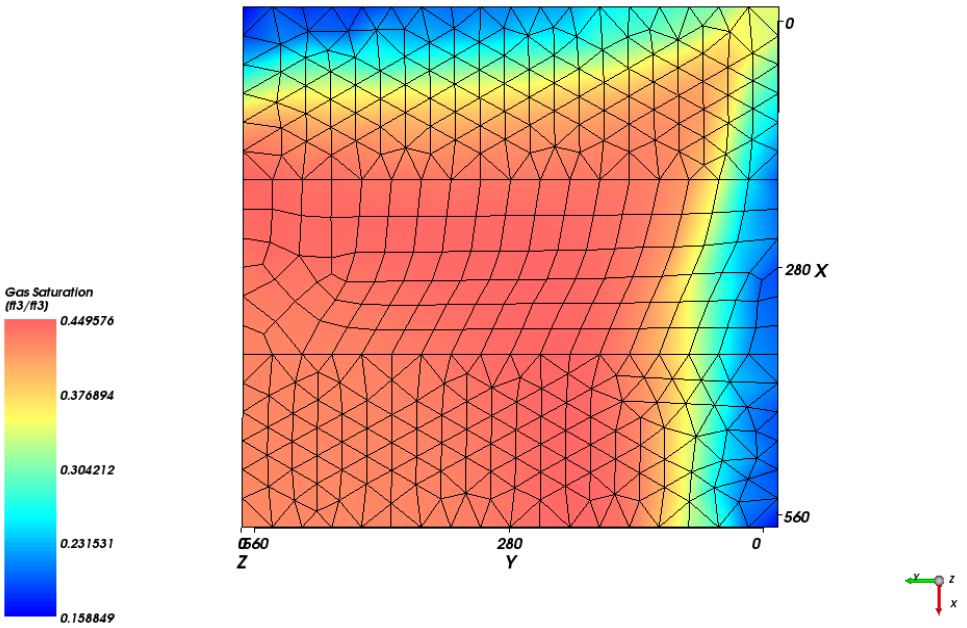

Figure 7.3.1.4. Gas saturation field for the two-dimensional unstructured grid application in conjunction with a hybrid mesh of triangles and quadrilaterals elements.

7.3.2 Three-dimensional Applications

This subsection presents four simulation case studies using the EbFVM approach implemented in the Coats (1980) formulation. The first case study was used to validate the implementation of the four element types used to model the reservoir geometry. The results of this case study are validated with the GPAS simulator using Cartesian meshes. Case 1 is the simulation of six-component gas injection in a quarter-of-five spot with the simultaneous flow of gas and oil. **Figures 7.3.2.1** through **7.3.2.4** present the four-refined grid configurations used for this case. **Table 7.3.2.1** presents the fluid and physical properties. As we can see from **Table 7.3.2.1**, an isotropic and homogeneous reservoir was considered. The relative permeability data for Corey's model are given in **Table 7.3.2.2**.

Table 7.3.2.1. Input data for Case 1

Grid blocks dimension in x, y, and z directions	Figures 7.3.2.1 through 7.3.2.4	
Length (m)	170.69	
Width (m)	170.69	
Thickness (m)	30.48	
Porosity (fraction)	0.35	
Rock compressibility (kPa^{-1})	$1.45x10^{-7}$	
Reservoir temperature (^oC)	71.1	
Permeability in x direction (m^2)	$1.0x10^{-14}$	
Permeability in y direction (m^2)	$1.0x10^{-14}$	
Permeability in z direction (m^2)	$1.0x10^{-14}$	
Water viscosity (Pa.s)	$1x10^{-3}$	
Water density (mol/m^3)	$55.55x10^3$	
Water compressibility (kPa^{-1})	$4.35x10^{-7}$	
Initial water saturation (fraction)	0.17	
Initial reservoir pressure (MPa)	10.34	
Producer bottom hole pressure (MPa)	8.96	
Gas injection rate (m^3/s)	0.3277	
Reservoir fluid initial composition	C1	0.50
	C3	0.03
	C6	0.07
	C10	0.20
	C15	0.15
	C20	0.05

Table 7.3.2.1 – Continued. Input data for Case 1

Injected fluid composition	C1	0.77
	C3	0.20
	C6	0.01
	C10	0.01
	C15	0.005
	C20	0.005

Table 7.3.2.2. Corey's model relative permeability data

	Water	Oil	Gas
End point relative permeability	0.4	0.9	0.9
Residual saturation	0.3	0.1	0.0
Exponent of relative permeability	3.0	2.0	2.0

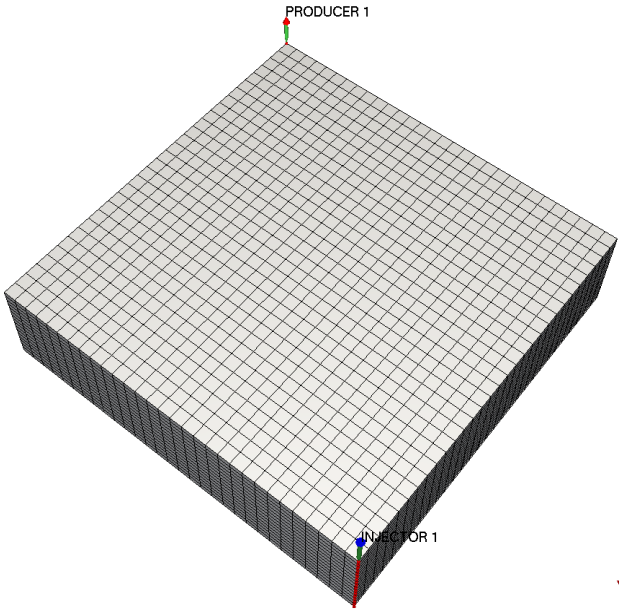

Figure 7.3.2.1 Hexahedron mesh for Case 1 (14,400 elements; 16,337 vertices).

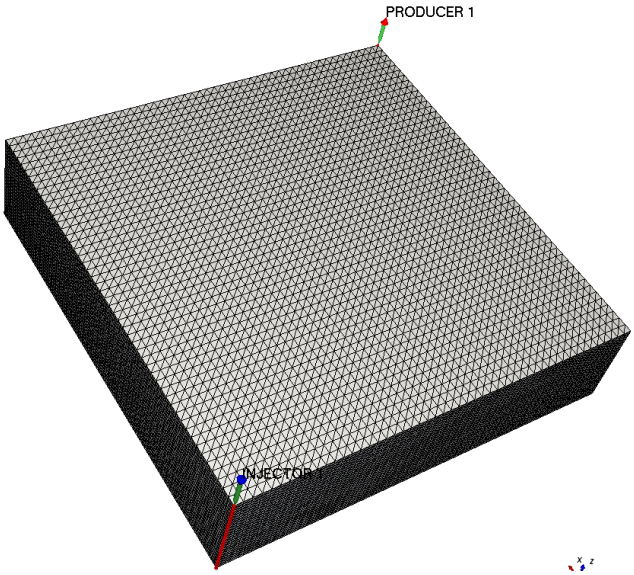

Figure 7.3.2.2. Tetrahedron mesh for Case 1 (375,000 elements; 67,626 vertices).

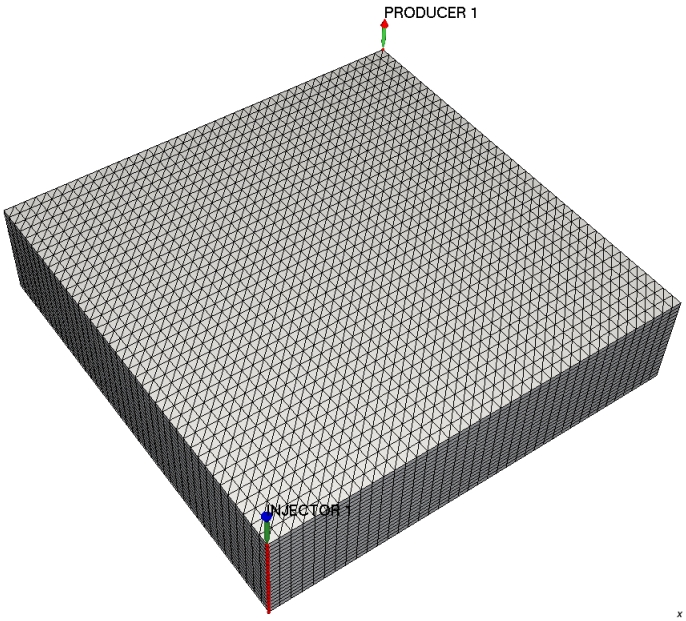

Figure 7.3.2.3. Prism mesh for Case 1 (64,000 elements; 35,301 vertices).

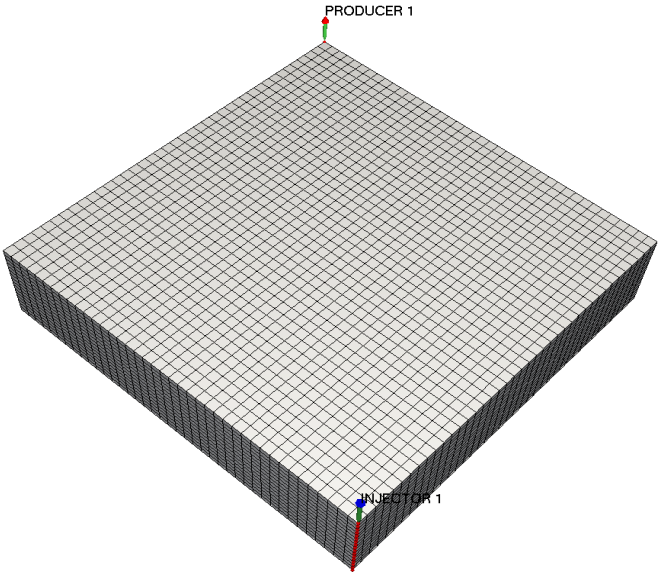

Figure 7.3.2.4. Pyramid mesh for Case 1 (153,600 elements; 54,177 vertices).

Figures 7.3.2.5 and **7.3.2.6** present the results of volumetric rate at standard conditions for oil, and gas phases, respectively, for Case 1 using all the four implemented elements. The results of this simulation using the GPAS simulator in conjunction with Cartesian grids are also shown. These figures show that the results of the present work using a Hexahedron (30x30x16 that is 14,400 elements; 16,337 vertices), a tetrahedron (50x50x25 that is 375,000 elements; 67,6226 vertices), a prism (40x40x20 that is 64,000 elements; 35,301 vertices), and pyramid (40x40x16 that is 153,600 elements; 54,177 vertices) mesh are quite similar for both oil and gas rates. We can also infer that the number of vertices of pyramid and tetrahedron elements is much larger compared to the hexahedron and prism elements. The reason for that is the shape functions used by the first two elements. It is important to mention that the number of vertices is equal to the number of control volumes. The number of vertices of tetrahedron mesh is about 3.16 times larger than the number of vertices of the hexahedron mesh. As mentioned by Maliska (2012), the numerical errors mainly of tetrahedron, prism, and pyramids elements cannot be classified as grid orientation effect, since these elements are randomly orientated along the domain. The errors exist, but they cannot be classified as grid orientation errors. We also can verify that the number of control volumes of the coarse Cartesian mesh is about 5.5 times larger than that of the hexahedron grid.

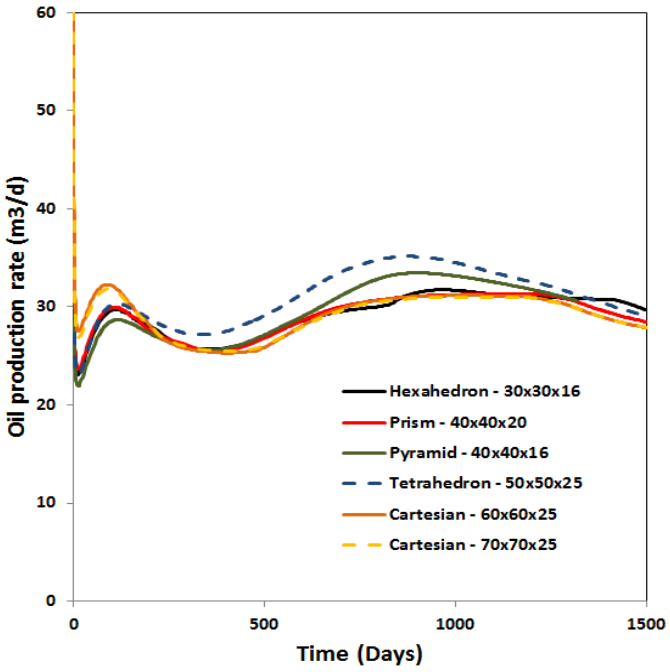

Figure 7.3.2.5. Results for Case 1 in terms of oil production rate vs. time.

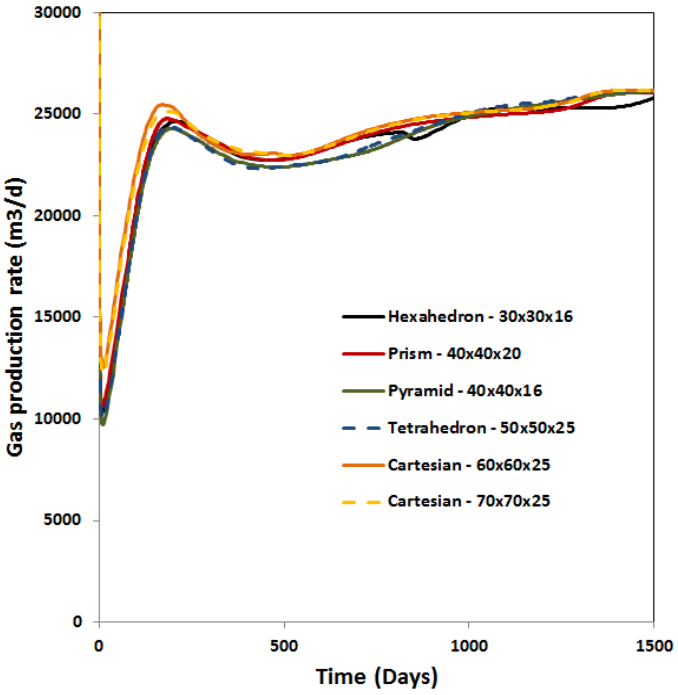

Figure 7.3.2.6. Results for Case 1 in terms of gas production rate vs. time.

The second case study also refers to gas injection in a quarter-of-five spot, but now an anisotropic and heterogeneous reservoir has been considered. Except for the porosity and absolute permeability field, all of the previous data presented for Case 1 were used. The K_{yy} component of the absolute permeability and porosity are presented in **Figures 7.3.2.7** and **7.3.2.8**. The K_{xx} component was equal set to K_{yy} component, K_{zz} component was equal set to one tenth of K_{xx} component, and the other components were set to zero.

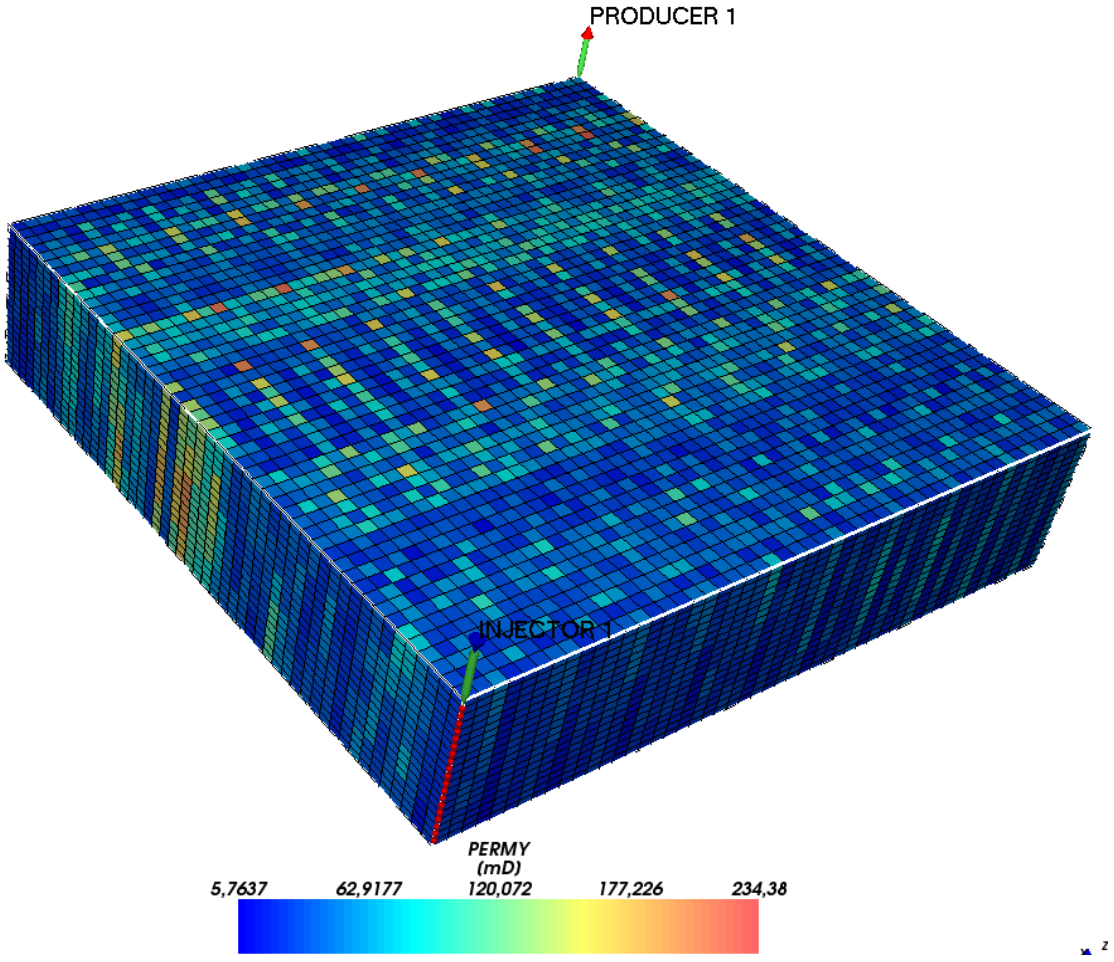

Figure 7.3.2.7 - Absolute permeability data used for Case 2.

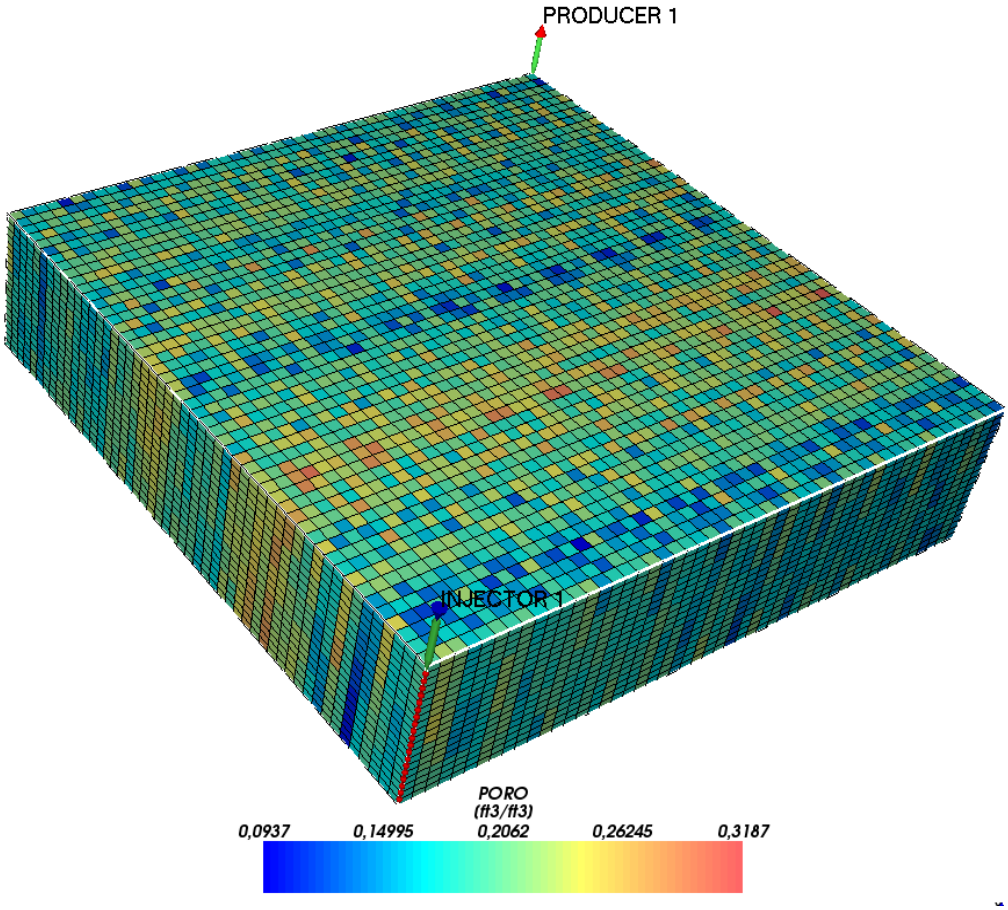

Figure 7.3.2.8. Porosity data used for Case 2.

The results in terms of volumetric rates of oil and gas at standard conditions obtained for Case 2 are shown in **Figures 7.3.2.9** and **7.3.2.10**. This case again refers to the characterization of six hydrocarbon components in a quarter of a five-spot. However, an anisotropic and a heterogeneous reservoir has been taken into account. Again, the results obtained in conjunction with the EbFVM for each one of the four types of elements are very close to each other for both oil and gas rates. The gas saturation obtained with the hexahedron element in two simulation times are presented in **Figures 7.3.2.11** and **7.3.2.12**. Due to the heterogeneity in porosity and permeability, the

saturation field is asymmetric in the beginning of the injection process. Later on, the effect disappears due to increase in saturation field.

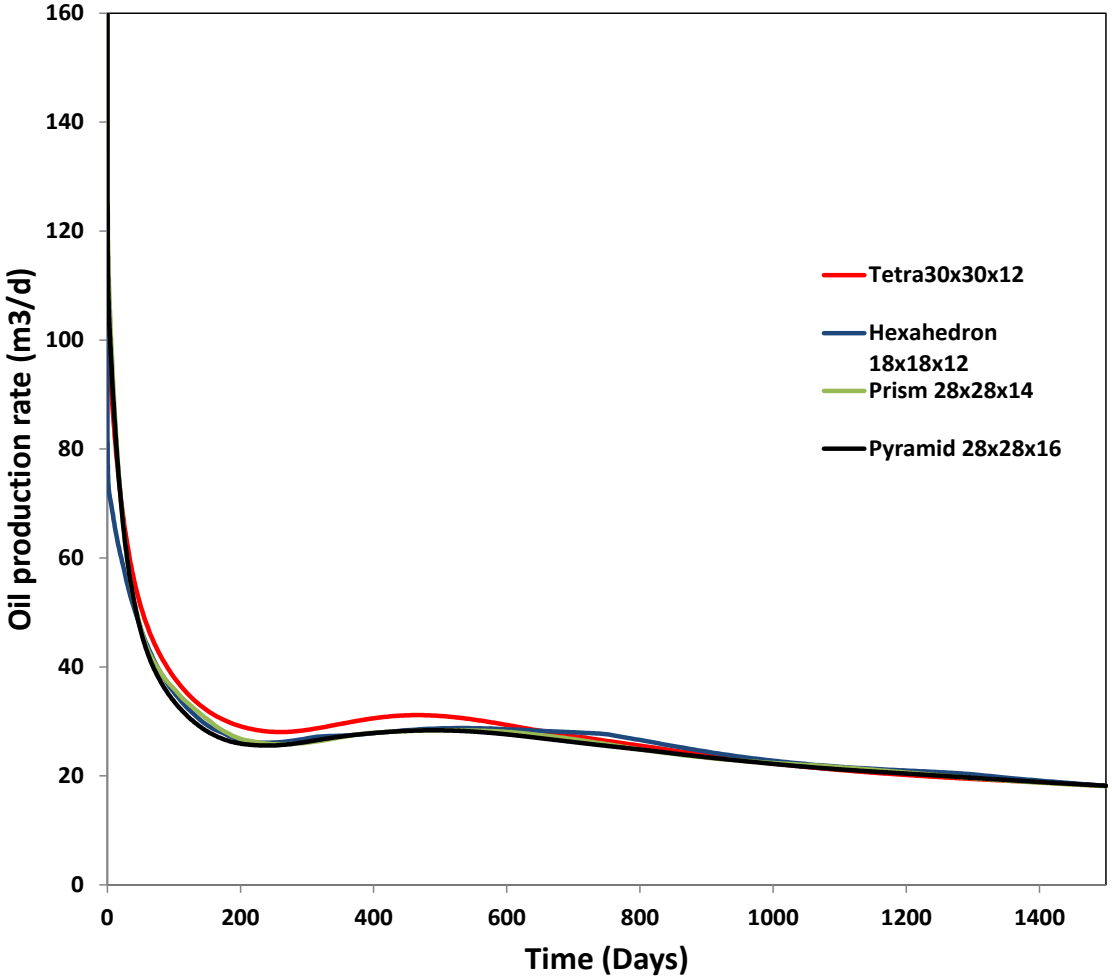

Figure 7.3.2.9. Oil production rate vs. time for Case 2.

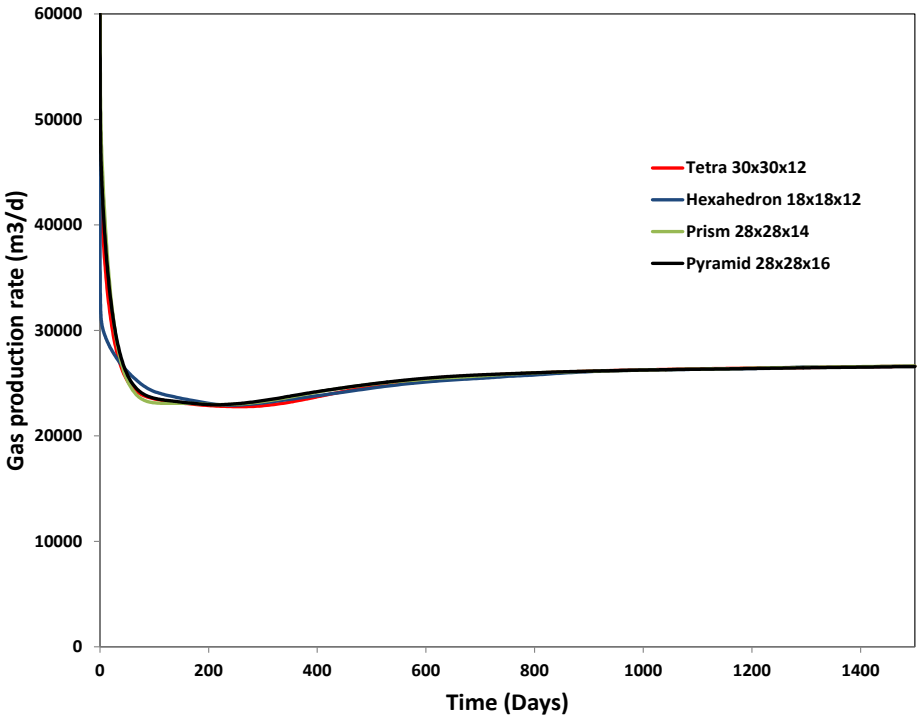

Figure 7.3.2.10. Gas production rate vs. time for Case 2.

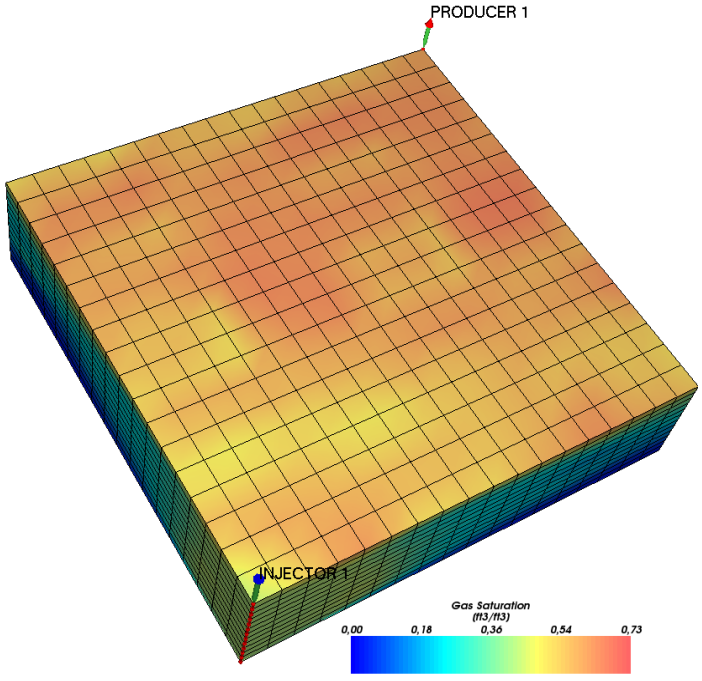

Figure 7.3.2.11. Gas saturation field – Hexahedron grid at 80 days.

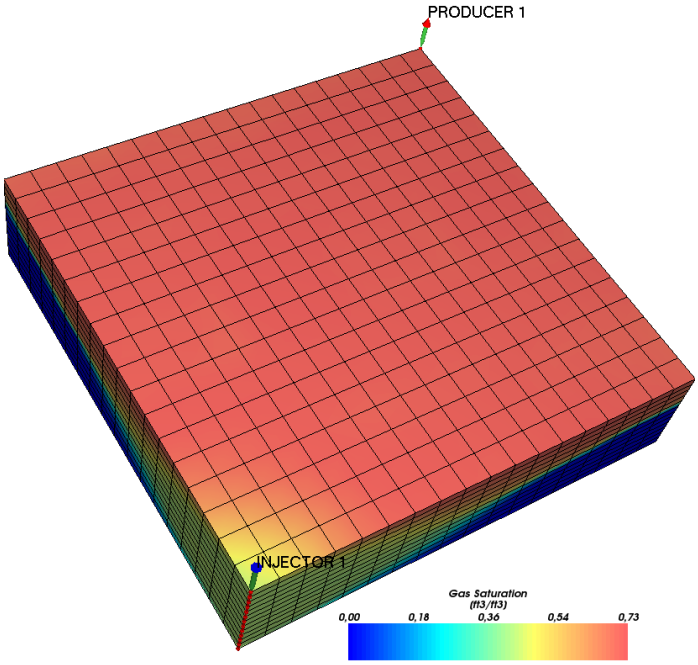

Figure 7.3.2.12. Gas saturation field – Hexahedron grid at 1001 days.

In order to present the three hydrocarbon phase capability of GPAS simulator, the third case study refers to the fluid flow simulation of three hydrocarbon phases (two liquid phases and a gas phase). The reservoir again refers to gas injection in a quarter-of-five spot. **Tables 7.3.2.3** and **7.3.2.4** present the fluid and physical properties and the relative permeability data for the Corey's model, respectively.

Table 7.3.2.3. Input data for Case 3

Length (m)	121.92	
Width (m)	121.92	
Thickness (m)	36.58	
Porosity (fraction)	0.30	
Rock compressibility (kPa^{-1})	$5.8x10^{-7}$	
Reservoir temperature (^oC)	18.33	
Permeability in x direction (m^2)	$1.0x10^{-13}$	
Permeability in y direction (m^2)	$1.0x10^{-13}$	
Permeability in z direction (m^2)	$1.0x10^{-13}$	
Water viscosity (Pa.s)	$8x10^{-4}$	
Water density (mol/m^3)	$55.55x10^3$	
Water compressibility (kPa^{-1})	$4.35x10^{-7}$	
Initial water saturation (fraction)	0.25	
Initial reservoir pressure (MPa)	6.21	
Producer bottom hole pressure (MPa)	6.21	
Gas injection rate (m^3/s)	0.3277	
Reservoir fluid initial composition	CO_2	0.01
	C1	0.19
	NC16	0.80
Injected fluid composition	CO_2	0.95
	C1	0.05
	NC16	0.00

Table 7.3.2.4. Corey's model relative permeability data for Case 3

	Water	Oil	Gas	Second oil
End point relative permeability	0.3	0.75	0.9	0.9
Residual saturation	0.25	0.2	0.0	0.0
Exponent of relative permeability	2.0	2.0	2.0	2.0

The results for Case 3, the three hydrocarbon phases, homogeneous, and isotropic reservoir, in terms of volumetric rates at standard conditions of oil and gas obtained in conjunction with hexahedron element are shown in **Figures 7.3.2.13** and **7.3.2.14**, respectively. The results obtained with GPAS in conjunction with Cartesian meshes are also shown. From these figures, we can observe that the volumetric rates of the hexahedron mesh are similar to the ones obtained with the Cartesian meshes, especially the more refined ones. The spikes in the curves are due to the phase change along the reservoir associated with phase composition and pressure changes. **Figures 7.3.2.15, 7.3.2.16** and **7.3.2.17** present the oil, gas, and second liquid saturation fields at 250 days, respectively. At this time, we can observe a rapid increase in gas production shown in **Figure 7.3.2.14**. Analyzing **Figures 7.3.2.15, 7.3.2.16** and **7.3.2.17** we can see that this is caused by the breakthrough of the second liquid phase in the production well.

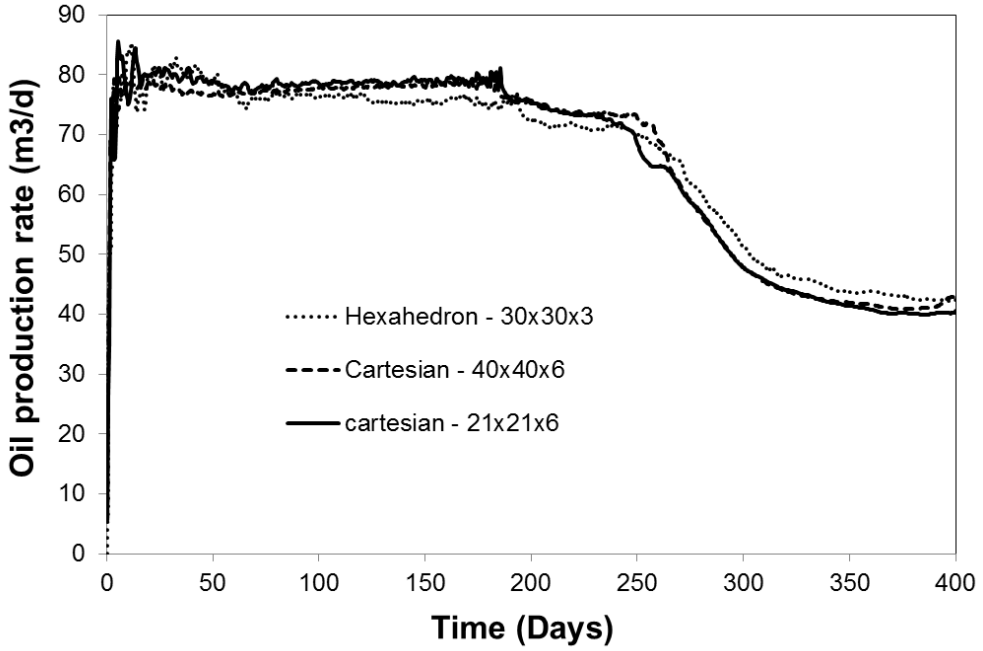

Figure 7.3.2.13. Oil production rate vs. time for Case 3.

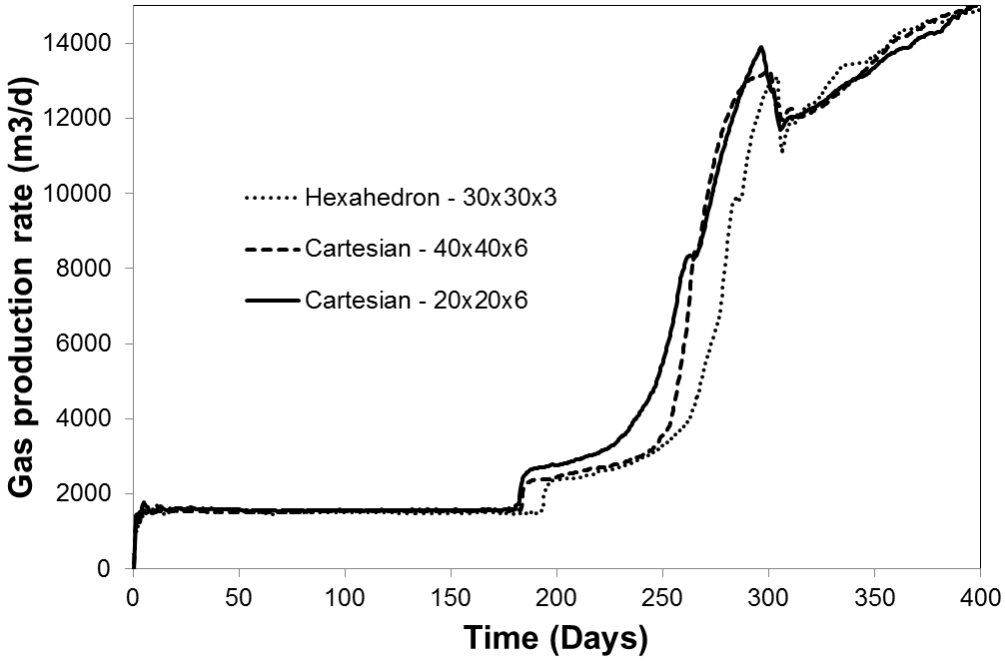

Figure 7.3.2.14. Gas production rate vs. time for Case 3.

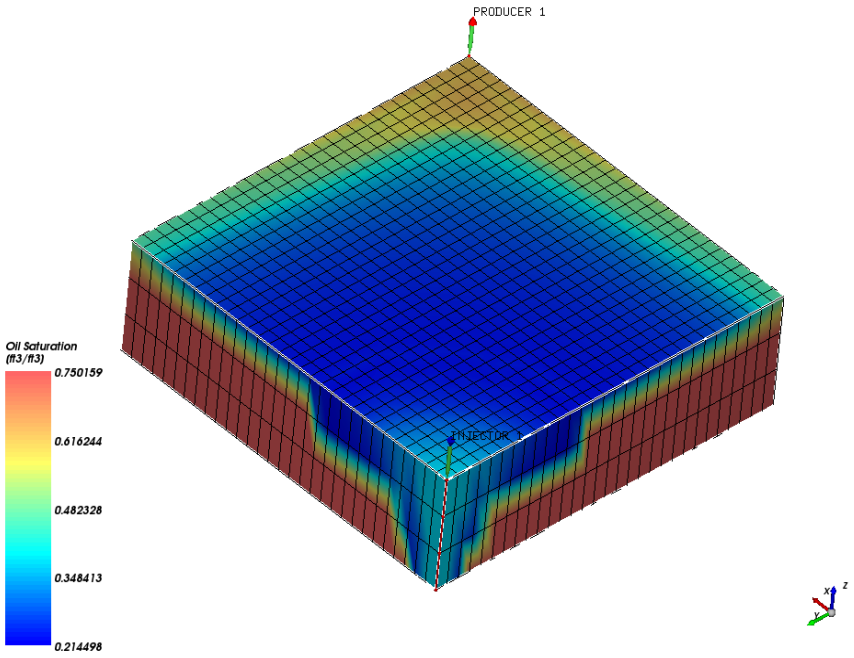

Figure 7.3.2.15. Oil saturation field at 250 days.

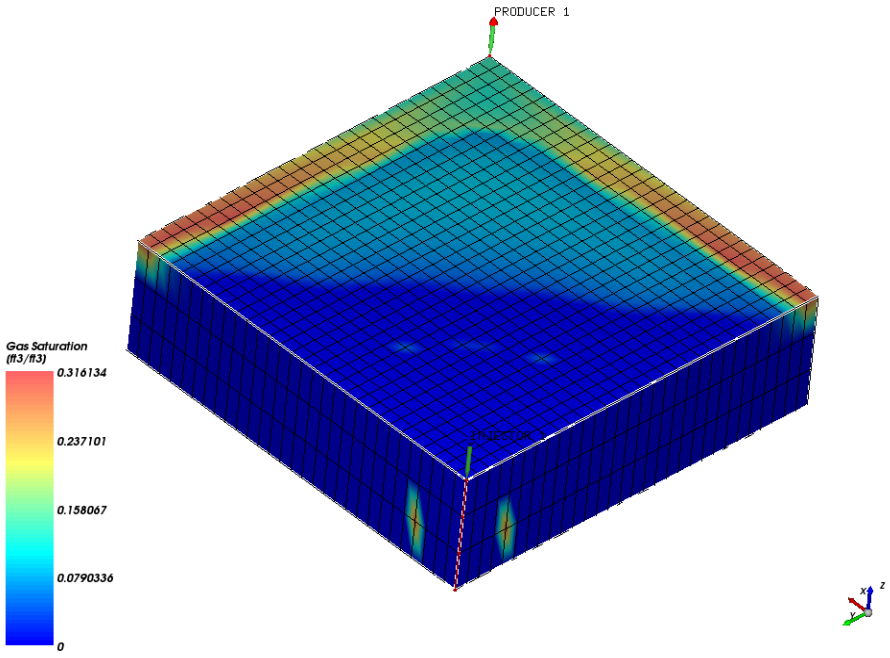

Figure 7.3.2.16. Gas saturation field at 250 days.

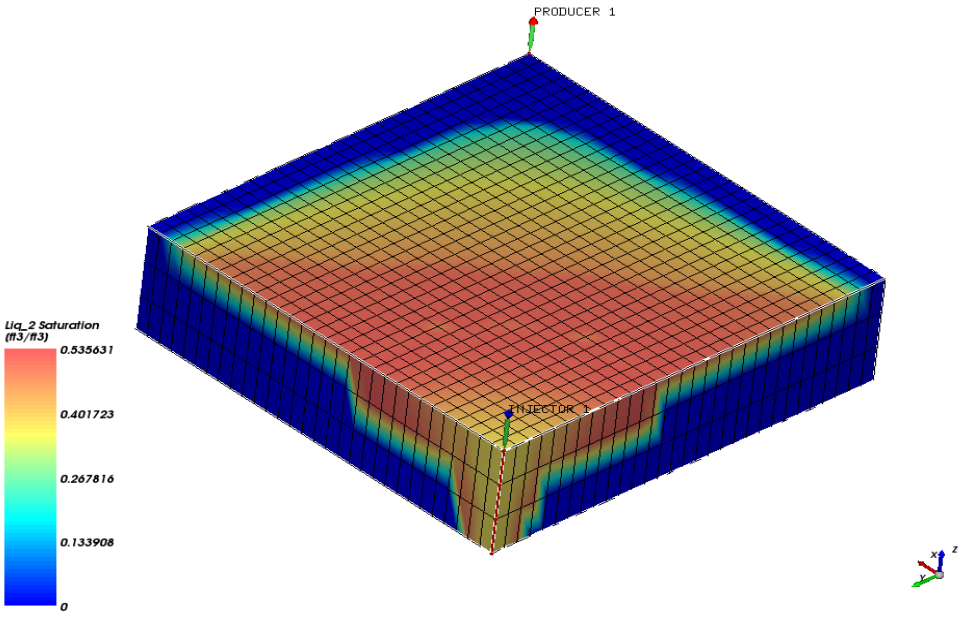

Figure 7.3.2.17. Second liquid saturation field at 250 days.

The last case study refers to the simulation of gas injection into an irregularly shaped reservoir. Except for the reservoir dimension and absolute permeabilities, we used the same properties shown in **Tables 7.3.2.1** and **7.3.2.2**. **Figures 7.3.2.18** and **7.3.2.19** show two grid-configurations employed for this reservoir. The first mesh, **Figure 7.3.2.18**, is composed only of hexahedrons, while the mesh shown in **Figure 7.3.2.19** is a hybrid mesh composed of tetrahedron, pyramid and hexahedron elements. **Figures 7.3.2.18** and **7.3.2.19** show the reservoir top and bottom topologies, respectively. From these figures, we can see that this reservoir is completely irregular in x, y, and z directions. The absolute permeabilities in x and y directions were 1.0×10^{-13} m^2 (100 mD), and the absolute permeability in z direction was 1.0×10^{-14} m^2 (10 mD). For each injection well, we used the volumetric rate given in **Table 7.3.2.1**.

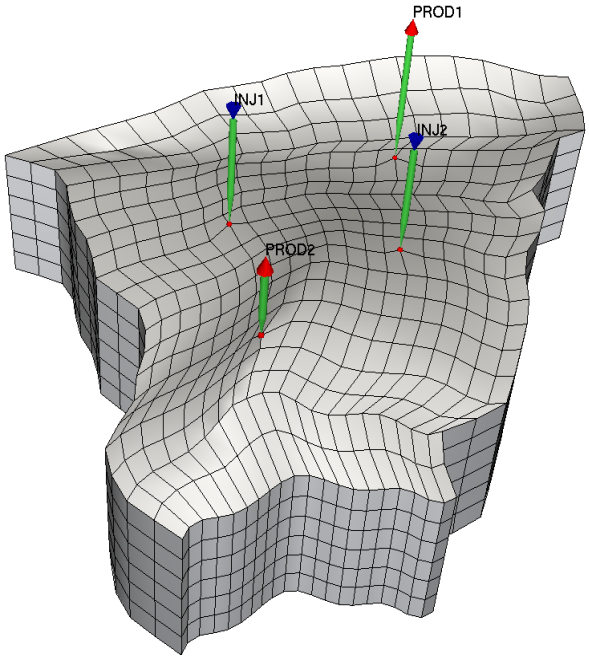

Figure 7.3.2.18. Hexahedron mesh used for Case 4 (3087 vertices; 2400 elements).

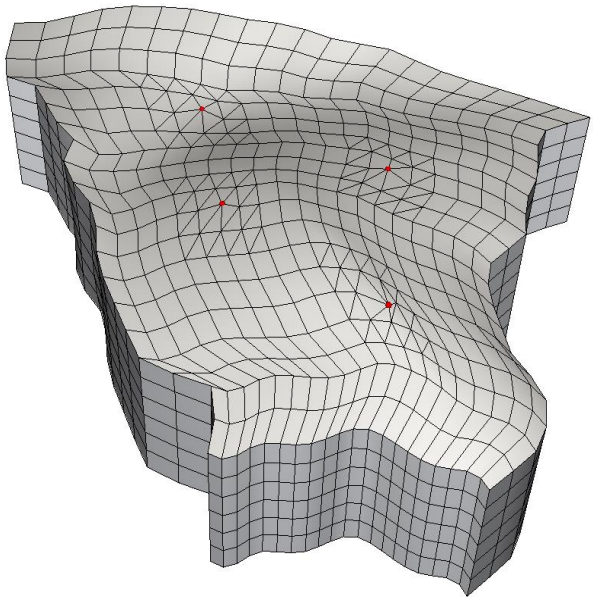

Figure 7.3.2.19. Hybrid mesh used for Case 4 (3475 vertices; 3086 tetrahedrons; 1632 hexahedron; 1925 pyramids).

Figures 7.3.2.20 and **7.3.2.21** present the results, in terms of oil and gas volumetric rates at standard condition, respectively, for the last case study in conjunction with the two meshes shown in **Figures 7.3.2.18** and **7.3.2.19**. Although the two grid configurations are different, the results in terms of oil and gas rates for both grids are in good agreement. The gas saturation field at two simulation times is shown in **Figures 7.3.2.22** through **7.3.2.25**, for the two grid configurations. From these figures, it is possible to observe a good agreement of the saturation field for both grid configurations investigated.

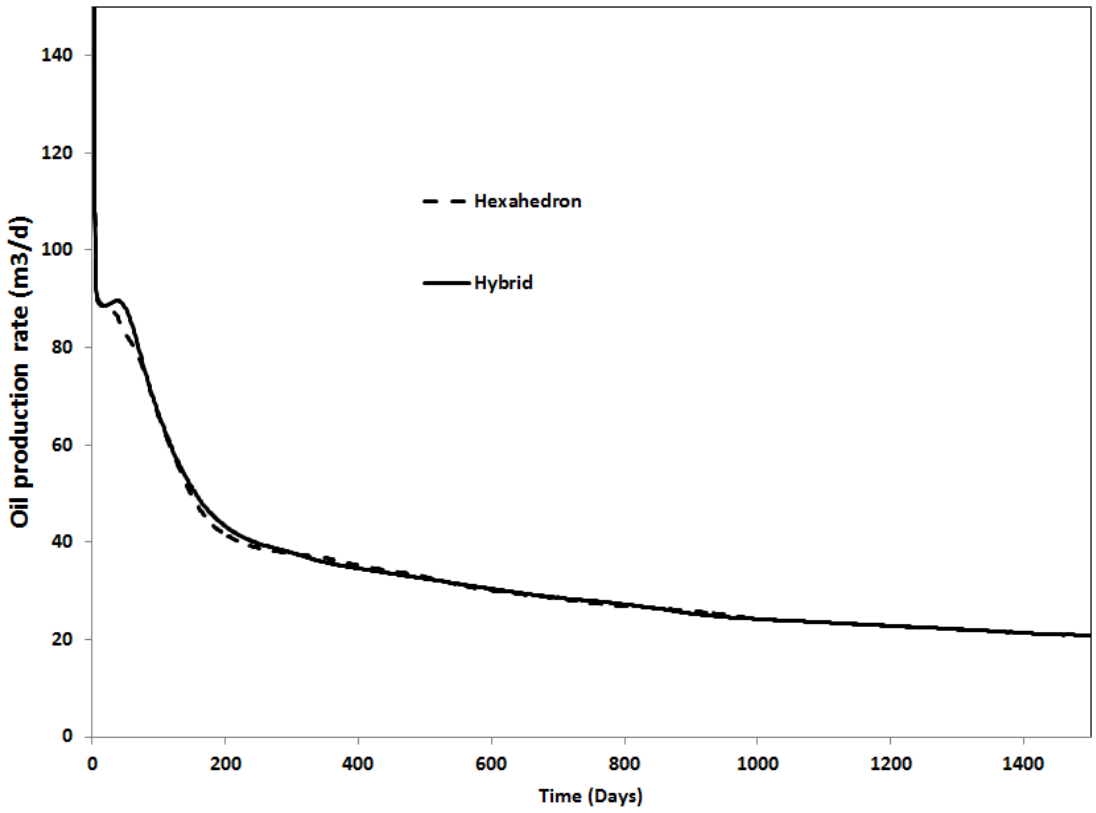

Figure 7.3.2.20. Oil production rate vs. time for Case 4.

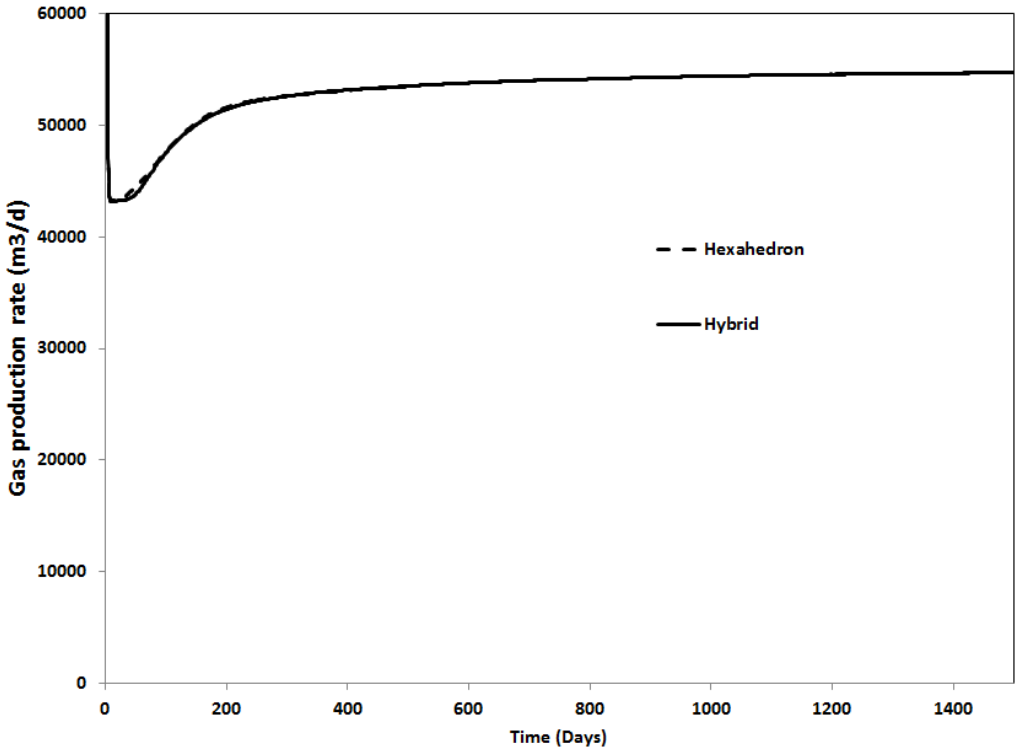

Figure 7.3.2.21. Gas production rate vs. time for Case 4.

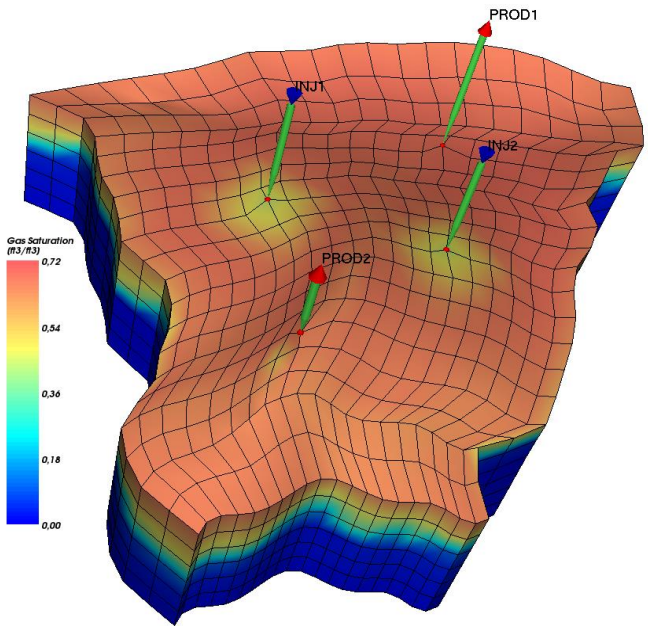

Figure 7.3.2.22. Gas saturation field using the hexahedron mesh at 80 days.

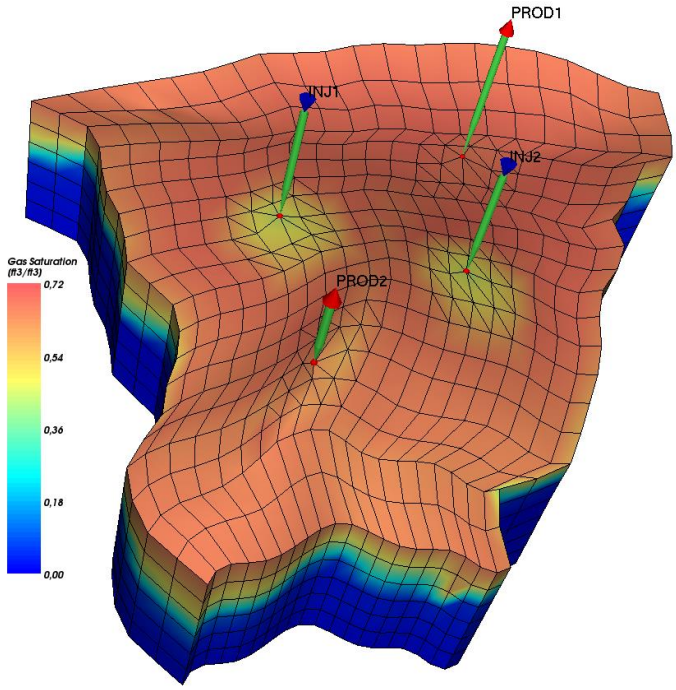

Figure 7.3.2.23. Gas saturation field using hybrid mesh at 80 days.

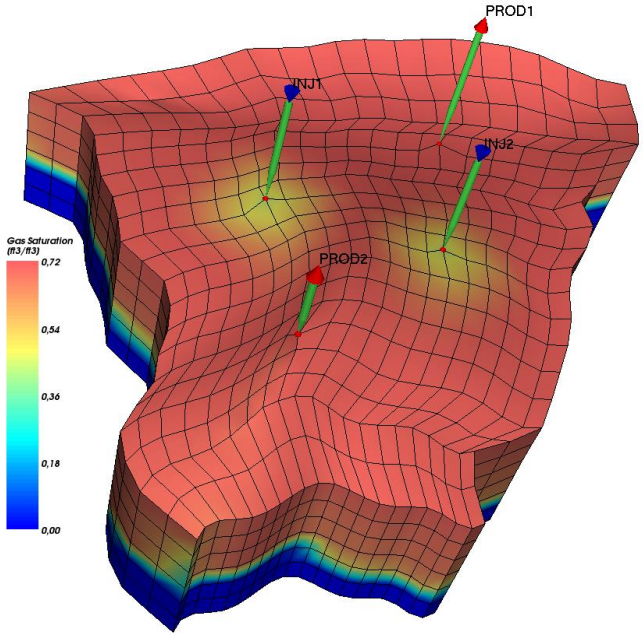

Figure 7.3.2.24. Gas saturation field using hexahedron mesh at 1000 days.

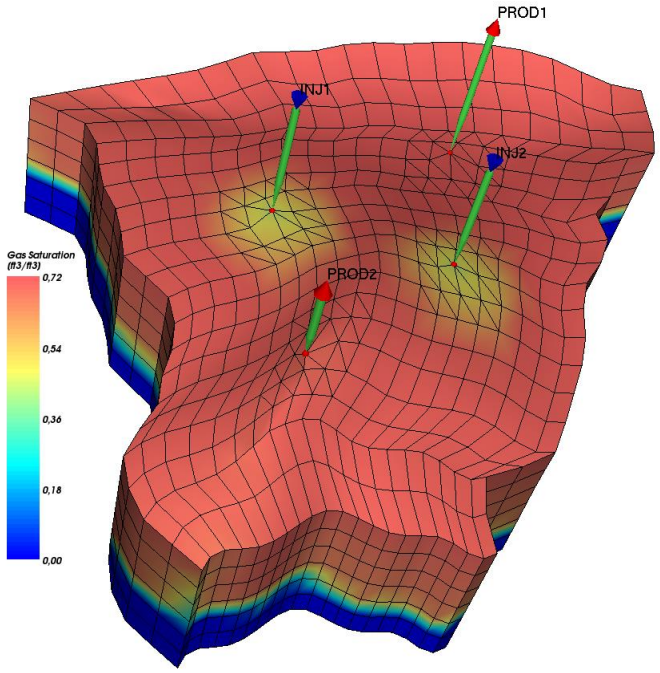

Figure 7.3.2.25. Gas saturation field using hybrid mesh at 1000 days.

Chapter 8. Summary, Conclusions and Recommendations

8.1 SUMMARY

A multi-formulation compositional reservoir simulator has been developed including features such as three-phase flash calculation (four-phase flow), physical dispersion, and unstructured grid.

Four different formulations were implemented: Coats (1980), Collins et al. (1992), Branco and Rodriguez (1996), and a sequential IMPEC.

Including the original GPAS formulation (Wang et al., 1997), five different formulations were compared in terms of total Newton iterations for various cases. These test cases included different physical problems such as miscible and immiscible gas injection, water flooding, condensate and lean gas production.

A three-phase flash capability was implemented for three of the formulations: Coats (1980), Branco and Rodriguez (1996), and the sequential IMPEC. Using this feature, we simulated cases for CO_2 injection where a third hydrocarbon phase appears.

An element-based finite volume approach for 2D and 3D compositional reservoir simulation using unstructured grids based on triangular and quadrilateral elements for 2D; and tetrahedron, prism, pyramid, and hexahedron elements for 3D was implemented for the Coats (1980) formulation. Results for the gas flooding simulation using the mentioned elements were compared to the results of the original formulation of the GPAS simulator in conjunction with Cartesian meshes.

Physical dispersion full tensor was implemented for Coats (1980) formulation for both Cartesian and unstructured formulations in conjunction with an element-based finite volume approach. The approach was tested for four different case studies: two tracer injections (1D and 2D), and two case studies involving solvent injection.

8.2 CONCLUSIONS

This section is subdivided into four subsections in order to better organize the conclusions for each of the subtopics included in this dissertation.

8.2.1 Comparison of Different Formulations

The results obtained suggest that different formulations can have different performance when simulating different problems. Two different semi-implicit formulations were included in our comparisons.

Compared to fully implicit formulations, we noticed a higher number of Newton iterations for all case studies using one of the semi-implicit formulations. Although both semi-implicit formulations significantly reduce the size of the Jacobian matrix, they have much larger number of Newton iterations in comparison to the fully implicit formulations considered. These results indicate that using a semi-implicit formulation can be beneficial in reducing the Jacobian size in an Adaptative Implicit Method (AIM) by combining advantages of a fully implicit scheme and a semi-implicit scheme.

One of the objectives of this research was to compare all the formulations implemented for solving different physical problems and identify if one formulation outperform the others for a specific physical problem. The comparison of the implemented fully implicit schemes in this dissertation shows that the Coats (1980) formulation performed better in terms of total number of Newton iterations for most simulated cases in our study as well as CPU times (as shown in Table 6.7.2). Therefore, we did not find a correlation among physical problem and formulation, but instead we found that, in general, the natural variables outperforms the other sets of primary variables for the cases we tested in this dissertation.

8.2.2 Three-phase Flash

The two CO_2 injection cases presented in Chapter 7 demonstrate the importance of having this feature available when handling super critical CO_2. Neglecting the appearance of the third hydrocarbon phase may lead to discrepancies in results and also to convergence problems.

The simulator performance is severely affected when using a three-phase flash option, which means that it is useful to have both options available (two-phase flash and three-phase flash) and only use three-phase flash when necessary. For this reason, we recommend a careful phase behavior analysis prior to the reservoir studies.

8.2.2 Unstructured Grid

The results of GPAS using fine Cartesian meshes were similar to those obtained using the EbFVM approach implemented and tested in the present work. The EbFVM method was less prone to grid orientation effects. However, as shown in the results, it can be noticed that the numerical error produced by tetrahedron and pyramid elements are larger than those of hexahedron and prism elements. When comparing these results to those obtained with GPAS Cartesian grids, it is observed that a simulation with Cartesian grids requires many more grid blocks than with the EbFVM approach.

The EbFVM approach is tested for several complex reservoir simulation problems. The results indicate the method is well suited for solving such problems.

8.2.3 Physical Dispersion

The results of 1D tracer injection were compared to the analytical solution and to the results of GPAS in conjunction with Cartesian meshes. The results suggest that the element-based approach reduces numerical dispersion, compared to the Cartesian

meshes. The results of the 2D tracer injection case study also indicate to be more accurate than those using Cartesian meshes.

Two additional applications were made using a heterogeneous quarter-of-five-spot and a reservoir with complex geometry. The results demonstrate the flexibility of the method in representing complex reservoirs and difficult phase behavior, in addition to its capacity to deal with heterogeneous media. In conclusion, the EbFVM approach was tested in various case studies involving physical dispersion. Based on the results, the approach proved advantageous when compared to the traditional Cartesian meshes.

8.3 RECOMMENDATIONS

1. Failures were observed when simulating miscible and immiscible gas injections problems. These failures occurred mostly because of issues in the phase behavior model, i.e. stability test, phase identification, and flash calculation. More research in these areas is needed to improve the robustness of the simulator.
2. Based on the implementations of Coats (1980) formulation, IMPSAT formulation (Branco and Rodriguez, 1996), and sequential IMPEC formulation, we suggest extending them to an AIM method (Adaptive Implicit Method). This implementation can improve the performance of GPAS by reducing the Jacobian size.
3. Other methods for reducing the Jacobian size can be tested, e.g. the inclusion of one of the mole fractions to the IMPSAT formulation.
4. Local grid refinement for the Cartesian and the corner point options should be implemented.
5. Better solvers should be tested for unstructured grids.

6. Parallel computing should be implemented for the unstructured grid formulations.
7. Higher order interpolation methods for the transmissibility terms should be implemented to reduce numerical dispersion.
8. An EOS flash calculation including aqueous phase should be implemented in GPAS to properly handle four-phase calculations.
9. A tracer component should be implemented in GPAS.
10. The relative permeability model should be improved, especially for applications involving four-phase flow.

Appendix A. Validation Cases

In this appendix we present some validation results comparing GPAS with other simulators such as CMG-GEM and UTCOMP, and comparing GPAS with the respective analytical result if it exists. These results were obtained by Xue Li in her master's thesis at The University of Texas at Austin (Li, 2012).

A.1 Linear Compressible Flow

The first case is a one-dimensional compressible flow and validates the conservation equation for a single-phase slightly compressible fluid. The case has a constant pressure boundary in one side and a no-flow boundary in the other. **Figure A.1.1** presents a schematic view of the numerical model this case. **Table A.1.1** presents the physical properties and initial conditions for this case.

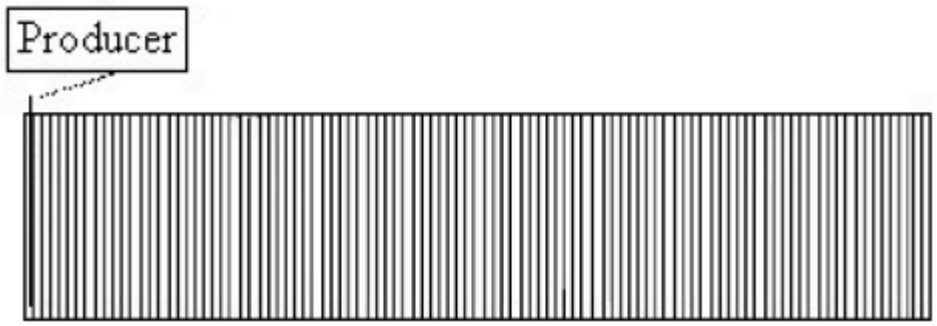

Figure A.1.1. Schematic view of the 1D linear compressible flow case (Li, 2012).

Table A.1.1. Physical properties and initial conditions for the 1D linear compressible flow case

Grid blocks dimension in x, y, and z directions	100 x 1 x 1	
Length (m)	609.6	
Width (m)	3.048	
Thickness (m)	3.048	
Porosity (fraction)	0.2	
Rock compressibility (kPa^{-1})	$7.25x10^{-5}$	
Reservoir temperature (^oC)	93.33	
Permeability in x direction (m^2)	$5.0x10^{-13}$	
Water viscosity (Pa.s)	$1x10^{-3}$	
Water density (kg/m^3)	999.6	
Water compressibility (kPa^{-1})	0.0	
Initial water saturation (fraction)	0.2	
Initial reservoir pressure (MPa)	13.79	
Producer bottom hole pressure (MPa)	13.1	
Initial composition	NC10	1.0

The governing partial differential equation for this case is given by Equation A.1.1 (Pope, 2003):

$$\frac{\partial^2 P}{\partial x^2} = \frac{\phi \mu c_t}{K} \frac{\partial P}{\partial t} \tag{A.1.1}$$

And the analytical solution for this particular case is given by Equation A.1.2:

$$P_D\left(x_D, t_D\right) = \sum_{n=1}^{\infty} \frac{2}{\gamma_n} \exp\left(-\gamma_n^2 t_D\right) \sin\left(\gamma_n x_D\right) \tag{A.1.2}$$

where P_D is the dimensionless pressure given by $P_D = \frac{P - P_e}{P_i - P_e}$, P_e is the constant pressure at the open boundaries, P_i is the initial pressure, x_D is the dimensionless distance to the open boundary and is given by $x_D = \frac{x}{L}$, L is the total length, γ_n is given by $\gamma_n = \frac{1}{2}(2n-1)\pi$, and t_D is the dimensionless time given by $t_D = \frac{Kt}{\phi \mu c_t L^2}$.

Figure A.1.2 presents the comparison of Coats (1980), Wang et al. (1997) formulations, and the analytical solution at t_D equal to 0.157. From this figure, we can see that both formulations match the analytical results for this case.

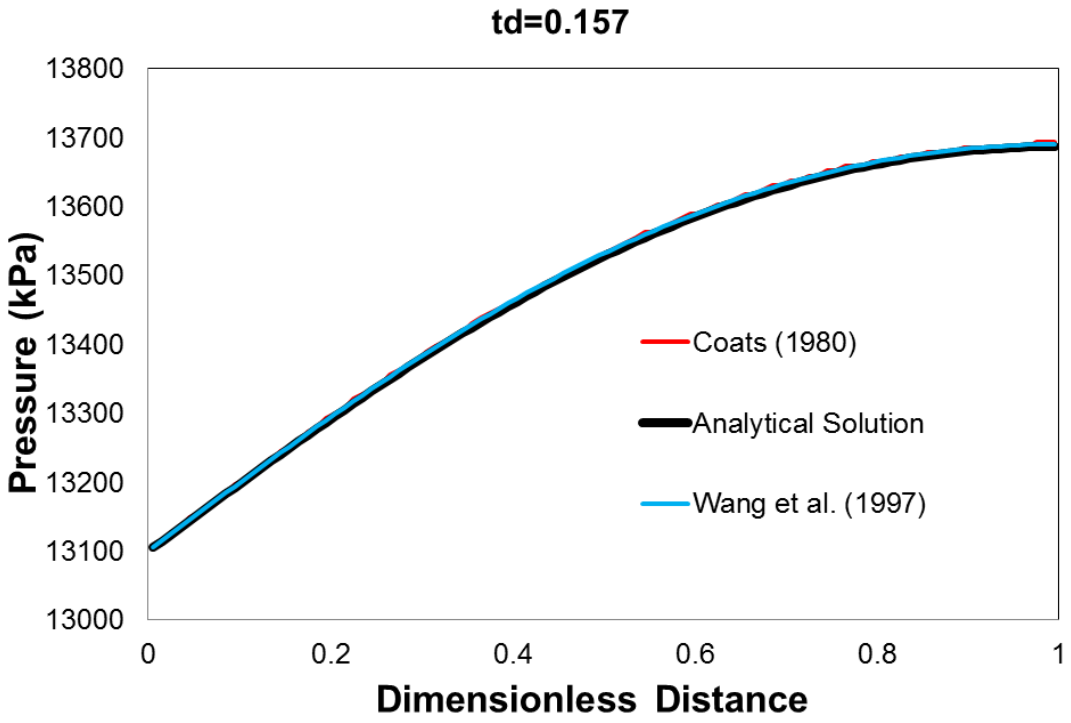

Figure A.1.2. Comparison of Coats (1980), Wang et al. (1997) formulations, and the analytical solution at t_D equal to 0.157.

A.2 TWO-DIMENSIONAL COMPRESSIBLE FLOW

This case is a two dimensional, single phase flow in a rectangular reservoir. **Figure A.2.1** presents a schematic view of the reservoir and its geometric properties. From this figure, we can also see that the well can be located anywhere in the reservoir and parameters L and q specify the location of this well.

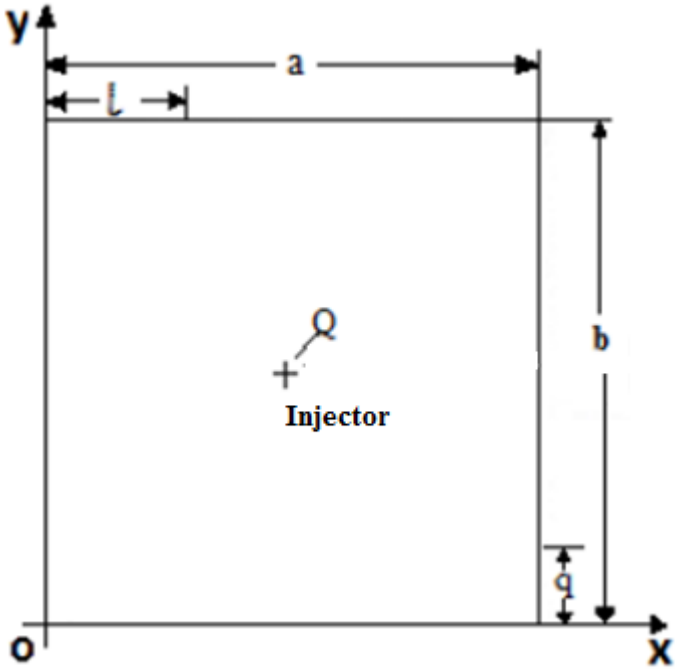

Figure A.2.1. Schematic view of the two-dimensional, single phase flow reservoir (Li, 2012).

The governing PDE for this case is given by Equation A.2.1 and the analytical solution for the pressure distribution is given by Equation A.2.2 (Hovanessian, 1961). **Table A.2.1** presents the physical properties and the initial conditions for this case.

$$\frac{\partial^2 P}{\partial x^2}+\frac{\partial^2 P}{\partial y^2}=\alpha\frac{\partial P}{\partial t}+\beta Q(l,q), \tag{A.2.1}$$

where $\alpha = C_1 \frac{\phi \mu c_t}{K}$, $\beta = C_2 \frac{B_o \mu}{K}$, C_1 and C_2 are constants which depend on the unit system, B_o is the oil formation volume factor, and Q is the production or injection rate.

$$P(x,y,t) = P_i - \frac{\beta Q}{ab}\left[\begin{array}{l} \frac{t}{\alpha} + 2\sum_{m=1}^{\infty} \frac{1}{\pi^2\left(\frac{m^2}{a^2}\right)}\left\{1-\exp\left[-\frac{\pi^2}{\alpha}\left(\frac{m^2}{a^2}\right)t\right]\right\}\cos\frac{m\pi l}{a}\cos\frac{m\pi x}{a} + \\ 2\sum_{n=1}^{\infty} \frac{1}{\pi^2\left(\frac{n^2}{b^2}\right)}\left\{1-\exp\left[-\frac{\pi^2}{\alpha}\left(\frac{n^2}{b^2}\right)t\right]\right\}\cos\frac{n\pi q}{b}\cos\frac{n\pi y}{b} + \\ 4\sum_{n=1}^{\infty}\sum_{m=1}^{\infty} \frac{1}{\pi^2\left(\frac{m^2}{a^2}+\frac{n^2}{b^2}\right)}\left\{1-\exp\left[-\frac{\pi^2}{\alpha}\left(\frac{m^2}{a^2}+\frac{n^2}{b^2}\right)t\right]\right\}\cos\frac{m\pi l}{a}\cos\frac{n\pi q}{b}\cos\frac{m\pi x}{a}\cos\frac{n\pi y}{b} \end{array}\right] \quad \text{(A.2.1)}$$

Table A.2.1. Physical properties and initial conditions for the 2D compressible flow case

Grid blocks dimension in x, y, and z directions	25 x 25 x 1	
Length (m)	609.6	
Width (m)	609.6	
Thickness (m)	0.3048	
Porosity (fraction)	0.2	
Rock compressibility (kPa^{-1})	7.25×10^{-5}	
Reservoir temperature (^oC)	93.33	
Permeability in x direction (m^2)	1.5×10^{-15}	
Permeability in y direction (m^2)	1.5×10^{-15}	
Water viscosity (Pa.s)	0.249×10^{-3}	
Water density (kg/m^3)	999.6	
Water compressibility (kPa^{-1})	0.0	
Initial water saturation (fraction)	0.2	
Initial reservoir pressure (MPa)	13.79	
Total injection rate (m^3/day)	0.235	
Initial composition	NC10	1.0

Figure A.2.2 presents the results in terms of the pressure profile at 365 days and *y* equals to 256 *m* given by Coats (1980) formulation, Wang et al. (1997) formulation, UTCOMP, and the analytical solution. From this figure, we can see that a good agreement was obtained for all the formulations and the analytical solution.

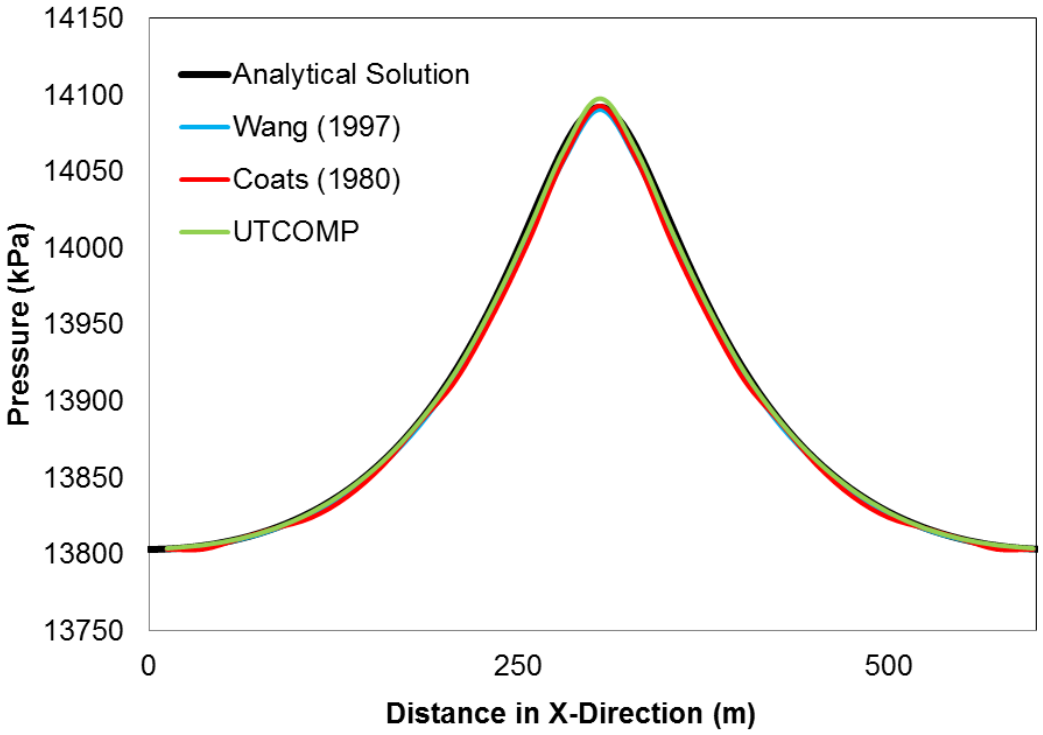

Figure A.2.2. Pressure profile given by Coats (1980), Wang et al. (1997) formulations, UTCOMP, and the analytical solution at *t* equal to 365 days and *y* equal to 256 *m*.

A.3 DIETZ DISPLACEMENT WITH IMMISCIBLE DISPLACEMENT

This case is a two dimensional immiscible displacement in a dipping reservoir. The model has two wells at the edges: one water injector and one oil producer. We used the EbFVM implementation for Coats (1980) formulation to model the geometry. **Figure A.3.1** presents the model using hexahedron element and the position of the wells. **Table A.3.1** presents the physical properties and the initial conditions for this case. **Table A.3.2** presents the Corey's parameters used for the relative permeability model. The solution was compared with UTCOMP.

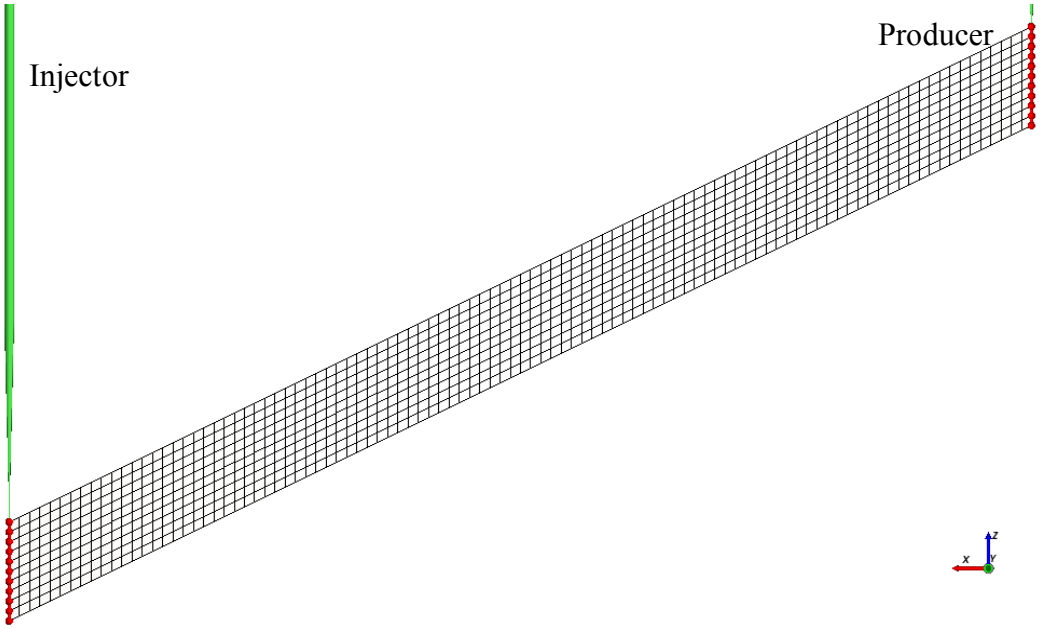

Figure A.3.1. Schematics of the EbFVM model used to simulate water flooding in a two-dimensional dip reservoir.

Table A.3.1. Physical properties and initial conditions for the 2D, immiscible displacement case

Grid blocks dimension in x, y, and z direction	100 x 1 x 10	
Length (m)	30.48	
Width (m)	3.048	
Thickness (m)	3.048	
Dip angle (degree)	30^{o}	
Porosity (fraction)	0.2	
Rock compressibility (kPa^{-1})	0.0	
Reservoir temperature (^{o}C)	15.56	
Permeability in x direction (m^2)	$5x10^{-13}$	
Permeability in z direction (m^2)	$5x10^{-13}$	
Water viscosity (Pa.s)	$0.5x10^{-3}$	
Water density ($gmol/m^3$)	$5.56x10^{4}$	
Water compressibility (kPa^{-1})	0.0	
Initial water saturation (fraction)	0.2	
Initial reservoir pressure (MPa)	13.79	
Total injection rate (m^3/day)	0.113	
Producer bottom hole pressure (MPa)	13.79	
Initial overall composition	C10	1.0

Table A.3.2. Corey's model relative permeability data for the 2D, immiscible displacement case

	Water	Oil	Gas
End point relative permeability	0.2	1.0	1.0
Residual saturation	0.2	0.35	0.0
Exponent of relative permeability	2.0	2.0	2.0

Figure A.3.2 presents the results of the water front position in four different times given by UTCOMP, CMG-STARS, and Coats (1980) formulation implemented in GPAS. As we can see from this figure, the results of the three simulators tested are in good agreement for the case simulated.

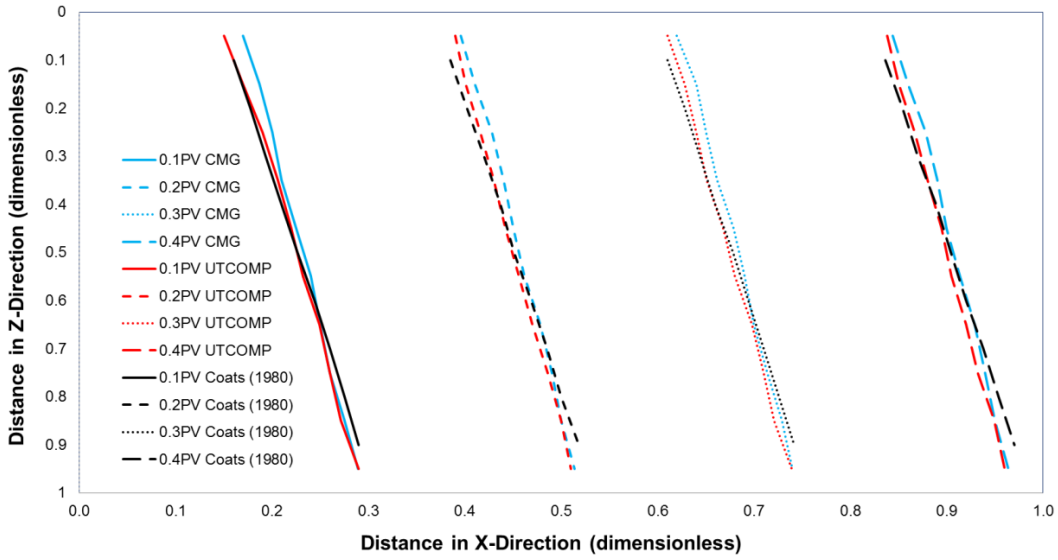

Figure A.3.2. Water front position in four different times (0.1PV, 0.2PV, 0.3PV, and 0.4PV) given by UTCOMP, CMG-STARS, and Coats (1980) formulation implemented in GPAS.

A.4 THREE-DIMENSIONAL WATER FLOODING

This case corresponds to a three-dimensional water flooding in a homogeneous quarter of five-spot reservoir. The reservoir was modeled with 40 x 40 x 5 grid blocks and the results of UTCOMP, CMG-GEM, the implementation of Wang et al. (1997) formulation implemented in GPAS, and the implementation of Coats (1980) formulation implemented in GPAS were compared. **Table A.4.1** summarizes the physical properties and initial conditions. **Table A.4.2** presents the Corey's parameters used for the relative permeability model.

Table A.4.1. Physical properties and initial conditions for the 3D, water flooding case

Grid blocks dimension in x, y, and z direction	40 x 40 x 5	
Length (m)	487.68	
Width (m)	487.68	
Thickness (m)	15.24	
Porosity (fraction)	0.2	
Rock compressibility (kPa^{-1})	0.0	
Reservoir temperature (^oC)	15.56	
Permeability in x direction (m^2)	$1x10^{-12}$	
Permeability in y direction (m^2)	$1x10^{-12}$	
Permeability in z direction (m^2)	$1x10^{-12}$	
Water viscosity (Pa.s)	$1.0x10^{-3}$	
Water density ($gmol/m^3$)	$5.56x10^4$	
Water compressibility (kPa^{-1})	0.0	
Initial water saturation (fraction)	0.2	
Initial reservoir pressure (MPa)	1.379	
Total injection rate (m^3/day)	556.4	
Producer bottom hole pressure (MPa)	1.379	
Initial overall composition	C10	1.0

Table A.4.2. Corey's model relative permeability data for the 3D, water flooding case

	Water	Oil	Gas
End point relative permeability	0.5	0.9	1.0
Residual saturation	0.2	0.1	0.0
Exponent of relative permeability	2.0	2.0	2.0

Figures A.4.1 and **A.4.2** present the results of CMG, UTCOMP, Wang et al. (1997) formulation, and Coats (1980) formulation in terms of volumetric oil rate and volumetric water rate, respectively. As we can see from these figures, the results given by GPAS and the other simulators are similar. UTCOMP presented some numerical instabilities; this problem probably occurred because of a large time step strategy during the simulation. Because these results came from Xue Li's thesis (Li, 2012), we prefer to keep in the same way they were published.

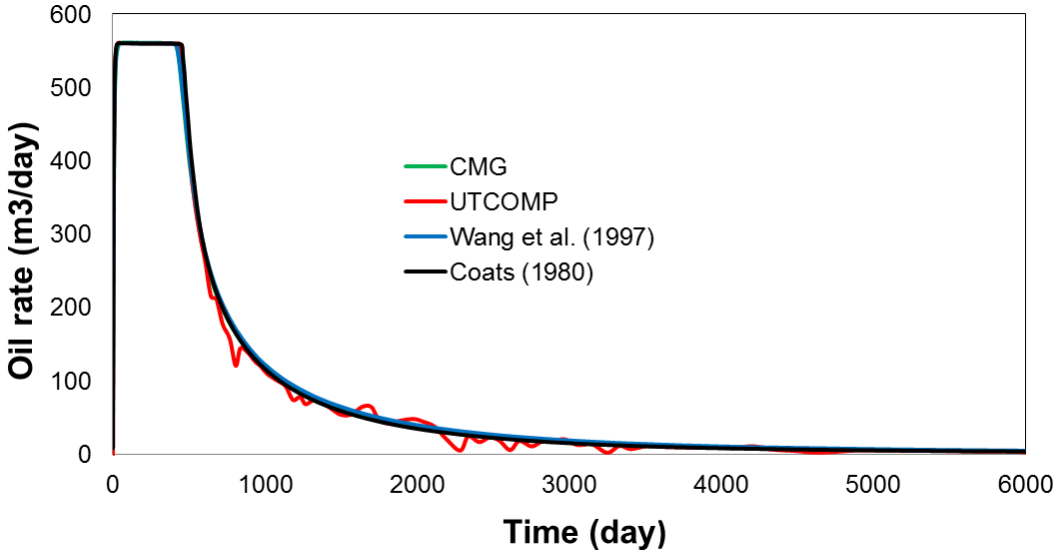

Figure A.4.1. Volumetric oil rate results given by various simulators for the three-dimensional water flooding case.

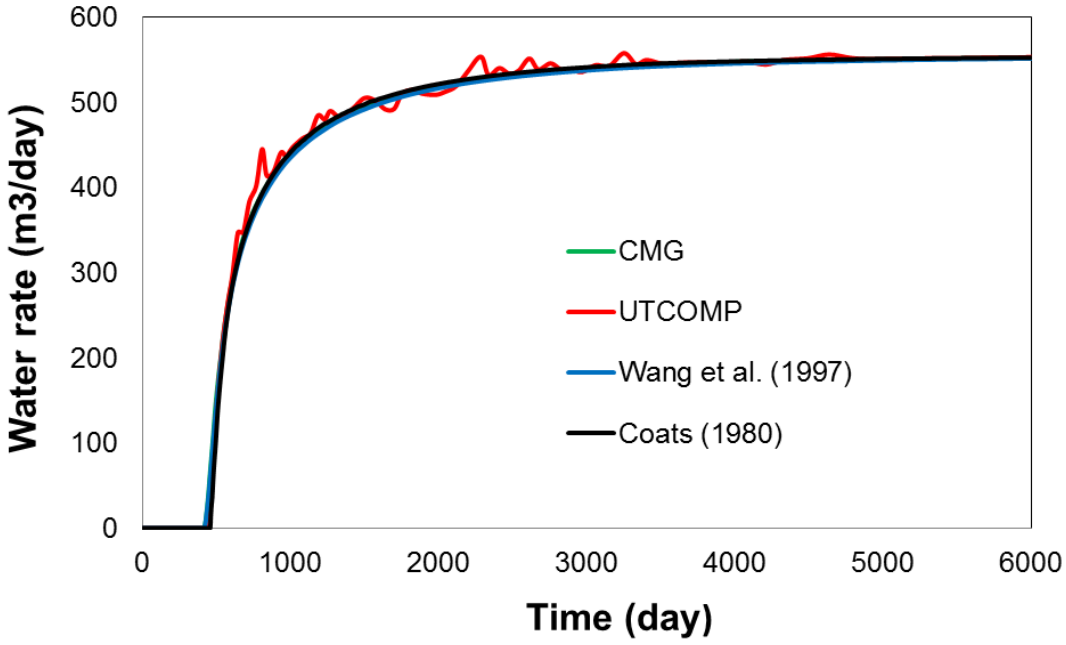

Figure A.4.2. Volumetric water rate results given by various simulators for the three-dimensional water flooding case.

A.5 THREE-DIMENSION MISCIBLE FLOODING

This case corresponds to a three-dimensional CO_2 flooding in a quarter of five-spot and compares the results of CMG-GEM, UTCOMP and the implementation of Coats (1980) formulation in GPAS. The fluid model has three components (CO_2, C1, and NC16) and the geometry was modeled using 40 x 40 x 5 grid blocks. A mixture of 95% of CO_2 and 5% of C1 is injected at a constant rate of 5.66×10^5 m^3/day. **Table A.5.1** summarizes the physical properties and initial conditions and **Table A.5.2** presents the Corey's parameters used for the relative permeability model.

Table A.5.1. Physical properties and initial conditions for the 3D, miscible gas flooding

Grid blocks dimension in x, y, and z direction	40 x 40 x 5	
Length (m)	487.68	
Width (m)	487.68	
Thickness (m)	60.69	
Porosity (fraction)	0.3	
Rock compressibility (kPa^{-1})	$5.8x10^{-7}$	
Reservoir temperature (^oC)	26.7	
Permeability in x direction (m^2)	$1x10^{-12}$	
Permeability in y direction (m^2)	$1x10^{-12}$	
Permeability in z direction (m^2)	$1x10^{-13}$	
Water viscosity (Pa.s)	$0.8x10^{-3}$	
Water density ($gmol/m^3$)	$5.56x10^4$	
Water compressibility (kPa^{-1})	$4.35x10^{-7}$	
Initial water saturation (fraction)	0.25	
Initial reservoir pressure (MPa)	20.68	
Total injection rate (m^3/day)	$5.66x10^5$	
Producer bottom hole pressure (MPa)	20.68	
Initial overall composition	CO_2	0.01
	C1	0.19
	NC16	0.80
Injected fluid composition	CO_2	0.95
	C1	0.05
	NC16	0.0

Table A.5.2. Corey's model relative permeability data for the 3D, miscible gas flooding

	Water	Oil	Gas
End point relative permeability	1.0	1.0	1.0
Residual saturation	0.25	0.0	0.0
Exponent of relative permeability	1.0	1.0	1.0

Figures A.5.1 and **A.5.2** present the results of CMG, UTCOMP, and Coats (1980) formulation in terms of volumetric oil rate and volumetric gas rate, respectively. As we can see from these figures, the results given by GPAS and the other simulators are similar, except for the breakthrough time. As discussed before in this dissertation, this difference in the breakthrough time occurs because of the differences in the three-phase relative permeability model used in GPAS.

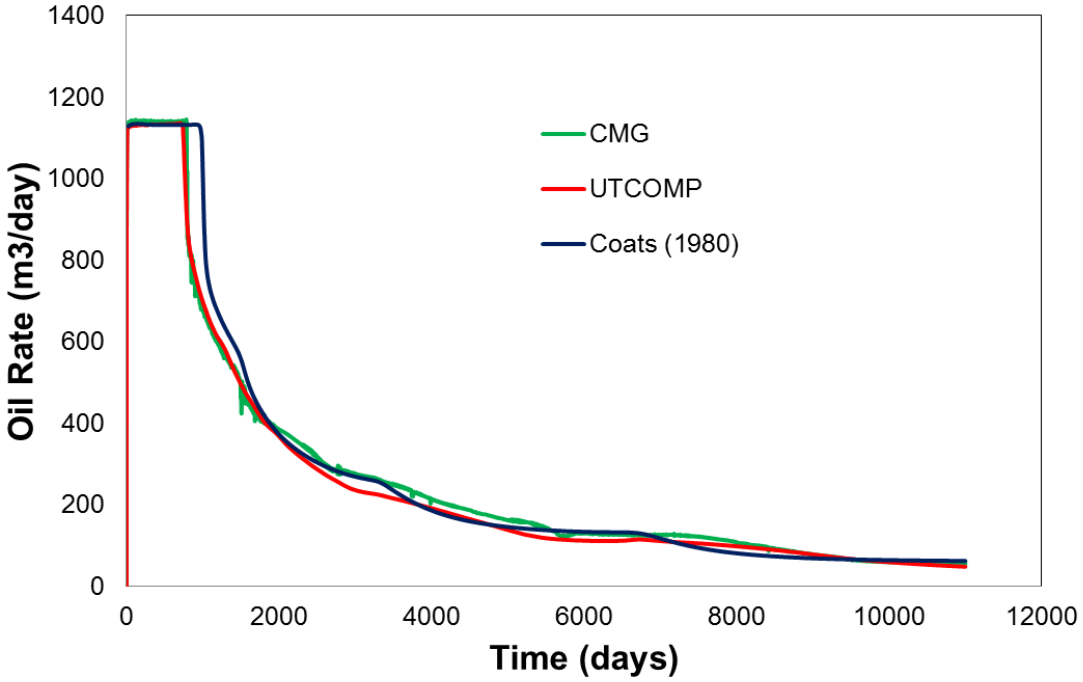

Figure A.5.1. Comparison of the volumetric oil rate results given by various simulators for the three-dimensional miscible gas flooding case.

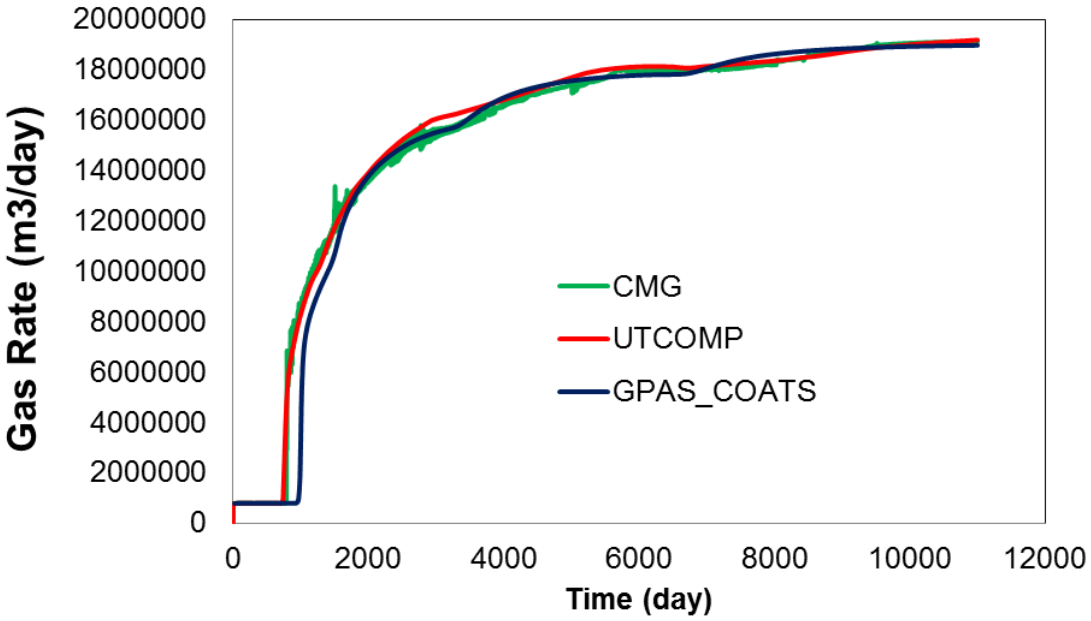

Figure A.5.2. Comparison of the volumetric gas rate results given by various simulators for the three-dimensional miscible gas flooding case.

Appendix B. Saturation Pressure Calculation

In his formulation, Coats (1980) suggests using a saturation pressure calculation in order to perform the stability test for each single hydrocarbon phase grid block. This methodology was tested in our research and we concluded that, although this methodology can be faster for easy cases (far from the critical point and from the cricondentherm), it is not as robust as Michelsen's stability test procedure (Michelsen, 1982).

In this appendix, we present one example of using a number of methodologies discussed in Chapter 3 to calculate the saturation pressure for several different temperatures. The results using the methodologies implemented in GPAS are compared to the results using Winprop (a commercial thermodynamic simulator developed by CMG).

This example consists of a six components problem. **Table B.1** presents the composition and the fluid model, **Table B.2** presents the binary interaction coefficients, and **Figure B.1** presents the phase envelope and the critical point.

Table B.1. Composition and fluid model for the six components case.

	Mole fraction	Pc (atm)	Tc (K)	Ac. Factor	MW	Vc (l/mol)
C1	0.75	45.4411	190.556	0.013	16	0.099
C3	0.03	41.9367	369.8333	0.152	44.1	0.203
FC6	0.02	29.7293	507.4444	0.301	86.2	0.344
FC10	0.1	20.686	617.667	0.488	142.3	0.521
FC15	0.05	13.609	705.556	0.65	206	1.027
FC20	0.05	11.023	766.667	0.85	282	0.777

Table B.2. Binary interaction coefficients.

	C1	C3	FC6	FC10	FC15	FC20
C1	0	0	0	0	0.05	0.05
C3	0	0	0	0	0.005	0.005
FC6	0	0	0	0	0	0
FC10	0	0	0	0	0	0
FC15	0.05	0.005	0	0	0	0
FC20	0.05	0.005	0	0	0	0

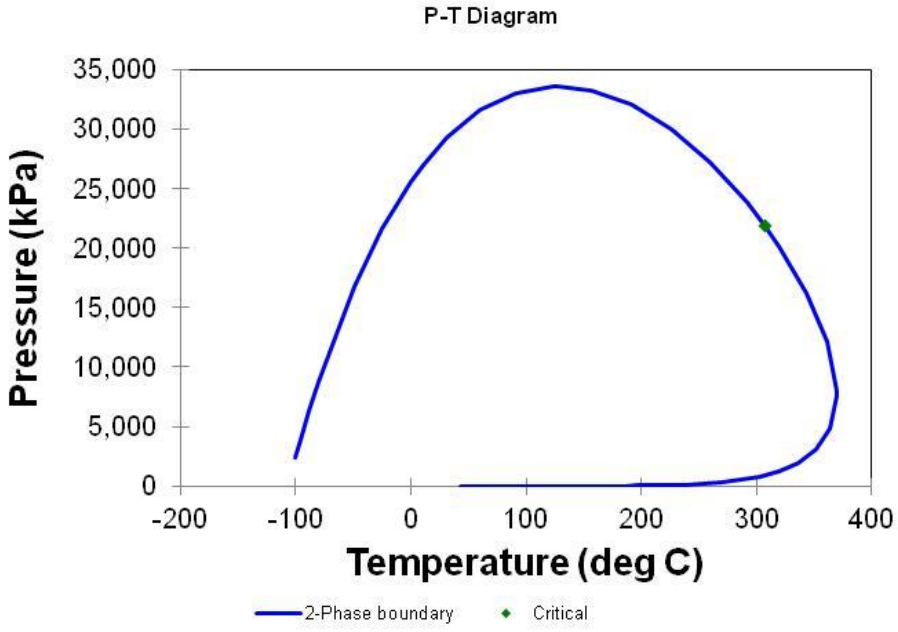

Figure B.1. Phase envelope and critical point for the six components case.

The critical point for this case is at *21953 kPa* and *306.7 ^{o}C*. **Table B.3** presents the results for the saturation pressure calculated using various methodologies implemented in GPAS and the respective results calculated using Winprop.

Table B.3. Saturation pressure calculated by various methods and by Winprop.

Temp (^{o}C)	Commercial	GPAS			Commercial	GPAS
	Psat (kPa)		Newton	Method	phase	
37.78	29888	29888	2	Baker	oil	oil
93.33	33136	33136	3	Baker	oil	oil
148.89	33453	33453	3	Baker	oil	oil
204.44	31378	31378	4	Baker	oil	oil
260.00	27188	27188	4	Baker	oil	oil
287.78	24291	24291	5	Baker	oil	oil
293.33	23640	23640	6	Baker	oil	oil
298.89	22900	22962	7	Baker	oil	oil
304.44	22242	22257	11	Baker	gas	oil
306.67	21960	21966	69	Michelsen	gas	oil
306.72	21953	FAIL	-	-	gas	-
306.78	21946	FAIL	-	-	gas	-
306.83	21939	FAIL	-	-	gas	-
306.89	21937	21937	173	Michelsen	gas	oil
306.94	21930	21930	13	Michelsen	gas	oil/gas
307.00	21922	21922	28	Baker	gas	gas/oil
307.06	21915	21915	29	Baker	gas	gas
307.22	21893	21893	16	Baker	gas	gas/oil
307.78	21819	21819	13	Baker	gas	gas/oil
308.33	21745	21745	12	Baker	gas	gas
308.89	21671	21671	11	Baker	gas	gas
310.00	21521	21521	9	Baker	gas	gas
315.56	20752	20752	7	Baker	gas	gas
343.33	16247	16247	3	Baker	gas	gas
365.56	FAIL	10664	2	Michelsen	-	gas
368.33	FAIL	9275	2	Michelsen	-	gas
368.89	FAIL	8852	2	Michelsen	-	gas
369.44	FAIL	7159	11	Michelsen	-	gas
369.50	FAIL	7268	11	Michelsen	-	gas
369.56	FAIL	7425	12	Michelsen	-	gas

As we can see from **Table B.3**, the methods implemented in GPAS had problems in calculating the saturation pressure close to the critical point, besides of that, the methods had problems identifying if the point calculated was a bubble point, or a dew point, which is important for proper phase identification. On the other hand, Winprop could calculate the saturation pressure close to the critical point, but did not identify the phase correctly. Also, Winprop failed to calculate the saturation pressure when it was close to the cricondentherm, but the methods implemented in GPAS performed the calculations correctly.

Because of the problems in calculating the saturation pressure, in this research we used Michelsen's stability test (Michelsen, 1982) for all the comparisons using the different formulations presented in this dissertation.

Appendix C. Corner Point Application

In this appendix, we present an application of Coats (1980) formulation in conjunction with the corner point feature implemented in GPAS. The corner point feature was originally implemented into GPAS framework by Marcondes et al. (2008). Therefore, the formulations tested in Chapter 6 benefited from this feature with further adaptations.

It is important to mention that the corner point implementation in GPAS considers full tensor permeability, which is different from the equivalent volume technique used in most commercial simulators. More details about the implementation of the corner point feature in GPAS can be found in Marcondes et al. (2008).

The case study is a quarter of five-spot model using 16x16x10 grid blocks. The reservoir fluid model has six components and the fluid injected is water. The case study was simulated using GPAS in conjunction with a Cartesian mesh, a orthogonal corner point mesh, and a distorted corner point mesh; then, the results of GPAS were compared with GEM-CMG. **Table C.1** presents the physical properties and the initial conditions for this case study.

Table C.1. Physical properties for the corner point case study

Grid blocks dimension in x, y, and z directions	16 x 16 x 10	
Length (m)	170.7	
Width (m)	170.7	
Thickness (m)	30.5	
Porosity (fraction)	0.35	
Rock compressibility (kPa^{-1})	$1.45x10^{-7}$	
Reservoir temperature (^oC)	71.1	
Permeability in x direction (m^2)	$1x10^{-14}$	
Permeability in y direction (m^2)	$1x10^{-14}$	
Permeability in z direction (m^2)	$1x10^{-14}$	
Water viscosity (Pa.s)	$1x10^{-3}$	
Water density (mol/m^3)	$55.55x10^3$	
Water compressibility (kPa^{-1})	$4.35x10^{-7}$	
Initial water saturation (fraction)	0.17	
Initial reservoir pressure (MPa)	10.34	
Water injection rate (m^3/day)	71.5	
Producer bottom hole pressure (MPa)	8.96	
Reservoir fluid initial composition	C1	0.5
	C3	0.03
	C6	0.07
	C10	0.2
	C15	0.15
	C20	0.05

Figures C.1 and **C.2** show the saturation field at 1500 days using GPAS and CMG-GEM in conjunction with an orthogonal corner point mesh and a Cartesian mesh, respectively. **Figure C.3** shows the saturation field at 1500 days using GPAS in conjunction with a distorted corner point mesh. From these three figures, we can see that the saturation field is similar for all the meshes tested.

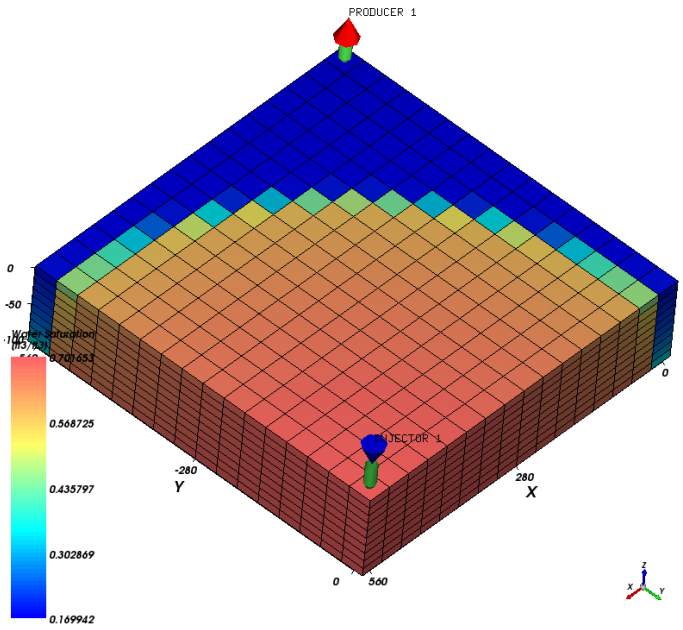

Figure C.1. Water saturation field at 1500 days using GPAS in conjunction with 16x16x10 orthogonal corner point mesh.

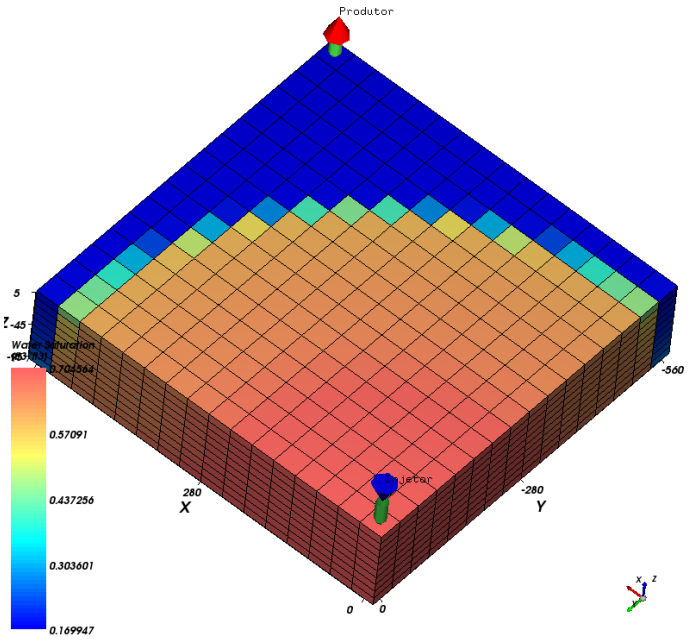

Figure C.2. Water saturation field at 1500 days using CMG-GEM in conjunction with 16x16x10 Cartesian mesh.

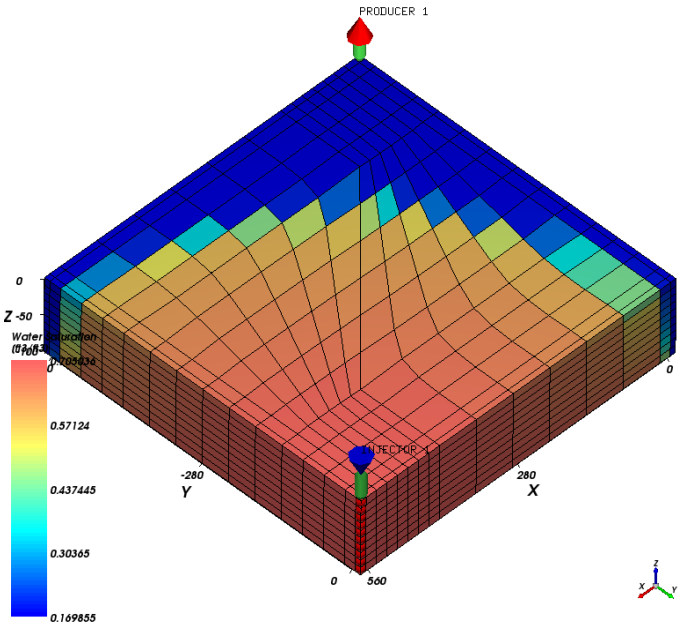

Figure C.3. Water saturation field at 1500 days using GPAS in conjunction with 16x16x10 distorted corner point mesh.

Figures C.4 and **C.5** present the results in terms of oil rate and gas rate versus time, respectively. From these figures we can compare the results of GPAS in conjunction with an orthogonal corner point mesh, GPAS using a Cartesian mesh, GPAS with a distorted corner point mesh, and CMG-GEM in conjunction with a Cartesian mesh. As we can see, the results are similar for all the simulations and it is important to mention that the results of the GPAS orthogonal corner point mesh match the results of GPAS Cartesian mesh as expected.

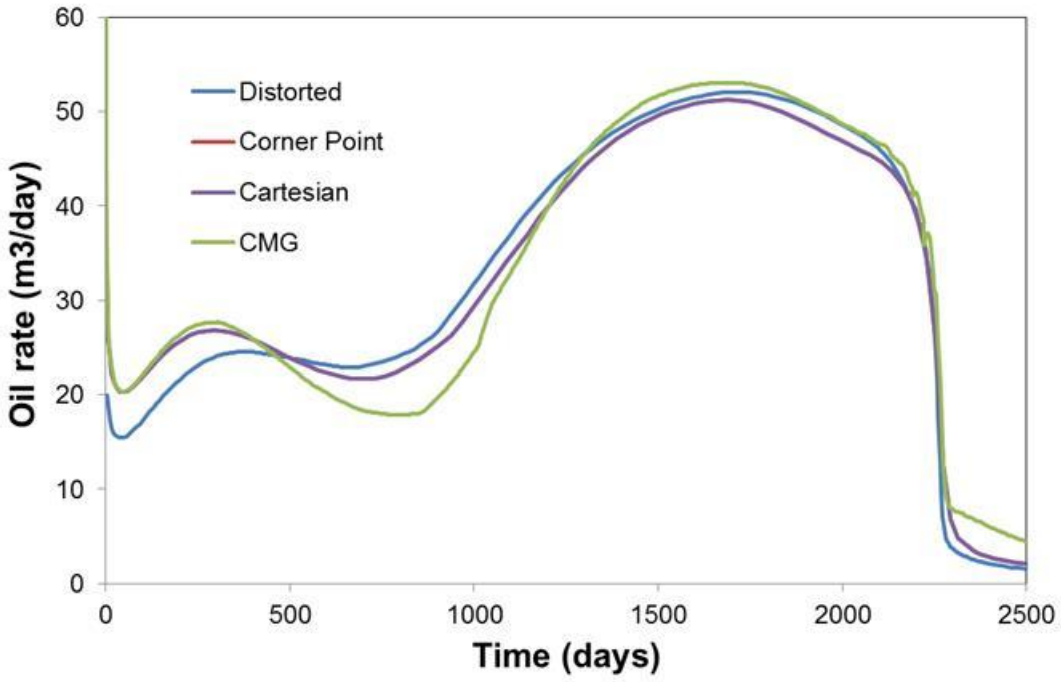

Figure C.4. Oil production rate versus time for the corner point case study.

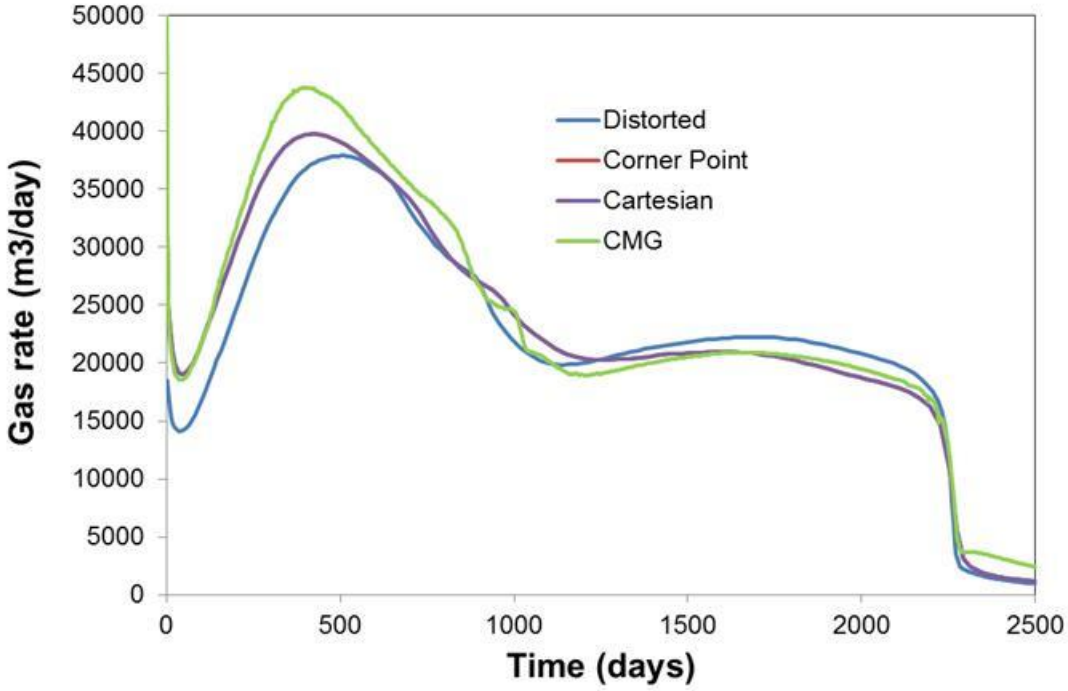

Figure C.5. Gas production rate versus time for the corner point case study.

Bibliography

Abbaszadeh-Dehghani, M. and Brigham, W.E., 1984. Analysis of well-to-well tracer flow to determine reservoir layering. *Paper SPE 10760, Journal of Petroleum Technology*, 36(10): 1753-1762.

Acs, G., Doleschall, S. and Farkas, E., 1985. General Purpose Compositional Model. *Paper SPE* 10515*, SPE Journal*, 25(4): 543-553.

Baker, L.E. and Luks, K.D., 1980. Critical Point and Saturation Pressure Calculations for Multicomponent Systems. *Paper SPE* 7478*, SPE Journal*, 20: 15-24.

Bear, J., 1988. Dynamics of fluids in porous media. Dover publications.

Bowen, G. and Crumpton, P., 2003. A New Formulation for the Implicit Compositional Simulation of Miscible Gas Injection Processes, *Paper SPE* 79692*, SPE Reservoir Simulation Symposium*.

Branco, C. and Rodriguez, F., 1996. A Semi-Implicit Formulation for Compositional Reservoir Simulation. *Paper SPE* 27053*, SPE Advanced Technology Series*, 4(1): 171-177.

Cao, H., 2002. Development of Techniques for General Purpose Simulators, *Ph.D. Dissertation, Department of Petroleum Engineering, Stanford University*.

Chang, Y., Pope, G.A. and Sepehrnoori, K., 1990a. A higher-order finite-difference compositional simulator. *Journal of Petroleum Science and Engineering*, 5(1): 35-50.

Chang, Y.B., 1990b. Development and Application of an Equation-of-State Compositional Simulator, *Ph.D. Dissertation, Department of Petroleum and Geosystems Engineering, The University of Texas at Austin*.

Chang, Y.B., Lim, M., Pope, G. and Sepehrnoori, K., 1994. CO2 flow patterns under multiphase flow: heterogeneous field-scale conditions. *Paper SPE* 22654-PA, *SPE Reservoir Engineering*, 9(3): 208-216.

Chien, M., Lee, S. and Chen, W., 1985. A New Fully Implicit Compositional Simulator, *Paper SPE* 13385*, 8th SPE Symposium on Reservoir Simulation*, Dallas, TX.

Coats, K.H., 1980. An Equation of State Compositional Model. *SPE Paper* 8284*, SPE Journal*, 20(5): 363-376.

Collins, D., Nghiem, L., Li, Y. and Grabonstotter, J., 1992. An Efficient Approach to Adaptive-Implicit Compositional Simulation with an Equation-of-State. *Paper SPE* 15133*, SPE Reservoir Engineering*, 7(2): 259-264.

Cordazzo, J., Maliska, C., C. da Silva, A.F. and V. Hurtado, F.S., 2005. An Element Based Conservative Scheme using Unstructured Grids for Reservoir Simulation, *18th World Petroleum Congress*.

Cordazzo, J., Maliska, C.R., Silva, A. and Hurtado, F.S.V., 2004a. The negative transmissibility issue when using CVFEM in petroleum reservoir simulation-1. Theory, *10o Brazilian Congress of Thermal Sciences and Engineering*.

Cordazzo, J., Maliska, C.R., Silva, A. and Hurtado, F.S.V., 2004b. The negative transmissibility issue when using CVFEM in petroleum reservoir simulation-1. Results, *10o Brazilian Congress of Thermal Sciences and Engineering*.

Creek, J. and Sheffield, J., 1993. Phase Behavior, Fluid Properties, and Displacement Characteristics of Permian Basin Reservoir Fluid/CO2 Systems. *Paper SPE* 20188-PA, *SPE Reservoir Engineering*, 8(1): 34-42.

Drexler, M., 1998. Towards a global convergence theory for Newton's method, *Stanford University Technical Report SCCM-98-06*, Stanford University.

Edwards, M.G., 2000. M-matrix flux splitting for general full tensor discretization operators on structured and unstructured grids. *Journal of Computational Physics*, 160(1): 1-28.

Edwards, M.G., 2002. Unstructured, control-volume distributed, full-tensor finite-volume schemes with flow based grids. *Computational Geosciences*, 6(3): 433-452.

Fanchi, J., 1983. Multidimensional numerical dispersion. *Paper SPE* 9018-PA, *SPE Journal*, 23(1): 143-151.

Fong, W., Sheffield, J., Ehrlich, R. and Emanuel, A., 1992. Phase Behavior Modeling Techniques for Low-Temperature CO2 Applied to McElroy and North Ward Estes Projects, *Paper SPE* 24184-MS, *SPE/DOE Enhanced Oil Recovery Symposium*.

Forsyth, P., 1990. A control-volume, finite-element method for local mesh refinement in thermal reservoir simulation. *Paper SPE* 18415*, SPE Symposium on Reservoir Simulation*.

Fung, L.S.K., Hiebert, A. and Nghiem, L.X., 1992. Reservoir simulation with a control-volume finite-element method. *Paper SPE* 21224*, SPE Symposium on Reservoir Simulation*, 7(3): 349-357.

Fussell, D. and Yanosik, J., 1978. An Iterative Sequence for Phase-Equilibria Calculations Incorporating the Redlich-Kwong Equation of State. *Paper SPE* 6050*, SPE Journal*, 18(3): 173-182.

Fussell, L. and Fussell, D., 1979. An Iterative Technique for Compositional Reservoir Models. *Paper SPE* 6891*, SPE Journal*, 19(4): 211-220.

Gottardi, G. and Dall'Olio, D., 1992. A control-volume finite-element model for simulating oil-water reservoirs. *Journal of Petroleum Science and Engineering*, 8(1): 29-41.

Gropp, W. et al., 1996. New Generation Framework For Petroleum Reservoir Simulation. *First Annual Report, Advanced Technology Initiative, Argonne National Laboratory and The University of Texas at Austin*.

Guler, B., Wang, P., Delshad, M., Pope, G.A. and Sepehrnoori, K., 2001. Three-and Four-Phased Flow Compositional Simulations of CO2/NGL EOR, *Paper SPE* 71485*, Anual Technical Conference and Exhibition*.

Haajizadeh, M., Fayers, F., Cockin, A., Roffey, M. and Bond, D., 1999. On the importance of dispersion and heterogeneity in the compositional simulation of miscible gas processes, *Paper SPE* 24184-MS, *SPE Asia Pacific Improved Oil Recovery Conference*.

Han, C., Delshad, M., Sepehrnoori, K. and Pope, G., 2005. A fully implicit, parallel, compositional chemical flooding simulator, *Pape SPE* 97217*, SPE Annual Technical Conference and Exhibition*.

Henry, R. and Metcalfe, R., 1983. Multiple-phase generation during carbon dioxide flooding. *Paper SPE* 8812-PA, *SPE Journal*, 23(4): 595-601.

Hovanessian, S., 1961. Pressure Studies in Bounded Reservoirs. *Paper SPE* 50-PA, *SPE Journal*, 1(4): 223-228.

Jessen, K. and Rastegar Moghadam, R., 2009. A Flow Based Lumping Approach for Compositional Reservoir Simulation, *SPE Paper* 119160*, SPE Reservoir Simulation Symposium*.

Kazemi, H., Vestal, C. and SHANK, D., 1978. An Efficient Multicomponent Numerical Simulator. *Paper SPE* 6890*, SPE Journal*, 18(5): 355-368.

Kendall, R., Morrell, G., Peaceman, D., Silliman, W. and Watts, J., 1983. Development of a Multiple Application Reservoir Simulator for Use on a Vector Computer, *Paper SPE* 11483*, Middle East Oil Technical Conference*, Manama, Bahrain.

Khan, S., Pope, G. and Sepehrnoori, K., 1992. Fluid characterization of three-phase CO2/oil mixtures, *Paper SPE* 24130-MS*, SPE/DOE Enhanced Oil Recovery Symposium*.

Lacroix, S., Vassilevski, Y.V. and Wheeler, M.F., 2000. Iterative solvers of the implicit parallel accurate reservoir simulator (IPARS), I: single processor case. *TICAM report 00-28*.

Lake, L.W., 1989. Enhanced oil recovery. Prentice Hall Inc.

Li, D., 2004. Four-Phase Streamline-Based Compositional Simulation of Gas Injections for a Viscous Oil, *SPE Paper* 88790*, Abu Dhabi International Conference and Exhibition*.

Li, X., 2012. A Collection of Case Studies for Verification of Reservoir Simulators, *Master's Thesis, Department of Petroleum and Geosystems Engineering, The University of Texas at Austin*, Austin.

Lins, A.G., 2010. Advanced Compositional Simulation of CO2 Processes, *Ph.D. Dissertation, University of Calgary*, Calgary.

Lins Jr, A., Nghiem, L. and Harding, T., 2011. Three-Phase Hydrocarbon Thermodynamic Liquid-Liquid-Vapour Equilibrium in CO2 Process, *Paper SPE* 148040*, SPE Reservoir Characterisation and Simulation Conference and Exhibition*.

Liu, J., Delshad, M., Pope, G.A. and Sepehrnoori, K., 1994. Application of higher-order flux-limited methods in compositional simulation. *Transport in Porous media*, 16(1): 1-29.

Maliska, C., 2012. Personal Communication. In: F. Marcondes (Editor).

Marcondes, F., Han, C. and Sepehrnoori, K., 2008. Effect of cross derivatives in discretization schemes in structured non-orthogonal meshes for compositional reservoir simulation. *Journal of Petroleum Science and Engineering*, 63(1): 53-60.

Marcondes, F., Santos, L.O.S., Varavei, A. and Sepehrnoori, K., 2013. A 3D Hybrid Element-based Finite-Volume Method for Heterogeneous and Anisotropic Compositional Reservoir Simulation. accepted by *Journal of Petroleum Science and Engineering*.

Marcondes, F. and Sepehrnoori, K., 2007. Unstructured Grids and an Element Based Conservative Approach for Compositional Reservoir Simulation, *19th International Congress of Mechanical Engineering*.

Marcondes, F. and Sepehrnoori, K., 2010. An element-based finite-volume method approach for heterogeneous and anisotropic compositional reservoir simulation. *Journal of Petroleum Science and Engineering*, 73(1): 99-106.

Michelsen, M.L., 1982. The Isothermal Flash Problem. Part I. Stability. *Fluid phase equilibria*, 9(1): 1-19.

Michelsen, M.L., 1985. Saturation Point Calculations. *Fluid phase equilibria*, 23(2-3): 181-192.

Nghiem, L. and Li, Y., 1986. Effect of Phase Behavior on CO2 Displacement Efficiency at Low Temperatures: Model Studies with an Equation of State. *Paper SPE* 13116-PA, *SPE Reservoir Engineering*, 1(4): 414-422.

Nghiem, L.X., Fong, D. and Aziz, K., 1981. Compositional Modeling with an Equation-of-State. *Paper SPE* 9306*, SPE Journal*, 21(6): 687-698.

Okuno, R., Johns, R. and Sepehrnoori, K., 2010. Three-Phase Flash in Compositional Simulation Using a Reduced Method. *Paper SPE* 125226-PA, *SPE Journal*, 15(3): 689-703.

Okuno, R., Johns, R. and Sepehrnoori, K., 2011. Mechanisms for High Displacement Efficiency of Low-Temperature CO2 Floods. *Paper SPE* 129846-PA, *SPE Journal*, 16(4): 751-767.

Orr, F.M., Yu, A.D. and Lien, C.L., 1981. Phase behavior of CO2 and crude oil in low-temperature reservoirs. *Paper SPE* 8813-PA, *SPE Journal*, 21(4): 480-492.

Paluszny, A., Matthäi, S. and Hohmeyer, M., 2007. Hybrid finite element–finite volume discretization of complex geologic structures and a new simulation workflow demonstrated on fractured rocks. *Geofluids*, 7(2): 186-208.

Pan, F., 2009. Development and application of a coupled geomechanics model for a parallel compositional reservoir simulator, *Ph.D. dissertation, Department of Petroleum and Geosystems Engineering, The University of Texas at Austin*.

Pan, F., Sepehrnoori, K. and Chin, L., 2007. Development of a coupled geomechanics model for a parallel compositional reservoir simulator, *Paper SPE* 109867*, SPE Annual Technical Conference and Exhibition*.

Parashar, M., Wheeler, J., Pope, G., Wang, K. and Wang, P., 1997. A new generation EOS compositional reservoir simulator: Part II-framework and multiprocessing, *Paper SPE* 37977-MS*, SPE Reservoir Simulation Symposium*.

Peng, D.Y. and Robinson, D.B., 1976. A new two-constant equation of state. Industrial & Engineering Chemistry Fundamentals, 15(1): 59-64.

Pope, G.A., 2003. Fluid Flow through Permeable Media. Petroleum and Geosystems Engineering. The University of Texas at Austin, Austin, TX.

Prevost, M., Edwards, M. and Blunt, M., 2002. Streamline tracing on curvilinear structured and unstructured grids. *SPE Paper* 78663-PA, *SPE Journal*, 7(2): 139-148.

Quandalle, P. and Savary, D., 1989. An Implicit in Pressure and Saturations Approach to Fully Compositional Simulation, *Paper SPE* 18423*, SPE Symposium on Reservoir Simulation*, Houston, TX.

Santos, L.O.S., Marcondes, F. and Sepehrnoori, K., 2013. A 3D Compositional Miscible Gas Flooding Simulator with Dispersion using Element-based Finite-Volume Method. submitted to *Journal of Petroleum Science and Engineering*.

Shelton, J.L. and Yarborough, L., 1977. Multiple phase behavior in porous media during CO2 or rich-gas flooding. *Journal of Petroleum Technology*, 29(9): 1171-1178.

Shrivastava, V., Nghiem, L. and Moore, R., 2002. A novel approach for incorporating physical dispersion in miscible displacement, *Paper SPE* 77724-MS*, SPE Annual Technical Conference and Exhibition*.

Shrivastava, V., Nghiem, L., Moore, R. and Okazawa, T., 2005a. Modelling physical dispersion in miscible displacement-Part 1: Theory and the proposed numerical scheme. *Journal of Canadian Petroleum Technology*, 44(5): 25-33.

Shrivastava, V., Nghiem, L., Moore, R. and Okazawa, T., 2005b. Modelling physical dispersion in miscible displacement-Part 2: Validation, Numerical Tests, and Applications. *Journal of Canadian Petroleum Technology*, 44(5): 34-43.

Solano, R., Johns, R. and Lake, L., 2001. Impact of reservoir mixing on recovery in enriched-gas drives above the minimum miscibility enrichment. *Paper SPE* 73829-PA*, SPE Reservoir Evaluation & Engineering*, 4(5): 358-365.

Stalkup, F., 1990. Effect of gas enrichment and numerical dispersion on enriched-gas-drive predictions. *SPE Paper* 18060-PA, *SPE Reservoir Engineering*, 5(4): 647-655.

Thele, K.J., Lake, L.W. and Sepehrnoori, K., 1983. A comparison of three equation-of-state compositional simulators, *Paper SPE 12245, SPE Reservoir Simulation Symposium*.

Turek, E., Metcalfe, R. and Fishback, R., 1988. Phase Behavior of Several CO2/West Texas-Reservoir-Oil Systems. *SPE Paper* 13117-PA, *SPE Reservoir Engineering*, 3(2): 505-516.

Varavei, A., 2009. Development of an equation-of-state thermal flooding simulator, *Ph.D. Dissertation, Department of Petroleum and Geosystems Engineering, The University of Texas at Austin*.

Verma, S. and Aziz, K., 1997. A control volume scheme for flexible grids in reservoir simulation, *Paper SPE* 37999*, SPE Symposium on Reservoir Simulation*.

Voskov, D. and Tchelepi, H., 2008. Compositional Parametrization for Multi-phase Flow in Porous Media, *Paper SPE* 113492*, SPE/DOE Symposium on Improved Oil Recovery*.

Voskov, D., Tchelepi, H. and Younis, R., 2009. General Nonlinear Solution Strategies for Multiphase Multicomponent EoS Based Simulation, *Paper SPE* 118996*, SPE Reservoir Simulation Symposium*, The Woodlands, TX.

Wang, P. et al., 1999. A Fully Implicit Parallel EOS Compositional Simulator for Large Scale Reservoir Simulation, *Paper SPE* 51885*, SPE Reservoir Simulation Symposium*.

Wang, P., Wheeler, M., Parashar, M. and Sepehrnoori, K., 1997. A New Generation EOS Compositional Reservoir Simulator: Part I - Formulation and Discretization, *Paper SPE* 37979*, SPE Reservoir Simulation Symposium*, Dallas - TX.

Wang, X. and Strycker, A., 2000. Evaluation of CO2 Injection with Three Hydrocarbon Phases, *International Oil and Gas Conference and Exhibition in China*.

Watts, J., 1986. A Compositional Formulation of the Pressure and Saturation Equations. *Paper SPE* 12244*, SPE Reservoir Engineering*, 1(3): 243-252.

Wei, Y., Michelsen, M., Stenby, E., Berenblyum, R. and Shapiro, A., 2004. Three-phase Compositional Streamline Simulation and Its Application to WAG, *SPE Paper* 89440*, SPE/DOE Symposium on Improved Oil Recovery*.

Wheeler, M. et al., 1999. A parallel multiblock/multidomain approach for reservoir simulation, *Paper SPE* 51884*, SPE Reservoir Simulation Symposium*.

Wilson, G.M., 1969. A modified Redlich-Kwong equation of state, application to general physical data calculations, *65th National AIChE Meeting*, Cleveland, OH.

Wong, T.W. and Aziz, K., 1988. Considerations in the Development of Multipurpose Reservoir Simulation Models, *First and Second International Forum on Reservoir Simulation*, Alpbach, Austria, pp. 12-16.

Young, L. and Stephenson, R., 1983. A Generalized Compositional Approach for Reservoir Simulation. *Paper SPE* 10516*, SPE Journal*, 23(5): 727-742.